2015

A New Role for Beta-Amyloid in Alzheimer's Disease: Initiation of Thrombotic and Inflammatory Processes Via Coagulation Factor XII and Fibrinogen

Daria Zamolodchikov

A NEW ROLE FOR BETA-AMYLOID IN ALZHEIMER'S DISEASE: INITIATION OF THROMBOTIC AND INFLAMMATORY PROCESSES VIA COAGULATION FACTOR XII AND FIBRINOGEN

A Thesis Presented to the Faculty of

The Rockefeller University

in Partial Fulfillment of the Requirements for

the degree of Doctor of Philosophy

by

Daria Zamolodchikov

June 2015

A NEW ROLE FOR BETA-AMYLOID IN ALZHEIMER'S DISEASE: INITIATION OF THROMBOTIC AND INFLAMMATORY PROCESSES VIA COAGULATION FACTOR XII AND FIBRINOGEN

Daria Zamolodchikov, Ph.D.

The Rockefeller University 2015

Alzheimer's disease (AD) is a progressive neurodegenerative disorder with no effective therapies. While abundant genetic, histological, and experimental evidence links the beta-amyloid (Aβ) peptide to disease onset and progression, the mechanisms behind neuronal dysfunction in AD are not completely understood.

It is now clear that AD is a complex, multifactorial disease characterized by vascular dysfunction, prothrombotic state, and inflammation, but whether these conditions are a cause or consequence of disease is debated. Prothrombotic and inflammatory states can contribute to alterations in cerebral blood flow resulting in hypoperfusion. Since neuronal function is dependent on an uninterrupted blood supply sustained by a healthy vasculature, agents capable of eliciting thrombosis and/or inflammation could play a key role in AD onset and progression.

The contact activation system, initiated by activation of the plasma protein FXII, is capable of launching both thrombotic and inflammatory pathways. I investigated whether Aβ could directly induce these pathways by interacting with FXII *in vitro,* in AD mouse models, and in AD patients. A prothrombotic state may also result from reduced clot degradation, as seen in mouse models of AD. I therefore investigated the mechanism by which clots formed in the presence of Aβ are structurally altered and resistant to degradation.

I established the ability of Aβ to initiate prothrombotic and inflammatory processes via activation of the FXII-driven contact system, and provided evidence for these processes in AD patients and mouse models. I also defined the regions involved in Aβ-fibrinogen binding and elucidated the mechanism by which this interaction results in delayed fibrinolysis. My results suggest new pathogenic mechanisms, diagnostic tests, and therapeutic targets for AD.

To my grandmother
Galina A. Lavnikova
March 7, 1922 – May 22, 2011

ACKNOWLEDGEMENTS

My mentor Sid Strickland provided me with unwavering support and enthusiasm while allowing me broad freedom to explore my ideas. I am grateful to Sid for giving me the opportunity to go down many paths, for helping me keep what is and isn't interesting in perspective, for creating a warm and sane lab environment, and for keeping me up to date on the latest developments in mobile phone technology.

I thank my faculty advisory committee members Seth Darst, Barry Coller, and Deena Oren for their time, attention to detail, and thoughtful feedback over the years. I also thank Dudley Strickland for taking the time to act as my external committee member.

Some of the work presented here was done in collaboration with lab members Hyung Jin Ahn, Marta Cortes-Canteli, and Zu-Lin Chen, who extended valuable mentorship and crucial experimental assistance. I am grateful for the friendship and advice provided by current and former lab members Anna Kruyer, Erin Norris, Emily Lowry, Alex Bounoutas, and Moses Feaster. I am also grateful to Manish Ponda for his bottomless medical knowledge and valuable scientific discussions.

Thomas Renné provided much needed expertise and guidance at a pivotal point in my research. I am thankful for being so warmly welcomed in his lab at the Karolinska Institute. I am grateful to Renné lab members Jenny Björkqvist, Katrin Nickel, Linda Labberton, and Anne Jämsä for being patient teachers and making me feel very much at home.

This work could not have been done without the assistance of current and former Rockefeller Resource Center scientists Deena Oren, Kunihiro Uryu, Joe Fernandez, Shivaprasad Bhuvanendran, and Kaye Thomas.

Finally, my family and friends have supported me through the many highs and lows of my graduate career, for which I am very grateful.

TABLE OF CONTENTS **Page**

LIST OF FIGURES **Page**

LIST OF TABLES

CHAPTER 1. INTRODUCTION

1.1. Alzheimer's disease: demographic and clinical features

Alzheimer's disease (AD) is the most common type of dementia, affecting over 5.2 million Americans and 26 million people worldwide. Age is the greatest risk factor: one in nine people age 65 and over (11%) and one third of those age 85 and over (32%) have AD[1]. As the global population achieves higher longevity due to advances in medicine, the prevalence of AD will continue to increase. By 2050, the number of Americans age 65 and over with AD is projected to triple to 13.8 million if treatments to prevent or slow disease are not developed. The disease is and will continue to be an immense financial burden: the cost of care for individuals with AD is projected to increase from $203 billion in 2013 to $1.2 trillion in 2050[1].

At its earliest stages, AD is clinically characterized by deficits in the ability to learn and remember new information. Symptoms progress to include impairment of semantic memory (concept-based knowledge), executive function (problem solving, planning, and execution), and visuospatial skills[2]. In late stages of disease, brain regions responsible for controlling life-sustaining functions become affected, leading to death. Neuropathologically, AD is characterized by the accumulation of the peptide beta-amyloid (Aβ) in the brain parenchyma (plaques)[3] and by the intraneuronal accumulation of filamentous hyperphosphorylated tau protein (tangles)[4]. In addition to these diagnostic criteria, other histological changes found in AD brains include vascular pathology, neuroinflammation, dystrophic neurites, and brain atrophy. The etiology of AD is complex and still poorly defined. Despite decades of research, the initiating event(s) behind neuronal dysfunction remain unclear. Many theories have emerged from the study of the neuropathological hallmarks described above, with most identifying the Aβ peptide as a critical player in AD pathogenesis.

1.2. AD etiology: Aβ hypothesis

Aβ is proteolytically derived from the ubiquitously expressed transmembrane protein amyloid precursor protein (APP). Cleavage of APP by the aspartyl protease β-secretase creates the N-terminus of the Aβ peptide. Release of Aβ is mediated by the γ-secretase catalytic component presenilin, which cleaves the remaining portion of APP at one of several sites, creating a 39 to 43 amino acid Aβ peptide (Figure 1.1). The most common form of Aβ generated is 40 amino acids long (Aβ40), with the 42 amino acid peptide (Aβ42) considered to be the more pathogenic form[5].

Normally, the generation of Aβ in the brain is balanced by its clearance, which is mediated by proteolytic degradation[6], cell-mediated clearance[7,8], perivascular drainage[9], and transport across the blood-brain barrier (BBB) into the circulation[10]. A rise in Aβ concentration leads to the formation of soluble Aβ oligomers, with subsequent fibrillization and deposition in the form of plaques[11] (Figure 1.1). Mutations in genes resulting in increased production of Aβ or in the production of Aβ with decreased potential for clearance are associated with elevated AD risk, providing a genetic link between Aβ and AD. For example, mutations in APP, presenilin 1, or presenilin 2 induce altered Aβ production and are responsible for an early onset, autosomal dominant form of the disease[12]. Furthermore, triplication of the APP-bearing chromosome 21 in Down Syndrome results in increased Aβ production, early Aβ plaque deposition, and dementia in 50-70% of individuals by age 60-70[13].

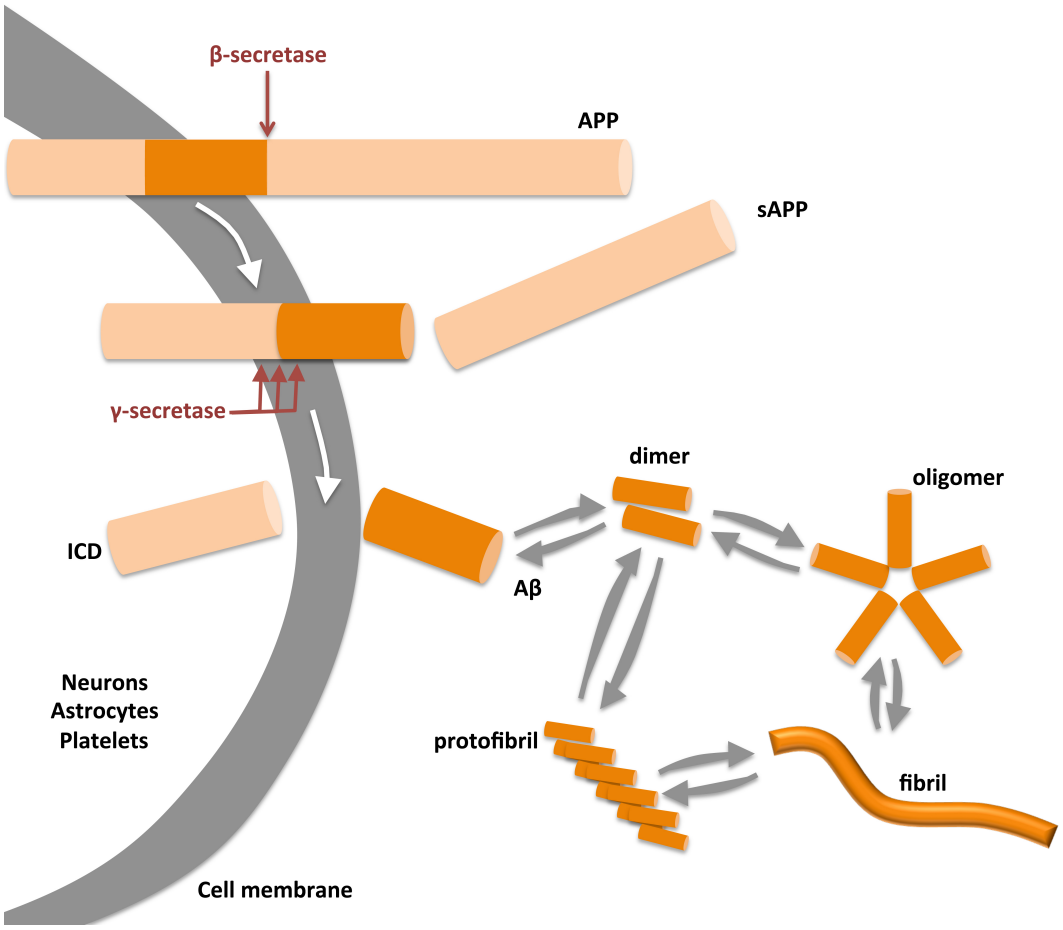

Figure 1.1. Production of Aβ from APP. The ubiquitously expressed transmembrane protein APP undergoes processing by β- and γ-secretases to release C-terminal soluble APP (sAPP), the Aβ peptide, and an N-terminal intracellular domain (ICD). Aβ can self-aggregate, resulting in the formation of dimers, various oligomeric forms, protofibrils, and fibrils.

In contrast to these early-onset AD cases, it is thought that the vast majority of sporadic (late-onset) AD stems from defective Aβ clearance and not increased Aβ production[14-16]. Indeed, the strongest genetic risk factor for late-onset AD is apolipoprotein E (*APOE*) genotype, with individuals carrying the *APOE* ε4 allele being at an increased risk of AD compared to ε3 and ε2 carriers[17,18]. While the role of ApoE in AD is complex and not fully understood, one aspect of its function is that it disrupts the transport of parenchymal Aβ across the BBB by LRP1 receptors, with the ε4 isoform disrupting the efficiency of Aβ clearance more than ε3 and ε2[19].

Correlations between Aβ accumulation and AD at both a histological and genetic level support the "Aβ hypothesis of AD," which states that a chronic imbalance in production versus clearance of Aβ leads to its gradual accumulation in the brain, which over the many years of AD development results in pathological changes characteristic of AD, including microgliosis, astrocytosis, neuronal dysfunction, and cognitive impairment[11]. The idea that Aβ accumulation can result in AD-related pathological and clinical changes is supported by experimental evidence of Aβ-mediated toxicity. Aβ oligomers induce neuronal mitochondrial dysfunction[20], synaptic dysfunction[21-23], and directly promote neuronal death[21]. Aβ deposits trigger microglial and astrocytic activation, which can contribute to neuronal dysfunction through inflammatory processes[24]. Thus, neuronal dysfunction due to Aβ's direct or glial cell-mediated toxicity can cause cognitive decline. However, Aβ deposits are also found in neurologically normal individuals[25-27], indicating that Aβ does not always induce neurotoxicity, and suggesting that other factors contribute to AD onset.

1.3. AD etiology: vascular hypothesis

A healthy brain vasculature is critical for neuronal viability and cognitive function. Oxygen and nutrients are supplied to the brain by arteries, which branch into arterioles and finally into capillaries. Capillary walls mediate exchange of substances between the

circulation and brain parenchyma and constitute the BBB. Brain function is dependent on a tightly regulated BBB and on consistent cerebral blood flow (CBF)[28], which can be dramatically affected by very small changes in cerebral vessel biology and structure[29]. While cerebrovascular dysfunction has traditionally been thought to cause a distinct disease called vascular dementia, a large body of evidence now indicates that significant overlap exists between vascular dementia and AD, blurring this distinction[30]. Indeed, cerebrovascular pathology is present in virtually all AD patient brains upon autopsy[31-36] and BBB dysfunction is increasingly recognized as an important aspect of AD pathology[28,37-39], but whether these changes play a causal role in AD or are simply co-morbidities is still debated.

The idea that vascular pathologies may be causative in AD stems from evidence that they precede AD development. Conditions associated with vascular disease such as diabetes, hypertension, hypercholesterolemia, atherosclerosis, silent brain infarcts, and white matter lesions increase the risk of developing AD[40-44], with nearly all of them present not only at AD onset but also decades before any loss of cognitive function develops[41]. Many of them can compromise CBF and induce brain hypoperfusion[29], which are observed early in the course of AD[28,45,46]. Disturbances in CBF and brain perfusion can lead to BBB dysfunction, dysregulation of nutrient transport, neuronal dysfunction, and eventually cognitive decline[41,47]. Hypoxia and energy deficits resulting from hypoperfusion can accelerate Aβ deposition, increase tau hyperphosphorylation, impair BBB functions, precipitate neuronal loss, and produce cognitive dysfunction[46,48-50], all of which are pathological hallmarks of AD. Even a relatively mild restriction in blood supply to brain tissue causes long-term dysfunction of synaptic transmission[51], underscoring the idea that small deficits in oxygen and nutrient supply can over time have significant effects.

The presence of morphological abnormalities in the AD brain vasculature, the epidemiologic connections between vascular disease risk factors and AD risk, and the

potential mechanistic connections between vascular and neuronal dysfunction provide a basis for an alternative theory known as the “vascular hypothesis of AD,” which states that deficiencies in vascular function and CBF gradually lead to the pathological and molecular characteristics of the disease[29,41]. Thus, the “Aβ hypothesis” identifies Aβ as a primary driver in AD, while the “vascular hypothesis” identifies vascular dysfunction as a cause of AD neuropathology and symptoms. But what exactly causes vascular dysfunction in individuals at risk for AD?

In this thesis, I would like to propose that Aβ itself could drive the vascular changes that may lead to AD onset and progression, providing a link between the Aβ and vascular hypotheses. Exploring this connection requires the introduction of two additional pathologic states associated with AD.

1.4. Prothrombotic state in AD

In keeping with a link between AD and vascular dysfunction, accumulating evidence suggests that AD patients and mouse models exhibit a prothrombotic or hypercoagulable state, defined as an increased tendency toward clot formation. Clot formation is mediated by activated platelets and the coagulation cascade, which involves the sequential activation of a series of factors resulting in the production of thrombin. AD patients have elevated plasma levels of activated Factor VII, prothrombin fragment 1+2, von Willebrand Factor[52,53], and activated platelets[54,55], all of which reflect or promote increased thrombin generation. The existence of a prothrombotic state in AD would be expected to increase the incidence thrombotic events. Indeed, AD patients are at a higher risk for microinfarcts[56,57] and stroke[58] compared to non-demented controls, microinfarct number correlates with cognitive decline [57], and AD mouse models have a greater propensity to form thrombi[59,60].

An important question is whether the prothrombotic state in AD patients is a cause or consequence of disease. Evidence for a causative role comes from epidemiological studies suggesting that prothrombotic states may contribute to disease onset and progression. Older adults with increased D-dimer and prothrombin fragment 1+2 levels, both markers of increased thrombin generation, are at higher risk for cognitive decline[61], and increased levels of coated platelets (a highly pro-coagulant subset of activated platelets[62]) correlate with future AD severity[63] and progression from MCI to AD[64]. Conditions characterized by hypercoagulability such as factor V Leiden (a prothrombotic mutation in factor V)[65], elevated plasma homocysteine levels[66-68], elevated plasma fibrinogen levels[69], silent brain infarcts[40], and stroke[70-72] place individuals at increased risk for AD. The hypothesis that a prothrombotic state contributes to AD is also supported by improvements in AD pathology and memory in AD patients[73-75] and mouse models[76,77] following treatment with anticoagulants.

1.5. Proinflammatory state in AD

Inflammation is a well-established component of AD pathology supported by proteomic, histological, genetic, and epidemiological evidence[24,78]. Inflammation in the AD brain parenchyma is characterized by increased levels of activated microglia and astrocytes (the cellular mediators of inflammation in the brain) as well as by increased levels of complement system components and cytokines[24]. Chronic activation of astrocytes diminishes their capacity to support neuronal health[79,80], and the release of proinflammatory molecules from chronically activated microglia and astrocytes combined with chronic complement activation can directly induce neuronal toxicity[81]. Inflammation in AD is observed not only in the brain parenchyma, but also in the periphery: AD plasma and serum have elevated levels of circulating proinflammatory cytokines, chemokines[24,78], and acute phase proteins, and AD blood cells produce increased levels of cytokines[78,82]. The idea that peripheral inflammation

can contribute to and/or reflect neuroinflammation and neuropathology is supported by studies in AD patients and mouse models demonstrating that elevated circulating levels of proinflammatory molecules correlate with increased microglial activation, neuronal loss, and cognitive decline[78].

Whether inflammation is a primary driver of AD, a toxic consequence of other AD-related processes, or a protective response delaying AD onset is debated[83]. However, several lines of evidence support a role for inflammation in driving AD onset and progression. Mouse models of AD show microglial activation prior to Aβ plaque deposition[84,85], microglial activation is seen in prodromal AD[86,87], and is increased in early to moderate AD compared to controls[88,89]. Further support comes from studies showing that peripheral markers of inflammation increase the risk of AD[90], that incidence of systemic infections increase the risk of dementia[91], and that cognitive impairment in AD individuals is exacerbated during and after systemic infection[92]. Finally, numerous epidemiological studies show that long-term nonsteroidal anti-inflammatory drug use reduces AD risk[24].

1.6. Contribution of prothrombotic and inflammatory states to vascular dysfunction

Thrombosis and inflammation can contribute to vascular dysfunction through multiple mechanisms. Thrombus formation in arterioles decreases CBF in downstream capillaries[93], while thrombosis in venules disrupts local CBF and decreases CBF in upstream capillaries[94]. Chronically decreased CBF can lead to vascular endothelial cell remodeling, endothelial cell death[95], and capillary collapse[47]. Thrombin itself can mediate endothelial cell permeability i*n vitro*[96-98] and precipitate BBB dysfunction and breakdown *in vivo*[99,100]. BBB dysfunction results in leakage of plasma proteins into the brain parenchyma, leading to vessel wall thickening and subsequent functional deterioration[101,102]. Furthermore, thrombin binding to protease activated receptors on endothelial cells promotes the release of proinflammatory cytokines[103,104], thereby contributing to inflammatory processes.

Inflammation-induced vascular dysfunction may stem from changes in the ability of chronically activated astrocytes to control vascular tone and BBB function[79,80] as well as from a proinflammatory state in the periphery. Circulating proinflammatory molecules such as cytokines, activated complement components, and bradykinin can modify vascular endothelial cell function and increase BBB permeability[105-109]. Indeed, mouse models with systemic inflammation have increased susceptibility to BBB permeability[110-112]. The ability of inflammatory processes to elicit clinically-relevant vascular dysfunction is illustrated by the etiology of vascular disease in humans. Inflammation-induced endothelial activation and leakage of blood components through a compromised endothelium can lead to chronic vascular diseases such as atherosclerosis[107,113] and cerebral small vessel disease[114,115], both characterized by vessel narrowing and stiffness[107,115,116].

Thus, changes to vascular biology, structure, and permeability induced by thrombotic and inflammatory mediators could be a key mechanism behind the vascular dysfunction, BBB dysregulation, and CBF reduction implicated in the initiation and/or progression of AD.

1.7. A possible role for Aβ in thrombosis and inflammation

If dysregulated coagulation and inflammation play a role in inducing and/or exacerbating vascular pathology, pathways capable of triggering these processes are of great interest to AD etiology. The contact activation system, which can launch both prothrombotic and proinflammatory pathways, is initiated when the plasma protein factor XII (FXII) is exposed to negatively charged surfaces (contact activation)[117]. Contact activated FXII (FXIIa) cleaves plasma prekallikrein to generate plasma kallikrein, which in turn cleaves high molecular weight kininogen (HK) to release the proinflammatory mediator bradykinin (Figure 1.2, kallikrein-kinin system). In addition to cleaving prekallikrein, FXIIa also activates factor XI (FXI) in the intrinsic coagulation cascade leading to thrombin generation, the conversion of fibrinogen to fibrin, and clot formation (Figure 1.2, intrinsic coagulation pathway). Activation

of the contact system also produces numerous proteases (including FXIIa, kallikrein, FXIa, and thrombin) capable of complement system activation[118-120] (Figure 1.2). In AD, a possible surface for FXII activation could be Aβ, which has been shown to stimulate FXII-dependent plasma kallikrein activity[121,122] and HK cleavage[121,123] *in vitro*.

Thrombotic potential is mediated not only by agents capable of modulating the coagulation cascade, but also by factors affecting the physical and biochemical stability of the forming fibrin clot, which is very sensitive to the conditions under which it is formed[124]. In this regard, binding of Aβ to fibrinogen[125] in the forming clot may further promote thrombosis by inducing changes in clot structure and stability[59].

The potential for interactions between Aβ and FXII and/or fibrinogen *in vivo* is supported by studies placing Aβ at sites of possible thrombosis and inflammation at increased concentrations. This includes locally elevated levels of Aβ at the luminal side of cerebral capillary walls, where Aβ enters the blood through the BBB[10], secretion of Aβ by activated platelets[126], and Aβ accumulation in atherosclerotic lesions[127]. Taken together, accumulating evidence supports the hypothesis that Aβ may act as both an initiator of coagulation and inflammation via interaction with FXII and as a modulator of clot stability via interaction with fibrinogen.

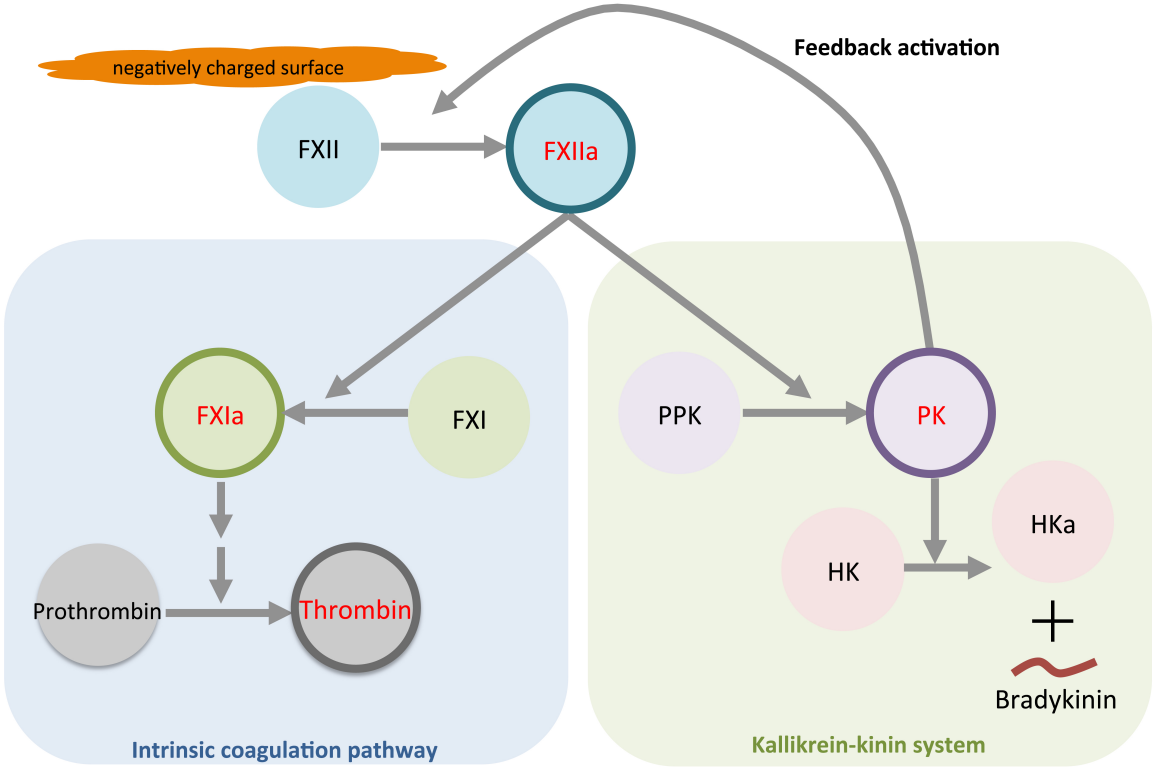

Figure 1.2. The contact activation system. Contact between FXII and negatively charged surfaces produces activated FXII (FXIIa), which can lead to activation of the intrinsic coagulation pathway (blue panel) and the plasma kallikrein-kinin system (green panel). Activation of FXI to FXIa triggers a cascade of proteolytic reactions ultimately resulting in the formation of thrombin, which mediates clot formation. Plasma kallikrein (PK) generated from FXIIa-mediated plasma prekallikrein (PPK) activation further activates FXII (feedback activation) and cleaves high molecular weight kininogen (HK), which releases bradykinin. Proteases capable of initiating complement system activation are designated in red.

1.8. Objectives

AD is an enormous and growing public health problem, due in large part to the fact that there are no effective therapies. Major roadblocks to the treatment of AD are the lack of adequate diagnostic tools and the absence of viable therapeutic targets, both stemming from an incomplete understanding of the mechanistic basis of AD etiology and progression.

The induction of prothrombotic and inflammatory states by Aβ could explain the epidemiological associations between AD, thrombosis, and inflammation. At the same time, Aβ-mediated activation of inflammatory and prothrombotic processes could be the missing link connecting the Aβ hypothesis with the vascular hypothesis of AD. Evaluation of the possibility that Aβ could act as a trigger for thrombosis and inflammation by interacting with plasma proteins FXII and fibrinogen is the focus of the work presented in this thesis. A detailed understanding of these interactions may reveal new pathological mechanisms, provide possibilities for earlier diagnosis, and pave the way for novel therapeutic targets in AD.

CHAPTER 2. MATERIALS AND METHODS

2.1. Identification of fibrinogen regions that interact with Aβ

Plasminogen was purified from human plasma (NY Blood Center) using lysine-sepharose as described[128], and co-purifying plasmin was inactivated with 10 mM diisopropyl fluorophosphate (Sigma). Human plasminogen-free fibrinogen (Calbiochem; 5 mg/ml in 50 mM Tris, pH 7.4, 150 mM NaCl, 5 mM iodoacetamide) was incubated with 0.6 μM plasminogen and 0.37 μM tPA (generously provided by Genentech) overnight at 37°C to generate small fibrinogen degradation products (FDPs) or with 140 nM plasminogen and 20 nM tPA for 6 hours (hrs) at 37°C to generate large FDPs. Digestions were stopped with aprotinin (Sigma). FDPs (500 μl) were incubated for 3 hrs at room temperature (RT) with synthetic N-terminally biotinylated Aβ42 (Anaspec; 200 nM or 2 μM final concentration) in phosphate buffered saline (PBS) adjusted to contain 500 mM NaCl, 0.01% NP-40 and protease inhibitor cocktail (Roche), the Aβ-interacting peptides pulled down with streptavidin-sepharose beads (Invitrogen) for 1 hr at RT, and the peptides eluted with sample loading buffer and analyzed by SDS-PAGE on a 4-20% gradient gel (Life Sciences) with colloidal blue staining (Invitrogen). Incubations that did not contain biotinylated Aβ42 served as a control for non-specific binding to the streptavidin-sepharose beads.

Mass spectroscopy was performed by the Rockefeller University Proteomics Resource Center as follows: protein gel bands were excised from the SDS-PAGE. Gel bands were reduced with 10 mM dithiothreitol (DTT) and alkylated with 55 mM iodoacetamide, then digested with Sequence Grade Modified Trypsin (Promega) in ammonium bicarbonate buffer at 37°C overnight. Digestion products were extracted twice with 0.1% trifluoroacetic acid, 50% acetonitrile, and 1.0% trifluoroacetic acid. The extracted mixture was dried by Speed-Vac and re-dissolved in 10 ml 0.1% trifluoroacetic acid. For LC-MS/MS analysis, the Dionex U3000 capillary/nano-HPLC system directly interfaced with the LTQ-Obritrap mass

spectrometer (Thermo Fisher), which was operated in the data-dependent acquisition mode using Xcalibur 2.0.7 software. The MS/MS scans from each LC-MS/MS run were converted from the .RAW file format to .DTA files using Bioworks 3.3.1 software. DTA files were analyzed using the MASCOT software search algorithm.

2.2. MALDI-TOF mass spectrometry and Edman sequencing

MALDI-TOF mass spectrometry and Edman sequencing were performed by the Rockefeller University Proteomics Resource Center. Coomassie blue-stained bands were excised from SDS-polyacrylamide, destained with 200 mM ammonium bicarbonate in 50% acetonitrile, and treated with 10 mM DTT in 0.1 M ammonium bicarbonate for protein reduction. Free cysteine residues were alkylated with freshly made 55 mM iodoacetamide in 0.1 M ammonium bicarbonate. Tryptic digestion was performed with 25 ng/µl Sequence Grade Modified Trypsin (Promega) in ammonium bicarbonate buffer for 16 hrs at 30°C with agitation. Digestion products were cleaned and concentrated using micro-C18 ZipTip (Millipore), mixed with 0.5 µl of 10 mg/ml α-cyano-4-hydroxysuccinnamic acid in 50% acetonitrile, 0.1% (v/v) TFA, and applied onto a MALDI plate. MALDI mass spectra were recorded with a PerSeptive Voyager-DE STR MALDI time-of-flight mass spectrometer operated in the reflectron mode. The mass measurement accuracy with internal calibration was, in general, better than 100 ppm. The measured peptide masses were used for database searching with ProFound algorithm. Edman sequencing was performed using an Applied Biosystems Procise sequencer.

2.3. Pulldown assay between Aβ and 49 amino acid fibrinogen β-chain fragment

A 49 amino acid fragment corresponding to fibrinogen β-chain residues 366-414 (TMTIHNGMFFSTYDRDNDGWLTSDPRKQCSKEDGGGWWYNRCHAANPNGR) was synthesized at Rockefeller University's Proteomics Resource Center. N-terminally biotinylated Aβ42 (200 nM) or vehicle was incubated with the 49-mer (1 µM) in PBS

containing 0.01% NP-40 and protease inhibitor cocktail (Roche) for 2 hrs at RT. Biotinylated Aβ42 and its binding partners were pulled down using streptavidin-sepharose beads for 1 hr at RT, washed, and eluted with sample buffer. Eluates were analyzed by SDS-PAGE on a 4-20% gradient gel followed by silver staining (Thermo Scientific).

2.4. Preparation and purification of fibrinogen fragment D

Fibrinogen fragment D was prepared and purified as described in [129]. Briefly, plasminogen-free human fibrinogen (Calbiochem) was reconstituted in 50 mM Imidazole, 5 mM $CaCl_2$, 150 mM NaCl, pH 7.4 and treated with 5 mM iodoacetamide (Sigma). Fibrinogen was digested with 0.01 mg TPCK trypsin (Pierce) per 1 mg fibrinogen for 4 hrs at 22°C. Digestion was stopped with soybean trypsin inhibitor (0.03 mg soybean trypsin inhibitor per 1 mg fibrinogen). Fragment D was affinity purified using the GPRPC peptide (prepared at the Rockefeller University Proteomics Resource Center) covalently immobilized on a SulfoLink Coupling Resin column (Thermo Scientific). The column was equilibrated with 50 mM imidazole, 5 mM $CaCl_2$, 150 mM NaCl pH 7.0, and fibrinogen degradation products were applied to the column and allowed to incubate for 15 minutes (min) with end-over-end rotation. The column was washed with 50 mM imidazole, 1 M NaBr, pH 7.2 and fragment D eluted with 50 mM NaAc, 1 M NaBr, pH 5.3. Eluted fragment D was neutralized with 2 M Tris, pH 8.0 and dialyzed into PBS. Affinity-purified fragment D was subjected to another step of fast protein liquid chromatography (FPLC) purification using a Superose 12 gel filtration column on an AKTA protein purification system (GE Healthcare), eluting in 50 mM Tris pH 7.0. The purity of the fragment D preparation was confirmed by SDS-PAGE followed by colloidal blue staining.

2.5. Western blot analysis

Non-reduced or reduced samples were subjected to SDS-PAGE on 10% or 4-20% gradient gels, transferred to polyvinylidene fluoride (PVDF) membranes (Millipore), and

incubated in blocking buffer (5% milk in PBS containing 0.1% Tween-20 (PBS-T)) for 30 min at RT. Membranes were incubated with primary antibody diluted in blocking buffer for 2 hrs at RT or overnight at 4°C. After washing with PBS-T, membranes were incubated with HRP-conjugated secondary antibodies in blocking buffer for 1 hr at RT. After washing, membranes were incubated with chemiluminescent substrate (Perkin-Elmer or GE) and exposed to film (Ewen-Parker). Blots were stripped with stripping buffer (Thermo Scientific) when analysis with multiple antibodies was necessary. For quantification, film exposures were chosen such that all bands were below saturation level, and images were imported into ImageJ software[130]. The density of each band was measured by selecting a rectangular area slightly larger than the band (the area of the rectangle was constant for all bands corresponding to the same protein) and measuring mean pixel intensity for that area. Rectangles of identical size were then used to measure background pixel intensity directly above or below each band, which was then subtracted from the corresponding band's pixel intensity.

2.6. Pulldown assay between Aβ or Aβ fragments and fibrinogen fragment D

Synthetic N-terminally biotinylated Aβ fragments 1-16, 15-25, 17-40, 22-41, 1-40, and 1-42 (200 nM, Anaspec) were incubated with fibrinogen (1 nM) or fibrinogen fragment D (200 nM) for 1 hr at RT in 50 mM Tris pH 8.0 containing 500 mM NaCl, 0.01% NP-40 and protease inhibitor cocktail. Streptavidin beads were added for 30 min, and elution was conducted as described above and analyzed by Western blot using a polyclonal antibody against fibrinogen (Dako). For some experiments, biotinylated Aβ42 (200 nM) was incubated with varying concentrations of non-biotinylated Aβ17-42 and a pulldown assay performed as described above. In some experiments, fibrinogen fragment D was biotinylated using Sulfo-NHS-biotin (Pierce). Pulldown assays were performed with biotinylated fragment D (200 nM) and Aβ42 I31P or Aβ42 G37D (1 μM) in 50 mM Tris pH 7.4 containing 150 mM NaCl, 0.01%

NP-40, protease inhibitor cocktail, and 0.1% bovine serum albumin (BSA) as described above. Western blots were probed with antibodies against fibrinogen (Dako) and Aβ (3D6, Elan).

2.7. Crystallization of fibrinogen fragment D-Aβ42 complex

Fragment D crystals were obtained with the assistance of the Rockefeller University Structural Biology Resource Center as described in [129]. Briefly, crystals were obtained by sitting drop vapor diffusion at RT from 50 mM Tris, pH 8.5, 70 mM $CaCl_2$, 2 mM sodium azide, 12-17% polyethylene glycol (PEG) 3,350 in drops of 10-20 µl, with fragment D (prepared as described in Methods 2.5) at 15 mg/ml. Aβ42, Aβ42 G37D, Aβ42 I31P, and Hylite fluor 555-Aβ42 (all from Anaspec) were reconstituted to 0.7-1.5 mg/ml in 50 mM Tris, pH 8.5 with 0.12% NH_4OH, then diluted 2-fold in 2X reservoir buffer (50 mM Tris pH 8.5, 4 mM sodium azide, 140 mM $CaCl_2$, 34% PEG 3,350) to yield Aβ peptides in 1X reservoir buffer. Fragment D crystals were then soaked in the various Aβ solutions (containing an excess of Aβ over fragment D) for two weeks at RT, frozen in the N_2 cryostream in reservoir buffer without cryoprotection, and diffracted to 3.3 Å (for Aβ42-soaked crystals) at the National Synchrotron Light Source, Brookhaven National Laboratory (Beam line X25, wavelength = 1.1 Å). We also obtained data to 2.9 Å for crystals not subjected to soaking (native crystals). Data reduction was performed using HKL2000 software[131]. Molecular replacement was performed with PHENIX software (PHENIX-dev-1555) using the PDB entry 1FZA for fragment D[132], resulting in successful determination of the phases and coordinates of fragment D atoms. Refinement was performed with PHENIX software[133].

2.8. Preparation of Aβ and control peptides for fibrinolysis experiments

Aβ42 (Anaspec) was reconstituted to 1 mg/ml in 50 mM Tris pH 7.4, 0.1% NH_4OH and stored at -80°C. Prior to use, Aβ42 was incubated at 37°C with shaking for 12 hrs to generate a range of oligomeric species. Insoluble Aβ42 was removed by centrifugation at

12,000 x g for 10 min[134]. The concentration of soluble Aβ42 was verified via bicinchoninic acid assay (BCA), and a representative transmission electron microscope (TEM) image of the Aβ42 preparation used is shown in Figure 3.5A. HiLyte Fluor 555-Aβ42 and HiLyte Fluor 555-Aβ(1-9) (Anaspec) were reconstituted to 0.5 mg/ml in the same buffer and not incubated prior to use unless otherwise indicated.

Amylin (Anaspec) was reconstituted to 2 mg/ml in dimethyl sulfoxide (DMSO). Prior to use, amylin was diluted to 0.2 mg/ml with 50 mM Tris pH 7.4 (10% DMSO final concentration) and incubated for 24 hrs at 37°C with shaking. Presence of amyloid fibrils was confirmed by TEM (Figure 3.5G) and Thioflavin T fluorescence (not shown).

2.9. Transmission Electron Microscopy

Samples were diluted to 0.1 mg/ml, applied to glow discharged CF200-Cu grids (Electron Microscopy Sciences), washed three times with ultrapure water (UV-treated with a Millipore system), and negatively stained with 2% uranyl acetate. Images were acquired using a JEOL JEM 100CX Transmission Microscope at the Rockefeller University Electron Microscopy Resource Center.

2.10. Preparation of fibrin monolayers

Fibrin monolayers were prepared in Fisherbrand High Binding 96-well plates (Fisher Scientific) as described[135,136]. Wells were treated with 2.5% glutaraldehyde in 0.1 M sodium bicarbonate buffer pH 9.5 for 2 hrs at 37°C. After washing with ultrapure water, 0.3 μM fibrinogen in PBS + 1 mM $CaCl_2$ (60 μl) was applied for 18 hrs at 4°C. Wells were washed 3 times with PBS, and free aldehyde groups were neutralized with 100 μl 0.3 M ethanolamine pH 7.4 during a 1 hr incubation at RT. Wells were washed 3 times with PBS, and immobilized fibrinogen was converted to fibrin with 1 U/ml thrombin (Sigma) in PBS (60 μl)

for 1 hr at 37°C. Fibrin-bound thrombin was eluted with 0.5 M NaCl, and fibrin monolayers were stored at 4°C in PBS + 20 mM lysine.

2.11. Clot turbidity analysis

Assays were performed at RT in Fisherbrand High Binding 96-well plates in triplicate using a Molecular Devices Spectramax Plus384 reader. Clot formation was detected as a change in absorbance at 350 nm, with readings taken every 30 seconds (s). For clot formation and lysis, fibrinogen (1.5 μM) with or without Aβ42 (3 μM) was mixed with plasminogen (125 nM-300 nM), α-thrombin (Sigma; 0.5 U/ml), tPA (0.15 nM-15 nM), and $CaCl_2$ (5 mM) in 20 mM HEPES (N-2-hydroxyethylpiperazine-N'-2-ethanesulfonic acid) buffer (pH 7.4) with 140 mM NaCl, in a volume of 150 μl. The absence of plasmin activity in the plasminogen preparation was confirmed by chromogenic substrate assay (not shown). In some experiments, Aβ42 I31P and 555-Hylite Fluor Aβ42 and 555 Hylite Fluor Aβ(1-9) were used.

For lysis of pre-formed clots, fibrinogen (2.2 μM) with or without Aβ42 (5 μM) was mixed with plasminogen (125 nM), thrombin (0.5 U/ml), and $CaCl_2$ (5 mM) in 20 mM HEPES buffer (pH 7.4) with 140 mM NaCl, in a volume of 100 μM. Clots were incubated at 37°C for 1 hr, then overlaid with a 100 μl solution containing 10-50 nM tPA, 250 nM plasmin (Sigma) or 1 μM bovine TPCK trypsin (Thermo Scientific). Clots overlaid with plasmin and trypsin did not contain plasminogen. Prior to lysis, some clots were overlaid with 5 μM Aβ42 for 1 hr, the overlays removed, and the clot surface washed three times with HEPES buffer.

2.12. Enzyme activity

Assays were performed at RT in Fisherbrand 96-well plates with a reaction volume of 150 μl. For plasmin activity, chromogenic substrate Pefa-5329 (Centerchem; 530 μM) was added to plasmin (440 nM) with various amounts of Aβ42. For tPA activity, chromogenic

substrate S-2288 (Diapharma; 530 μM) was added to tPA (100 nM) with various amounts of Aβ42. For tPA-mediated plasminogen activation, plasminogen (440 nM) and tPA (100 nM) were mixed with various amounts of Aβ42, and Pefa-5329 was added to monitor plasmin generation.

To monitor plasmin activity and clot turbidity simultaneously and under the same reaction conditions, parallel clots were prepared containing fibrinogen (1.5 μM), plasminogen (300 nM), tPA (0.15 nM) or streptokinase (Sigma; 0.75 nM), thrombin (0.5 U/ml), $CaCl_2$ (5 mM) and either Pefa-5329 (400 μM) or buffer only (modified from [137,138]). Readings were taken at dual wavelengths of 405 nm (A_{405}) and 350 nm (A_{350}). Plasmin activity was detected in the samples containing Pefa-5329 at A_{405}, from which the signal arising from the changing turbidity (A_{405}) of the forming and lysing clot without Pefa-5329 was subtracted. Clot turbidity and plasmin activity were plotted together to best visualize the temporal relationship of the two processes.

Fibrin monolayers were overlaid with 60 μl of Aβ42 (2 μM) or vehicle in PBS and incubated for 18 hrs at 4°C. The Aβ was removed, and the well surface washed three times with PBS containing 0.05% Tween-20. Fibrin monolayers or control wells were then overlaid with 150 μM of plaminogen (300 nM) and tPA (1.5 nM), and plasmin activity measured with 530 μM of the chromogenic substrate Pefa-5329.

2.13. Clot structure and binding studies: Laser scanning confocal microscopy

Samples were visualized at RT using a Zeiss LSM 510 confocal laser scanning system and a Zeiss Axiovert 200 microscope with a 40x-Axiovert 1.2/water objective (3x optical zoom) at the Rockefeller University Bio-Imaging Resource Center. Laser scanning was done in multi-track scanning mode with excitation at 488 nm and emission at 500-530 nm (for Alexa Fluor 488 fibrinogen) and excitation at 543 nm and emission at 565-615 nm (for 555

HiLyte Fluor Aβ). All images were acquired using LSM 510 version 3.2 software (Zeiss) 50 μm above the glass surface. Five μm z-stacks taken every 0.5 μm (11 slices per image) were projected two dimensionally to produce the final image.

Aβ binding to fibrin(ogen): Clots (30 μM final volume) were formed in 1.5 mm glass-bottom dishes (Mattek). Fibrinogen (2.7 μM) and Alexa-Fluor 488 fibrinogen (Invitrogen; 0.3 μM) were mixed with thrombin (0.5 U/ml) and $CaCl_2$ (5 mM) in 20 mM HEPES (pH 7.4) with 140 mM NaCl with or without Aβ. For clots with Aβ, non-labeled Aβ42 (1.5 μM) was mixed with HiLyte Fluor 555 Aβ42 (1.5 μM) or HiLyte Fluor 555 Aβ(1-9) (1.5 μM). Clots were incubated in the dark at 37°C for 1 hr prior to imaging. For overlay experiments, clots formed as described were overlaid with HiLyte Fluor 555 Aβ42 (3 μM), HiLyte Fluor 555 Aβ(1-9) (3 μM) or vehicle for 1 hr, the overlays removed, and the clot surfaces washed with HEPES buffer. The fluorescent label does not alter Aβ's ability to delay clot lysis (not shown). For some experiments, clots were visualized in the absence of fluorescently labeled Aβ but with Aβ42 or Aβ42 I31P (1.5 μM).

Plasminogen binding to fibrin: Clots (30 μM final volume) were formed in 1.5 mm glass-bottom dishes with fibrinogen (3 μM), fluorescein isothiocyanate (FITC) labeled Glu-plasminogen (Oxford Biomedical; 125 nM), thrombin (0.5 U/ml), $CaCl_2$ (5 mM), with or without Aβ42 (5 μM) in 20 mM HEPES (pH 7.4) buffer with 140 mM NaCl. Samples were visualized as above, but using single track mode with excitation at 488 nm and emission at 500-530 nm. Five sections were captured from random locations in three separate control and Aβ-influenced clots. Representative 5 μM z-stacks composed of 11 slices and projected two dimensionally were also acquired for each control and Aβ-containing clot. FITC-plasminogen binding to fibrin was analyzed using ImageJ[130], with total fluorescence in each section used as a measure of plasminogen binding.

2.14. Plasminogen binding to fibrin monolayer: ELISA

Fibrin monolayers were incubated with Aβ42 (2 μM) or vehicle for 18 hrs at 4°C. Non-bound Aβ was removed and the monolayers washed with PBS with 0.05% Tween-20 three times. Plasminogen (500 nM) was then applied to the monolayers in PBS with 4% milk and 0.01% Tween-20 for 2 hrs at 37°C. Plasminogen was removed, and monolayers washed with PBS with 0.05% Tween-20 three times. Monoclonal plasminogen antibody 10A1 (Santa Cruz; 1:2000) in PBS with 4% milk and 0.01% Tween-20 was applied to the monolayer for 1 hr at RT. After washing, HRP-conjugated anti-mouse antibody (GE Healthcare; 1:5000) in the same buffer was applied for 1 hr at RT. After washing, the ELISA was developed using a tetramethylbenzidine (TMB) peroxidase substrate (Vector Labs) and reactions stopped using 1N H_2SO_4. Absorbance was measured at 450 nm. All conditions were tested in triplicate.

2.15. Preparation of Aβ for FXII activation studies

Aβ42, Aβ40, and Aβ42 E22Q Dutch (Anaspec) monomers and oligomers were prepared as in [139] with some modifications. Aβ peptides were monomerized by treatment with hexafluoroisopropanol (Sigma-Aldrich). Monomerized Aβ was dissolved to 5 mM with dimethyl sulfoxide (Sigma-Aldrich). For monomer (fresh) preparations, Aβ was dissolved to 100 μM in ultrapure ice-cold water and used immediately. For oligomers, Aβ in DMSO was dissolved to 100 μM in Ham's F12 medium (Caisson Labs) and incubated at 4°C for 16 hrs with rotation. For fibrils, non-monomerized Aβ42 was dissolved into a minimum volume of 1% NH_4OH, then adjusted to 200 μM with tris buffered saline (TBS) and incubated at 37°C with shaking for 7 days. All Aβ preparations were confirmed by TEM.

2.16. Human blood collection and plasma preparation

Studies with human volunteers were approved by the Rockefeller University Institutional Review Board or by the Karolinska Institute. Blood was drawn from 10 healthy volunteers

giving informed, written consent using 21 gauge 0.75 inch butterfly needles (BD) with a multi-adapter for S-Monovette (Sarstedt) into S-Monovette 5 ml tubes containing 1/10 volume 0.106 mM trisodium citrate solution at the Rockefeller University Hospital and Karolinska Institute Hospital. To obtain platelet rich plasma (PRP), blood was centrifuged at 130 x g for 10 min at RT, and the top 1/2 of the PRP removed. To obtain platelet poor plasma (PPP), blood was centrifuged twice at 2000 x g for 10 min at RT. PPP was frozen immediately at -80°C. All experiments with PRP and PPP were repeated using plasma from at least 3 volunteers.

2.17. Mouse lines

For thrombin generation experiments, $FXII^{-/-}$ and $FXI^{-/-}$ mice backcrossed for >10 generations[140,141] and age-matched C57Bl/6 control mice (Charles River) were used.

For brain immunofluorescence and Western blot experiments, transgenic Tg6799 (Jackson Laboratory) and TgCRND8 (kindly provided by A. Chishti and D. Westaway, University of Toronto, Canada) mouse models of AD were used. Tg6799 mice are double transgenic for APP/Presenilin 1 and express five familial AD mutations: three in APP (K670N/M671L, Swedish; I716V, Florida; V717I, London), and two in Presenilin1 (M146L, L286V) under the mouse thy1 promoter. Tg6799 mice develop amyloid plaques at 2 months of age and cognitive impairment by 4-5 months of age[142]. TgCRND8 mice express a double mutant form of APP695 (K670N/M671L, Swedish; V717F, Indiana) under the human prion protein promoter. TgCRND8 mice develop Aβ pathology and cognitive deficits as early as 3 months of age[143]. Non-transgenic littermates were used as controls. For analysis of plasma contact system activation, Tg6799 mice and littermate controls were used. For Aβ42 injection experiments, 2 month old C57BL/6 mice (Jackson Laboratory) were used.

2.18. Analysis of thrombin generation in human and mouse plasma

Real time thrombin generation in normal human plasma or FXII-deficient plasma (from individuals genetically deficient in FXII; George King Biomedical) was measured by CAT as described in [144]. In some cases, plasma was pre-incubated for 30 min with an antibody against FXIIa[145] or active-site inhibited factor VII (ASIS; Novo Nordisk). Some reactions also contained FXIa (3 pM). All samples were run in duplicate, and curves are representative of at least 3 separate experiments run with plasma from different donors (for normal plasma). Real time thrombin generation in FXII-/-, FXI-/-, and C57Bl/6 mouse plasma was measured as described above, except a smaller amount of mouse PPP (40 µl) was used to obtain stronger signal (as in [146]).

2.19. Analysis of FXII, FXI, and prekallikrein activation *in vitro*

Chromogenic substrate assay: Assays were performed at 37°C in flat-bottom 96-well polystyrene plates (Fisher Scientific) coated with 1% Polyethylene glycol 20,000 in HEPES-buffered saline (HBS) for 2 hrs. To measure FXII activation, Pefachrome FXIIa (H-D-CHA-Gly-Arg-pNA-2AcOH; Centerchem), final concentration 0.8 mM, was added to a mixture containing 100 nM FXII (Haematologic Technologies) and 3 µM Aβ or vehicle. To measure FXII-dependent prekallikrein activation, Pefachrome PK (H-D-But-CHA-Arg-pNA-2AcOH; Centerchem), final concentration 0.8 mM, was added to a mixture containing 10 nM FXII, 10 nM plasma prekallikrein (Enzyme Research Laboratories) and 3 µM Aβ or vehicle. To measure FXII-dependent FXI activation, Pefachrome FXIa (Z-Aad-Pro-Arg-pNA-AcOH; Centerchem), final concentration 0.8 mM, was added to a mixture containing 5 nM FXII, 15 nM FXI (Haematologic Technologies), and 3 µM Aβ or vehicle. Enzyme activity was detected as change in absorbance at 405 nm every 45 s using a Molecular Devices Spectramax Plus 384 microplate reader.

Western blot: Coagulation factor activation was analyzed in a purified protein system and in human plasma. For FXII activation, FXII (200 nM) was incubated with Aβ42 (3 μM), dextran sulfate 500 kDa (DS500; Sigma; 10 μg/ml), or vehicle for 30 min at 37°C. In some experiments, prekallikrein (150 or 300 nM) and high molecular weight kininogen (HK; 300 nM) were added to the reaction. Reactions were stopped by adding reducing sample buffer and heating for 5 min at 85°C. Immunoblots were probed with an antibody against FXII (Hematologic Technologies). For FXI activation, FXII (200 nM), prekallikrein (150 nM), HK (Molecular Innovations; 300 nM), and FXI (150 nM) were incubated with Aβ (3 μM), kaolin (Fisher; 100 μg/ml), DS500 (10 μg/ml), or vehicle for 30 min at 37°C. Immunoblots were probed with a monoclonal antibody against FXI (Haematologic Technologies). For prekallikrein activation and HK cleavage, FXII (40 nM), prekallikrein (60 nM), and HK (60 nM) were incubated for 5 min at 37°C, and immunoblots were analyzed using a polyclonal antibody against plasma prekallikrein (Affinity Biologicals) or a monoclonal antibody against the light chain of HK (Abcam). For experiments in human plasma, plasma from healthy volunteers or FXII-deficient plasma was diluted 1:10 in HBS and incubated with activators for 1 hr at 37°C followed by Western blot analysis using the antibodies described above. For FXII activation, plasma was incubated with Aβ42 (20 μM). For prekallikrein activation, plasma was incubated with Aβ42 (20 μM) or kaolin (100 μg/ml). For HK cleavage, plasma was incubated with various concentrations of Aβ and kaolin.

ELISA: Normal human plasma or FXII-deficient plasma were diluted 1:10 in HBS buffer and incubated with Aβ42, Aβ42 Dutch (20 μM), kaolin (10 μg/ml), or vehicle at 37°C for 1 hr. Reactions were transferred to a 96-well plate pre-coated with a monoclonal antibody against FXI (3 μg/ml) overnight at 4°C, washed with PBS containing 0.05% Tween-20 (PBS-T), and blocked with PBS containing 2% milk (blocking buffer) for 1 hr at RT. Reactions were incubated in wells for 1 hr at RT, removed, and wells washed 3 x 5 min with PBS-T. A

polyclonal antibody against C1 inhibitor (Cedarlane) or alpha-1-antitrypsin (3 µg/ml; Thermo Scientific) in blocking buffer was applied to the wells for 1 hr at RT. After washing, an HRP-conjugated anti-goat antibody (Jackson; 1:2000) in blocking buffer was applied for 1 hr at RT. The ELISA was developed with TMB peroxidase substrate (Thermo Scientific). Absorbance was measured at 450 nm. All conditions were tested in triplicate.

2.20. Binding between Aβ and FXII, FXI

N-terminally biotinylated Aβ42 (200 nM) was incubated with FXII (200 nM) or FXI (100 nM) in PBS containing 0.01% NP-40 and protease inhibitor cocktail for 2 hrs at RT. Pulldown assays were performed as described above and analyzed by Western blot using monoclonal antibodies against FXII and FXI (Haematologic Technologies). For pulldown assays in normal human plasma, plasma was diluted 1:5 in PBS containing 0.01% NP-40 and protease inhibitor cocktail and incubated with biotinylated Aβ42 (500 nM) or N-terminally biotinylated amylin (500 nM; Anaspec) for 2 hrs at RT.

2.21. AD patient and control plasma samples

Experiments with human plasma were approved by the Rockefeller University Institutional Review Board. Plasma from AD patients and ND controls was obtained from the University of Kentucky Sanders-Brown Center on Aging (Group 1) and Washington University Knight Alzheimer's Disease Research Center (Group 2). For Group 1, blood from 18 AD and 11 ND individuals giving written, informed consent was drawn into heparinized Vacutainer tubes with a 23 or 21 gauge needle. AD cases were defined by a clinical diagnosis of AD as well as a postmortem Consortium to Establish A Registry for Alzheimer's Disease (CERAD) neuritic plaque score[147] of B or C, corresponding to probable or definite AD, respectively. ND cases had CERAD scores of 0 and no clinical diagnosis of AD. AD and ND cases were gender and age-matched (Table 1). For Group 2, blood from 10 AD and 10 ND individuals was drawn using EDTA-coated syringes into polypropylene tubes containing

a final concentration of 5 mM EDTA. Plasma was prepared by centrifuging blood at 2000 x g for 15 min, and flash frozen on dry ice prior to storage at -80°C. AD cases were defined by a Clinical Dementia Rating (CDR) score14 of ≥0.5 and CSF Aβ42 levels <500 pg/ml, and ND cases were defined by a CDR score of 0 and CSF Aβ42 levels >500 pg/ml (Table 2). CSF Aβ42 cut-off values for AD vs. ND were based on correlations between CSF Aβ42 levels and cortical amyloid load as assessed by positron emission tomography with Pittsburgh Compound B[148].

2.22. Analysis of contact system activation in AD patient plasma by Western blot

Plasma protein concentration was measured by BCA, and equal amounts of total protein (20 µg) from each sample were analyzed by non-reducing or reducing Western blot with monoclonal antibodies against FXII heavy chain (Haemotologic Technologies), HK light chain (Abcam), FXI (Haematologic Technologies), C1 esterase inhibitor (Proteintech), and transferrin (Abcam). Purified FXI, FXII, HK, C1 inhibitor (Athens Research and Technology), and FXII-deficient plasma were loaded as positive controls for some experiments.

2.23. Measurement of kallikrein-like activity in human and mouse plasma

Plasma kallikrein-like activity was measured using the chromogenic substrate S-2302 (Chromogenix) based on the method described in [149] with some modifications. Plasma (diluted 1:30) in 20 mM HEPES with 140 mM NaCl was mixed with S-2302 (0.67 mM final concentration) in duplicate, and absorbance at 405 nm was read for 30 min at RT in a Molecular Devices Spectramax 384 Plus spectrophotometer. The rate of substrate conversion over time was calculated for each plasma sample by the data acquisition software (Softmax 6.1; Molecular Devices), and expressed as a percentage of the rate found for normal human or wild type mouse plasma fully activated with dextran sulfate 500 kDa. S-2302 can also be cleaved by FXIIa, FXIa, and plasmin. To determine whether S-2302 cleavage was mediated by members of the contact activation pathway (kallikrein,

FXIIa, or FXIa) or plasmin, plasmin activity in all samples was determined using a different substrate (Pefachrome-5329, Pentapharm) and found not to differ between AD and ND plasma (not shown).

2.24. Analysis of contact system activation in AD mouse plasma

All animal experiments were conducted in accordance with the guidelines of the US National Institutes of Health Guide for the Care and Use of Laboratory Animals and with approval from the Animal Care and Use Committee of The Rockefeller University. Tg6799 mice (n=7) or littermate control mice (WT; n=7) at 6 months of age were anesthetized with atropine (500 mg/kg body weight) and avertin (0.04 mg/kg body weight) intraperitoneally. Blood (100 µl) was collected via retro-orbital bleeding through gel-repel (Sigma) and polybrene (Santa Cruz) coated capillaries into EDTA-coated tubes (BD) containing 5 mM EDTA. Plasma was prepared by centrifugation (1500 x g for 15 min, twice), and stored in polypropylene tubes containing 5 mM EDTA. Total protein concentration was determined by BCA, and plasma from each mouse containing 20 µg total protein was analyzed by Western blot using monoclonal antibodies against HK light chain (R&D) and transferrin (Abcam) in that order. Blots were stripped between antibody incubations. Protein levels were quantified by densitometric analysis.

2.25. Analysis of contact system activation in C57Bl/6 mice injected with Aβ

Aβ42, scrambled Aβ42, and amylin (Anaspec) were prepared as follows: peptides were resuspended in a minimum amount of 1% NH_4OH, then diluted to 1 mg/ml with PBS. Peptide concentration was determined by BCA, and the state of aggregation was determined by TEM. Aβ42, scrambled Aβ42, amylin, or vehicle (6 mg/kg body weight) were administered via retro-orbital injection into 2 month-old C57BL/6 mice under anesthesia using avertin and atropine as described above. After 6 hrs, blood was collected and processed as described above. Western blot analysis was performed as described above.

Levels of plasma Aβ42 were determined at 6 hrs post injection using an Aβ42-specific ELISA kit (Life Technologies) according to the manufacturer's instructions.

For analysis of the effect of different anticoagulants on *ex-vivo* contact activation, plasma from non-injected WT mice was collected into EDTA or heparin tubes. Plasma was then incubated with 20 μM Aβ42, scrambled Aβ42, amylin, or vehicle for 1 hr at 37°C, then analyzed by Western blot as described above.

2.26. Analysis of brain tissue in AD patients and mouse models

Immunofluorescence: Mice were saline/heparin-perfused and brains were fixed in 4% paraformaldehyde, cryoprotected in 30% sucrose, and frozen. Coronal sections (20 μm) were blocked for 1 hr in PBS containing 0.25% Triton X-100 and 3% donkey serum (Jackson Laboratory), incubated overnight at 4°C with anti-Aβ monoclonal antibody 6E10 (Covance) and FXII antibodies (Novus, HTI), followed by 1 hr incubation with Alexa-Fluor secondary antibodies. Controls for secondary antibody non-specific binding were performed by omitting primary antibodies. Sections were dehydrated and cover slips were applied with Vectashield (Vector labs). Images were acquired using an inverted TCS SP8 laser scanning confocal microscope (Leica DMI 6000) at the Rockefeller University's Bio-Imaging Resource Center and analyzed by ImageJ.

Western blot: Mouse (whole brain) and human (temporal pole) frozen tissue was homogenized in 5 volumes (g/ml) of PBS containing 1% NP-40, 0.5% sodium deoxycholate, 0.1% SDS, and protease inhibitor cocktail (Roche). The homogenates were centrifuged at 10,000 x g for 10 min at 4°C to yield a supernatant containing the soluble protein fraction. Protein concentration was determined by BCA, and equal amounts were run on a 10% polyacrylamide Criterion gel (Bio-Rad) followed by Western blot analysis with the following

antibodies: murine HK (R&D Systems), tubulin (Abcam), human HK light chain (Abcam), actin (Abcam), albumin (Thermo Scientific), hemoglobin (Abcam), and fibrinogen (Dako).

2.27. Antibodies

Table 2.1. List of antibodies used

Antigen	Details	Source	Applications
Aβ	Mouse monoclonal 6E10	Covance	immunofluorescence
Aβ	Mouse monoclonal 3D6	Elan	Western blot
Actin	Chicken polyclonal	Abcam	Western blot
Albumin	Goat polyclonal	Thermo Scientific	Western blot
Alpha-1-antitrypsin	Goat polyclonal	MyBioSource	ELISA
C1 esterase inhibitor	Goat polyclonal	Cedarlane	ELISA
C1 esterase inhibitor	Rabbit polyclonal	Proteintech	Western blot
Fibrinogen	Rabbit polyclonal	Dako	Western blot
FXI	Mouse monoclonal	Hameatologic Technologies	ELISA, Western blot
FXII	Mouse monoclonal	Haematologic Technologies	Western blot
FXII	Rabbit polyclonal	Novus	Immunofluorescence
FXII	Sheep polyclonal	Haematologic Technologies	Immunofluorescence
FXIIa	Fully human monoclonal 3F7	Larsson et al. [145]	Inhibition studies
Hemoglobin	Rabbit monoclonal	Abcam	Western blot
HK (human)	Rabbit monoclonal to light chain	Abcam	Western blot
HK (mouse)	Rat monoclonal to light chain	R&D	Western blot
Plasminogen	Mouse monoclonal 10A1	Santa Cruz	ELISA
Prekallikrein	Sheep polyclonal	Affinity Biologicals	Western blot
Transferrin (human)	Rabbit polyclonal	Abcam ab88165	Western blot
Transferrin (mouse)	Rabbit polyclonal	Abcam ab82411	Western blot
Tubulin	Rat monoclonal	Abcam	Western blot

2.28. Statistical analysis

Data are presented as column graphs with mean ± standard deviation (SD) or as vertical scatter plots with medians and reported as means ± SD or medians in the text. Unless otherwise indicated, comparisons between two groups were performed using the unpaired, two-tailed t-test for parametric data or using the two-tailed Mann-Whitney test for non-parametric data. Comparisons between multiple groups were performed using Kruskal-Wallis test followed by Dunn's Multiple Comparison Test. For some experiments, comparisons between groups were performed using 1 way ANOVA followed by Dunnett's Multiple Comparison Test for multiple groups with a single control. Two-way ANOVA with Bonferroni post-test was used for comparisons between groups affected by two factors. Correlation analysis was performed using Pearson's correlation coefficient (*r*). P values ≤0.05 were considered significant (*), with values ≤0.01 designated (**), values ≤0.001 designated (***), and values ≤0.0001 designated (****) in figures. Statistical analyses were performed using GraphPad Prism software, version 5.0f.

CHAPTER 3. Mechanisms through which binding between Aβ42 and fibrinogen lead to delayed fibrinolysis

3.1. Background

If the prothrombotic state observed in AD patients and mouse models contributes to AD etiology, a better understanding of the mechanisms responsible for eliciting such a state is crucial. One way to achieve a prothrombotic state is through impaired fibrin degradation (fibrinolysis), which could prevent timely clearance of clots as well as increase the likelihood that clots will form, since the thrombotic-fibrinolytic equilibrium during clot formation would be disturbed. In this regard, the Strickland laboratory has shown that clots formed in the presence of Aβ42 are structurally altered and more resistant to fibrinolysis than normal clots[59], and that fibrinogen, the main protein component of clots, can bind Aβ42 specifically with a K_d of 26.3 ± 6.7 nM[125]. However, the mechanisms by which Aβ42-fibrin(ogen) binding delays fibrin clot lysis have not been defined. To better understand how Aβ42 binding to fibrin(ogen) can result in abnormal clot structure and to the decreased susceptibility of the fibrin clot to fibrinolysis, I investigated the biochemical and structural details of the Aβ42-fibrinogen interaction.

3.2. Biochemical details of the Aβ–fibrinogen interaction

Binding region for Aβ on fibrinogen. Fibrinogen is a 340 kDa glycoprotein composed of three pairs of chains (α, β, and γ) organized into three structural regions, where two identical D domains (fragment D) are joined by a central E domain (fragment E; Figure 3.1A). The Strickland laboratory has previously shown that Aβ binds to fragment D of fibrinogen[125]. To determine where within fragment D Aβ42 binds, I partially digested fibrinogen, generating fibrinogen degradation products (FDPs). FDPs were pulled down using biotinylated Aβ42 and streptavidin, and the Aβ42-interacting peptides visualized using SDS-PAGE. The ~7 kDa Aβ-binding fragment (Figure 3.1B; Fragment 1) was analyzed by liquid

chromatography-tandem mass spectrometry (LC-MS/MS) at the Rockefeller University's Proteomics Center, which mapped a portion of the ~7 kDa fragment to the C-terminal region of the fibrinogen β-chain (β396-407). Consistent with this result, N-terminal sequencing of the ~7 kDa fragment placed it within the C-terminal region of the β-chain (β366-370) (Figure 3.1C). The exact size of the fragment was determined using matrix-assisted laser desorption ionization-time of flight (MALDI-TOF) analysis, resulting in a mass corresponding to 49 amino acids, placing it between β366 and β414 (Figure 3.1C). These results indicate that Aβ42 interacts with fibrinogen near the C-terminus of the fibrinogen β-chain, a region that encompasses the functional domain called the b-hole (within the globular β-chain domain; green in Figure 3.1A). The 49 amino acid peptide (β366-414) corresponding to the identified fragment was synthesized at Rockefeller University's Proteomics Resource Center, and its ability to bind Aβ42 was confirmed by pulldown assay (Figure 3.1D) and by AlphaLISA assay by Hyung Jin Ahn[125], which demonstrated the ability of the 49-mer to inhibit Aβ-fibrinogen binding.

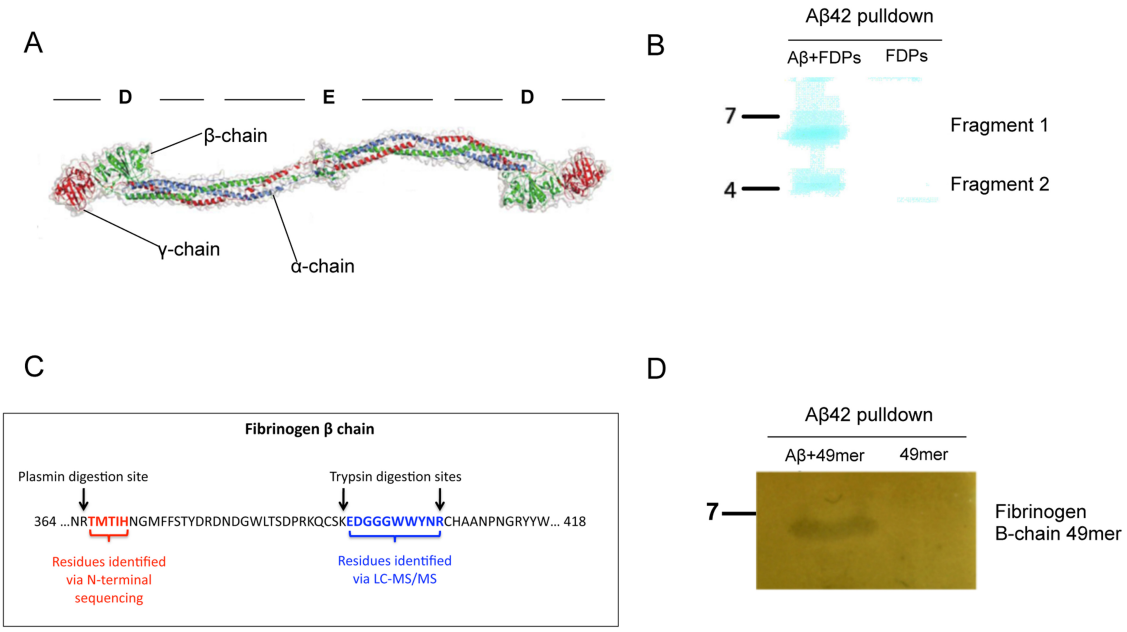

Figure 3.1. Localization of the Aβ42 binding site within fibrinogen fragment D. (A) Fibrinogen is composed of two sets of α, β, and γ chains and organized into an E domain flanked by two D domains (adapted from [150]). (B) Biotinylated Aβ42 pulled down two plasmin-generated fibrinogen degradation products (FDPs). Only the ~7 kDa fragment was analyzed successfully. (C) The ~7 kDa fragment mapped to the C-terminus of the fibrinogen beta chain by N-terminal sequencing and LC-MS/MS. MALDI-TOF identified 49 amino acids in the fragment. (D) Silver-stained SDS-PAGE showing that biotinylated Aβ42 pulls down the 49 amino acid fragment.

Binding region for fibrinogen on Aβ. To determine which region of Aβ42 is responsible for fibrinogen binding, fibrinogen and fragment D were pulled-down with biotinylated sub-regions of Aβ42. Fragments Aβ17-40 and Aβ22-41 had the strongest affinity for fragment D, while Aβ1-16 had the least (Figure 3.2A, top), indicating that the C-terminal two thirds of the molecule are involved in binding fragment D. Pulldown of fibrinogen with the same Aβ sub-regions yielded similar results, although more binding was detected to N-terminal Aβ peptides (Figure 3.2A, bottom), suggesting that fibrinogen may have additional Aβ binding sites outside of fragment D which may be mediated by N-terminal Aβ residues. This interpretation is supported by data demonstrating an additional binding site for Aβ42 on the fibrinogen α chain outside of fragment D (not shown, in collaboration with Hyung Jin Ahn). Consistent with the binding site for fragment D on Aβ being located closer to its C-terminus, incubation of biotinylated Aβ42 with fragment D in the presence of increasing concentrations of Aβ17-42 resulted in a dose-dependent decrease in fragment D pulldown (Figure 3.2B).

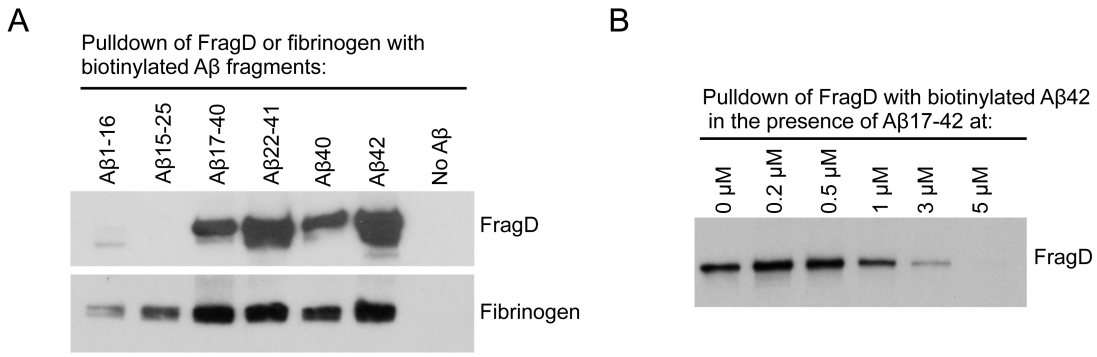

Figure 3.2. Localization of the fibrinogen binding site on Aβ42. Western blots showing streptavidin pulldown assays probed with a polyclonal anti-fibrinogen antibody (Dako). (A) Biotinylated Aβ fragments were used to pull down fibrinogen fragment D or fibrinogen. (B) Aβ17-42 blocks the ability of biotinylated Aβ42 to pull down fragment D in a dose-dependent manner.

3.3. Structural details of the Aβ–fibrinogen interaction

Structural details of the Aβ42-fibrinogen interaction were investigated via X-ray crystallography in collaboration with Hyung Jin Ahn and under the guidance of Deena Oren of The Rockefeller University's Structural Biology Resource Center. We sought to obtain a crystal structure of the complex between Aβ42 and fragment D, due to results indicating that fragment D is the major binding region for Aβ on fibrinogen and to the smaller size and ease of manipulation of fragment D.

Our strategy was to soak Aβ42 into pre-formed fragment D crystals due to the large solvent channels present in the fragment D structure. Fragment D crystals were obtained using the method of [129] as detailed in Methods 2.7 (Figure 3.3A), and the ability of Aβ42 to penetrate into the crystal lattice was tested by soaking fragment D crystals with fluorescently labeled TAMRA (5-Carboxy-tetramethylrhodamine)-Aβ42. Non-specifically bound TAMRA-Aβ42 was removed by repeatedly washing the crystal until no decrease in fluorescence was observed. Persistent fluorescence confirmed binding of Aβ42 within the crystals (Figure 3.3B). One challenge presented by soaking Aβ42 into fragment D crystals is the rapid oligomerization of Aβ42, resulting in a wide range of species. To circumvent this problem, we soaked crystals with the synthetic Aβ42 mutants I31P and G37D, which are less prone to aggregation[151,152], but can still bind fragment D (Figure 3.3C). Crystals were also soaked in Aβ42, Hylite fluor 555-labeled Aβ42, or not soaked at all, and data sets were collected at the National Synchrotron Light Source. The structure was solved by molecular replacement as described in Methods 2.7. Soaking of Aβ42 did not damage fragment D crystals, since in most cases the space groups and unit cell dimensions obtained were isomorphous with dimensions found in unsoaked (native) crystals, and relatively well with published dimensions for fragment D[129] (Figure 3.3D). Analysis of electron density showed subtle changes to the structure of fragment D soaked with all Aβ42 preparations compared to data

obtained for a native (unsoaked) crystal, suggesting interaction between fragment D and Aβ42. Specifically, a loop in the fragment D β-chain (β384-393), which forms part of the 49 amino acid Aβ42 binding region identified in Figure 3.1, was shifted away from the coiled coil region in multiple crystals soaked with Aβ42 and 555-Aβ42 (Figure 3.3E; data shown only for Aβ42-soaked crystal). This loop is shifted in a similar but not as dramatic a manner in fragment D structures crystallized in the presence of b-hole binding peptides (as in PDB 1FZG[153], among others; Figure 3.5F), suggesting that Aβ interacts with residues near the b-hole. Peptides binding the b-hole also induced a flip in a nearby loop (β395-400), which was not observed in our structure, suggesting that Aβ may not fit all the way in the b-hole as the peptides do. We also observed patches of density unaccounted for by the fragment D coordinates possibly corresponding to Aβ42. These patches of density were found in the region of fragment D in special proximity to the 49 amino acid binding site on the β-chain the binding site, but the density was not sufficient to conclusively place Aβ42 in that region (not shown).

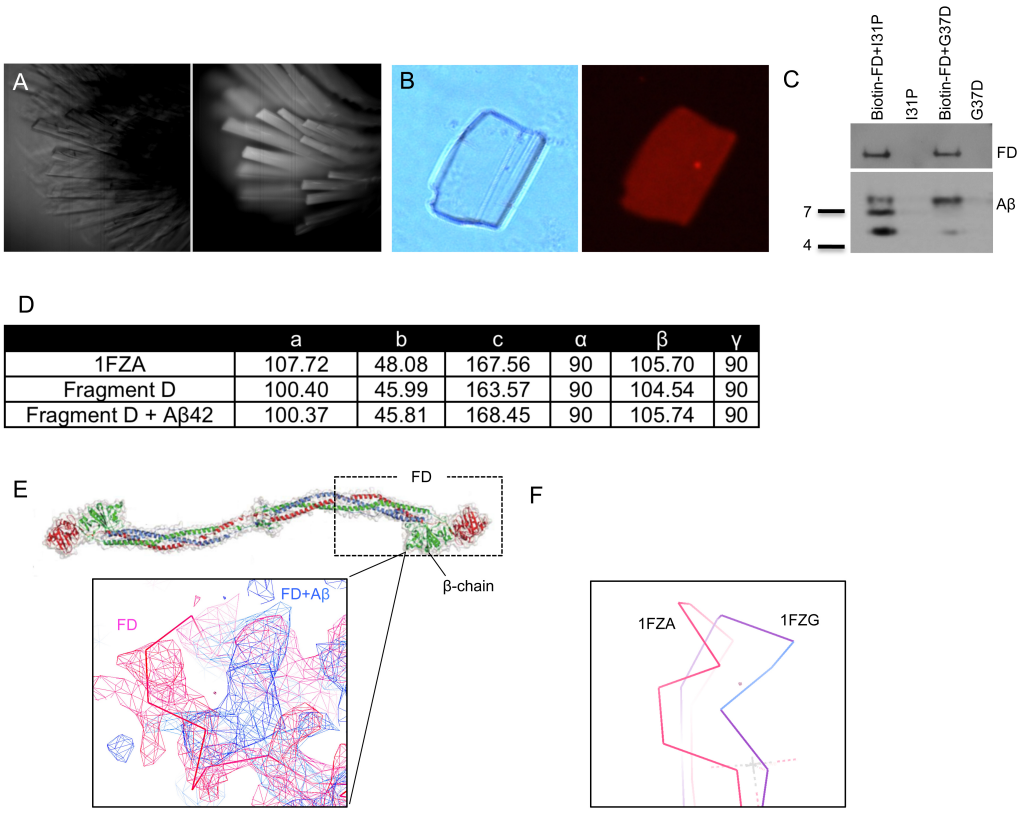

	a	b	c	α	β	γ
1FZA	107.72	48.08	167.56	90	105.70	90
Fragment D	100.40	45.99	163.57	90	104.54	90
Fragment D + Aβ42	100.37	45.81	168.45	90	105.74	90

Figure 3.3. Altered fragment D structure in the presence of Aβ42. (A) Bright field (left) and UV fluorescence (right) images of fragment D crystals, indicating crystals are proteinacious. (B) Left: Bright field image of a fragment D crystal that had been subjected to soaking in TAMRA-Aβ42 followed by extensive washing. Right: Persistent red fluorescence after washing indicated that TAMRA-Aβ42 was binding within the crystal. (C) Western blot analysis of a pulldown assay demonstrating that Aβ42 I31P and Aβ42 G37D bind to fragment D. The blot was probed with antibodies against fibrinogen (top) and Aβ (bottom) to demonstrate Aβ pulldown by biotinylated fragment D. (D) Unit cell dimensions of published, non-soaked, and Aβ42-soaked fragment D crystals. Only Aβ42-soaked crystal unit cell dimensions are shown, since data from other Aβ peptide soaks were similar. (E) Diagram of fibrinogen indicating fragment D (FD; dashed line box) and where differences between non-soaked and Aβ42-soaked fragment D crystals were found (solid line box). Superimposed 2Fo-Fc maps from non-soaked (pink; R_{work}/R_{free} = 0.24/0.33) and Aβ42-soaked (blue; R_{work}/R_{free} = 0.28/0.39) fragment D crystals with coordinates of non-soaked crystals. (G) Protein backbone diagram showing the shift of the β384-393 loop from native (1FZA) to b-hole-peptide bound (1FZG) fragment D.

3.4. Mechanism of fibrin formation and fibrinolysis

Upon exposure to thrombin, fibrinogen undergoes cleavage at the N-termini of its α and β chains within the central E domain to reveal A- and B-knobs, respectively, yielding a fibrin monomer. These knobs can interact with corresponding a- and b-holes in the D domains of an adjacent fibrin(ogen) molecule to begin the process of fibrin polymerization (Figure 3.4, blue panel). Fibrin monomers polymerize end-to-end into two-stranded protofibrils, which then aggregate laterally into fibrils, which branch to form a gelationous fibrin network (Figure 3.4, green panel).

Fibrin clot degradation (fibrinolysis) is mediated by plasmin, a serine protease that cleaves the fibrin network at specific sites, generating fibrin degradation products (Figure 3.4, yellow panel). Plasmin is derived from the zymogen plasminogen by tissue plasminogen activator (tPA) in the presence of fibrin, which itself enhances the rate of the reaction. One fibrin site initially involved in plasminogen activation by tPA includes residues 148-160 on the α-chain (Figure 3.4, pink panel; reviewed in [154]). This site becomes exposed and available for plasminogen binding after the conversion of fibrinogen to fibrin[155], but could remain hidden if clots are formed in the presence of Aβ, leading to delayed clot lysis. This hypothesis is derived from our data indicating that Aβ binds the fibrinogen β-chain near the b-hole (Figure 3.1 and [125]), which is in close spatial proximity to residues 148-160 of the α-chain (Figure 3.4, pink panel and [132]). Another potential explanation for delayed clot lysis is based on the relationship between fibrin structure and its susceptibility to fibrinolysis. Tighter fibrin networks composed of thin fibers are degraded less efficiently by plasmin than those composed of thick fibers[138,156-158] because 1) there are more fibers to be cleaved[157,159], requiring plasmin to detach from and move between fibers more frequently[160]; and 2) decreased network porosity of tighter fibrin networks results in impeded diffusion of

fibrinolytic enzymes throughout the clot (reviewed in[161]). Potential effects of Aβ on fibrin fiber thickness could thus be another mechanism of Aβ-mediated impaired fibrinolysis.

To determine the mechanism of Aβ42-mediated delay of fibrinolysis, I investigated the effects of Aβ42 itself and of the Aβ2-influenced fibrin network on the activity and function of the fibrinolytic factors tPA, plasminogen, and plasmin.

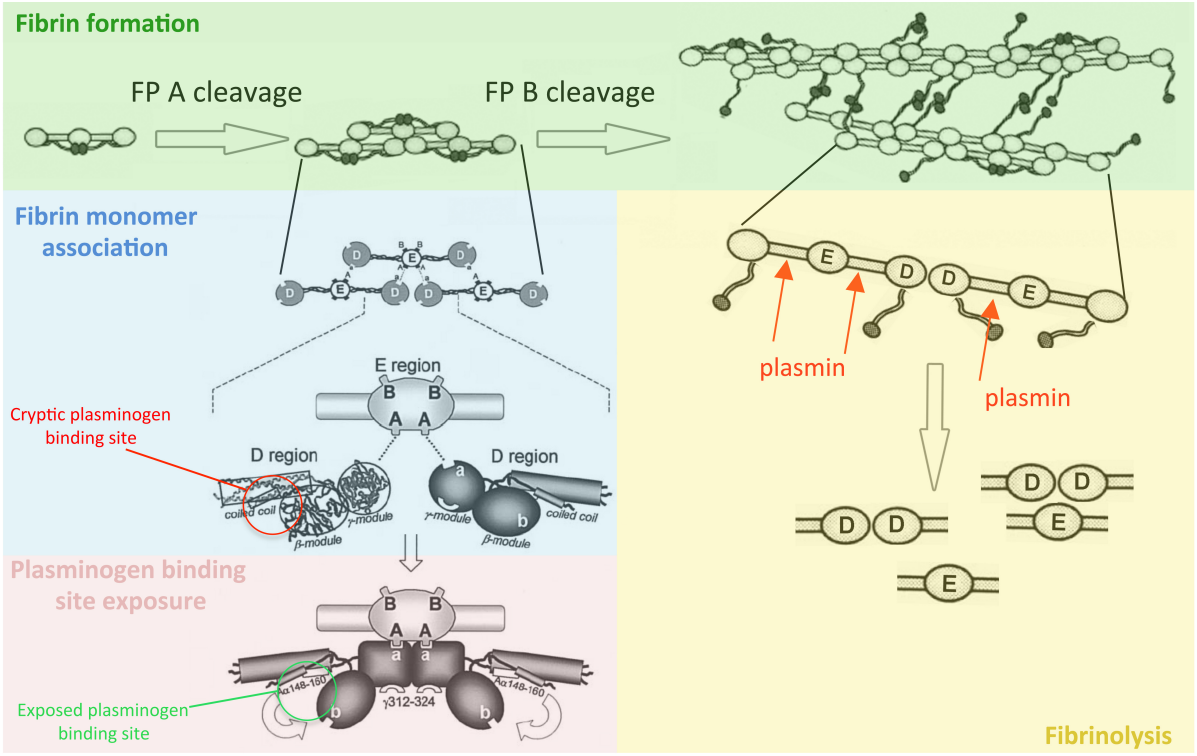

Figure 3.4. Fibrin formation and fibrinolysis. Cleavage of fibrinopeptides A and B within fibrinogen fragment E results in the formation of a fibrin monomer with exposed A- and B-knobs. These knobs interact with the a- and b-holes of fragment D domains on nearby fibrin monomers to begin the process of fibrin polymerization (blue panel). Fibrin monomers polymerize end-to-end into two-stranded protofibrils, which aggregate laterally into fibrils (green panel). Fibrinolysis is initiated by binding of plasminogen and tPA to the forming fibrin. The binding site for plasminogen on residues 148-160 of the α-chain is cryptic in fibrinogen (blue panel) but becomes exposed in polymerizing fibrin (pink panel). Activation of bound plasminogen to plasmin by tPA results in plasmin-mediated cleavage of the fibrin network and the production of fibrin degradation products (yellow panel). Images adapted from [162], [154].

3.5. Aβ42 present during or after clot formation results in delayed fibrinolysis

The effect on clot lysis of an Aβ42 preparation containing a mixture of monomeric, oligomeric, and fibrillar species (Figure 3.5A, inset) was evaluated using two methods. In one method, tPA was added to the clotting mixture at the start of clot formation to simulate internal fibrinolysis, which is thought to approximate physiological conditions[163]. Lysis rates were compared using half-lysis times, which were calculated as the time from when maximum turbidity was achieved to when the clot reached half its maximum turbidity. The effect of Aβ42 on clot lysis was tested over a wide range of tPA concentrations (Figure 3.5A; only one tPA concentration shown for clarity), since tPA levels can increase dramatically from their base levels in response to injury. A significant delay in lysis relative to control was observed at all three tPA concentrations tested (Figure 3.5B), suggesting that the effect may be relevant in chronic as well as acute injury states. Furthermore, the delay in lysis is Aβ concentration-dependent, with concentrations from 500 nM to 3 μM producing significant and increasing delays in lysis (Figure 3.5C,D). In a complementary method, pre-formed clots made with or without Aβ42 were overlaid with tPA to initiate fibrinolysis, a system that is more relevant to the pharmacological treatment of thrombosis[163]. In this system, half lysis time was defined as the time from tPA overlay until the clot reached half its maximum turbidity, and was significantly increased for Aβ42-containing clots (Figure 3.5E,F).

Aβ42 can adopt β-sheet structure, and it is possible that β-sheet structure alone was responsible for delayed fibrinolysis. However, clots formed with the amyloid peptide amylin, which had been aged and confirmed by TEM to contain fibrils (Figure 3.5G, inset), did not exhibit delayed lysis (Figure 3.5G). Furthermore, a truncated Aβ peptide (Aβ1-28) had no effect on clot lysis (Figure 3.5H). Thus, β-sheet structure alone is not enough to elicit delayed clot lysis, and a specific interaction between Aβ42 and fibrin(ogen) is crucial for the effect.

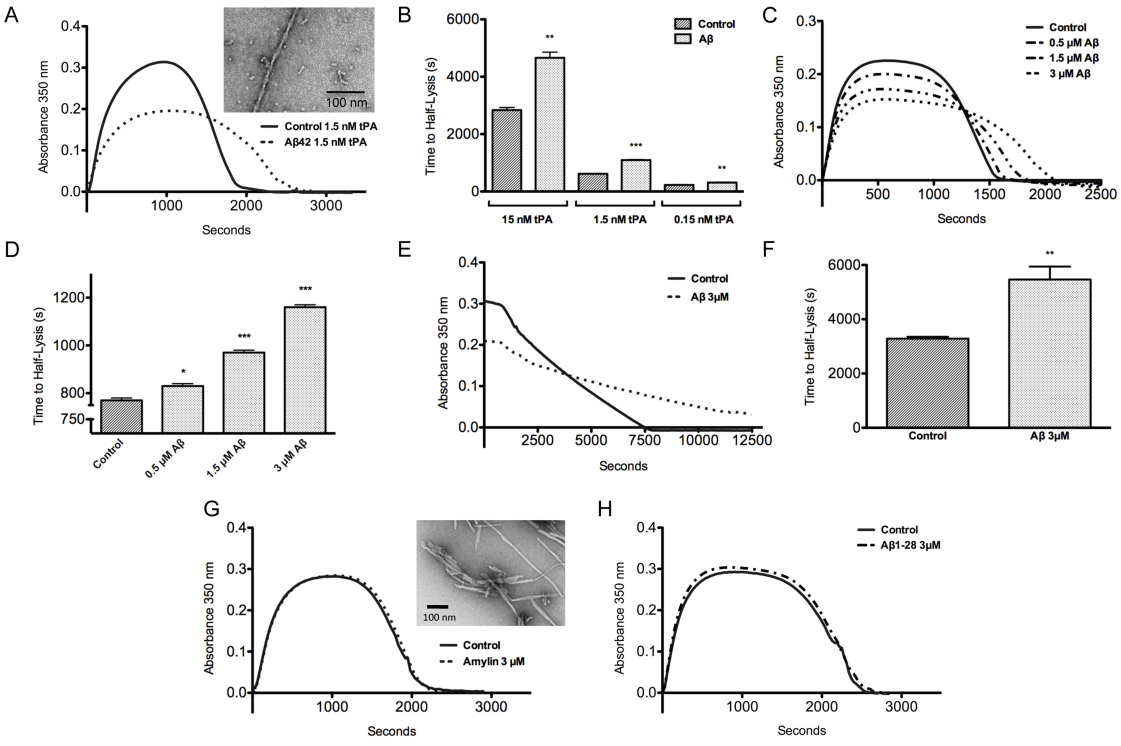

Figure 3.5. Aβ42 delays fibrinolysis in dose-dependent manner. (A) Clot formation and lysis were monitored by turbidity assay as described in methods. The presence of 3 μM Aβ42 (labeled as Aβ on graphs) in the clotting solution resulted in decreased maximum turbidity and delayed fibrinolysis (inset: TEM of Aβ42 used). (B) Time to half-lysis was significantly higher for clots formed in the presence of Aβ42 compared to control clots for all tPA concentrations tested. (C) Clots were formed with 0.5 μM, 1.5 μM, 3 μM Aβ42, or vehicle and 1.5 nM tPA. (D) Time to half-lysis of Aβ42 clots was significantly delayed in a dose-dependent manner. (E) Pre-formed clots prepared as described in methods were overlaid with 50 nM tPA. (F) Time to half-lysis of Aβ42 clots was significantly higher than control clots. (G) Clotting and lysis in the presence of 3 μM amylin confirmed by TEM to be fibrillar (inset) did not differ from control. (H) Clotting and lysis in the presence of 3 μM Aβ1-28 did not differ from control.

3.6. Aβ42 does not directly inhibit fibrinolytic enzyme activity

It is possible that Aβ42 interacts directly with fibrinolytic enzymes in solution and reduces their activity. I assessed the effect of a range of Aβ42 concentrations on the activities of tPA and plasmin. No effect of Aβ42 on tPA (Figure 3.6A) or plasmin (Figure 3.6B) activity was observed. It has been shown that the conversion of plasminogen to plasmin by tPA is enhanced in the presence of Aβ42, particularly for aggregated forms of $A\beta42^{164\text{-}166}$. Since Aβ42 preparations can vary dramatically, I wanted to exclude the possibility that our preparation would decrease the conversion of plasminogen to plasmin. In agreement with published results, I found that the generation of plasmin from plasminogen by tPA was increased in the presence of Aβ42 in solution (Figure 3.6C). These data indicate that the inhibitory effect of Aβ42 on clot lysis exists despite its ability to potentiate the generation of plasmin in solution.

3.7. Aβ42-associated fibrin is a weaker enhancer of plasmin generation and a poorer substrate for plasmin cleavage

Fibrin enhances the activation of plasminogen by tPA, and any changes introduced into the fibrin network by Aβ42 could alter the efficiency of tPA/plasminogen interactions with fibrin. To evaluate this possibility, I included the plasmin activity-monitoring chromogenic substrate Pefa-5329 in clotting reactions, and the rate of plasmin generation was monitored during clotting and lysis. Clots formed with Aβ2 showed delayed lysis and had reduced plasmin activity compared to control clots (Figure 3.7A,B). Since the reduced activity in Figure 3.7A is not due to sequestration of plasminogen by Aβ (not shown) or direct inhibition of plasmin activity by Aβ42 (in solution – Figure 3.6B; in clot overlay – not shown) , it implies a decrease in the rate of plasmin generation and may reflect Aβ-mediated disruption of the interaction between fibrin and tPA/plasminogen. To determine whether the decrease in plasmin generation is fibrin-related, I used streptokinase (SK) instead of tPA to activate

plasminogen, since the rate of plasminogen activation by SK, unlike tPA, is not enhanced in the presence of fibrin. Accordingly, there was no difference in plasmin generation between Aβ42 and control when clots were lysed with SK and plasminogen (Figure 3.7C). Despite similar rates of plasmin generation, the lysis of Aβ-influenced clots was still delayed with SK-initiated lysis (Figure 3.7C,D). This result could be due to the reduced capability of SK-generated plasmin[167] to bind or process fibrin fibers in Aβ-influenced clots versus control clots.

To test this possibility, I initiated clot lysis using pre-formed plasmin in order to bypass the plasminogen activation step. In agreement with the SK/plasminogen result, we observed an increase in half-lysis time of Aβ42-influenced clots compared to control clots (Figure 3.8, A and B). Plasmin interacts with fibrin through several binding domains and a catalytic domain[160]. The serine protease trypsin is also able to dissolve fibrin clots[160], but in contrast to plasmin, it operates entirely through its catalytic domain. When pre-formed clots were overlaid with trypsin, no delay of lysis of Aβ42-influenced clots was observed (Figure 3.8, C and D), suggesting that Aβ interferes with plasmin's access to its binding site and not its cleavage site on fibrin.

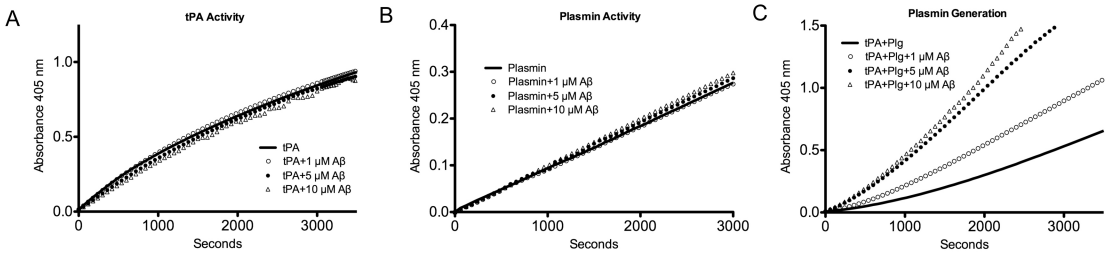

Figure 3.6. Aβ42 does not directly inhibit fibrinolytic enzyme activity. Aβ42 at 1 μM, 5 μM, and 10 μM or vehicle was combined with (A) tPA and the chromogenic substrate S-2288 to monitor tPA activity; (B) plasmin and the chromogenic substrate Pefa-5329 to monitor plasmin activity; or (C) tPA, plasminogen (plg), and Pefa-5329 to monitor plasmin generation from plasminogen. Representative results from ≥3 separate experiments.

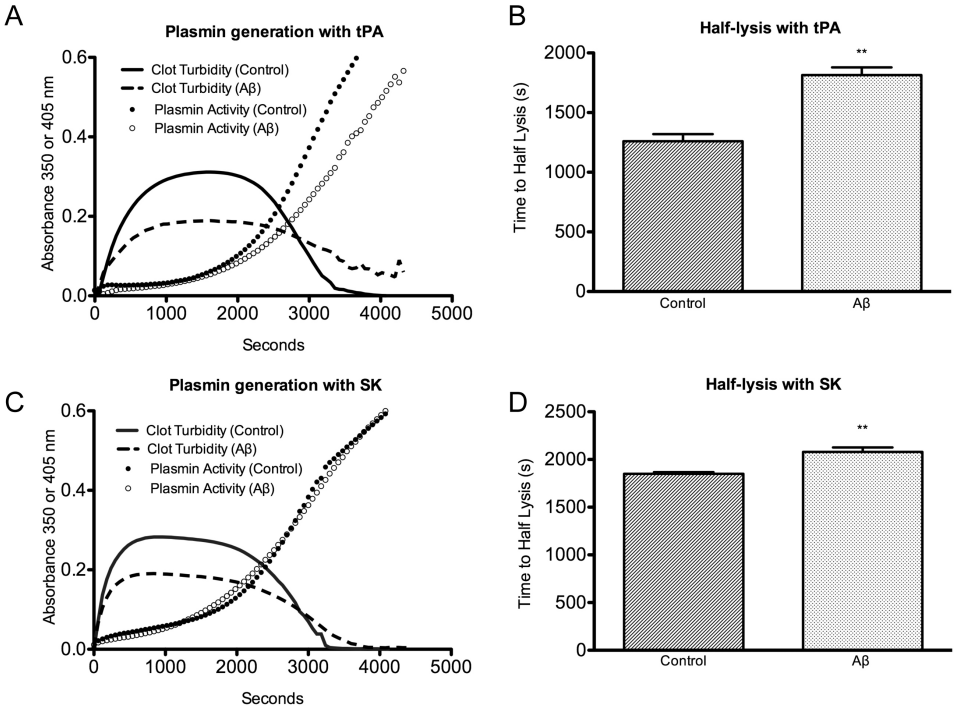

Figure 3.7. Plasmin generation by tPA, but not streptokinase, is decreased in Aβ42-influenced clots. (A) Fibrinogen, plasminogen, tPA, thrombin, $CaCl_2$, and Pefa-5329 or vehicle were mixed with or without 3 μM Aβ42. Absorbance was measured at 350 nm to follow clot formation and lysis and at 405 nm to monitor plasmin activity. Curves of A_{405} without Pefa-5329 were subtracted from Pefa-5329 A_{405} curves to control for A_{405} arising from clot turbidity and not plasmin activity. (B) Half-lysis of tPA/plasminogen-lysed clots was delayed in the presence of Aβ compared to control ($p = 0.011$). (C) Same as (A), except streptokinase (SK) was substituted for tPA. (D) Half-lysis of SK/plasminogen-lysed clots was delayed in the presence of Aβ42 compared to control ($p = 0.005$).

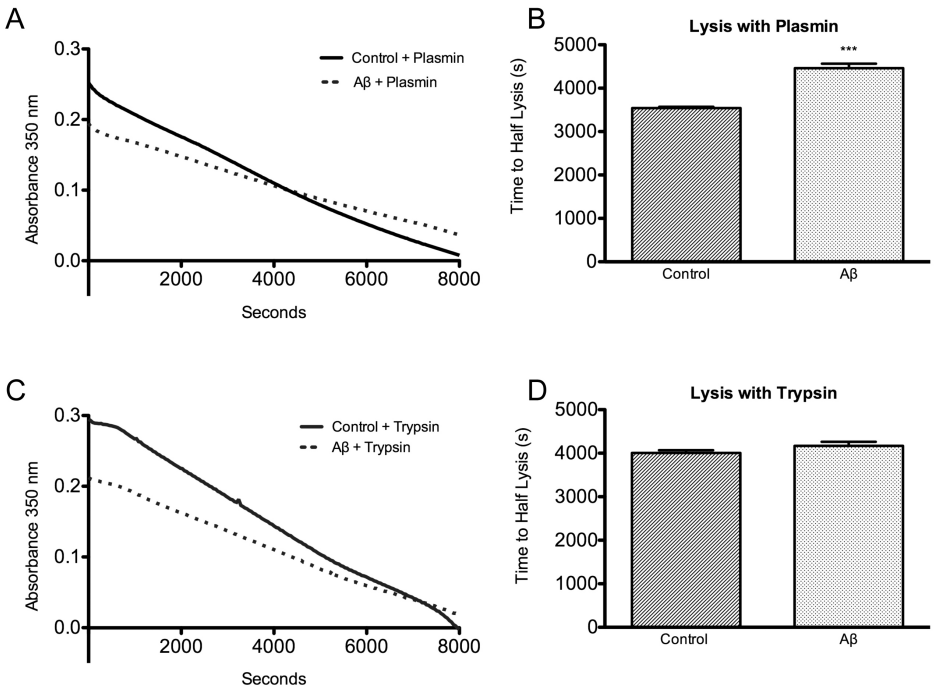

Figure 3.8. Aβ42-influenced clots are resistant to lysis by plasmin but not trypsin. (A) Pre-formed clots prepared as described in methods with or without 5 μM Aβ42 were overlaid with 250 nM plasmin. (B) Half-lysis was significantly slower in clots containing Aβ42 ($p = 0.0001$). (C) Pre-formed clots as in (A) were overlaid with 1 μM trypsin. (D) There was no significant difference between half-lysis times of control and Aβ42 clots ($p = 0.12$).

3.8. Aβ42 is incorporated into fibrin fibers throughout the clot network

The Strickland laboratory has previously shown that Aβ42-influenced clots are characterized by irregular clusters punctuating the fibrin network, and Congo Red staining (which stains amyloid fibrils) suggested that Aβ42 was confined to these clusters[59]. My hypothesis that Aβ42 interferes with plasmin(ogen)'s access to fibrin throughout the fibrin network requires its regular distribution along fibrin strands. This prompted me to more closely analyze Aβ42 localization within clots. Tracer amounts of Alexa Fluor-488-labeled fibrinogen (fibrinogen-488) were used to visualize the fibrin network, and HiLyte Fluor-555-labeled Aβ42 (Aβ42-555), was used to visualize Aβ42. In agreement with previous results, clots formed in the absence of Aβ42 showed a regular fibrin network (Figure 3.9A), while clots formed in the presence of Aβ42 contained irregular clusters (Figure 3.9C, E,I). Aβ42-555 labeling of irregular clusters (Figure 3.9F,H; arrowhead) confirmed our previous conclusion that Aβ42 binds to fibrin aggregates. However, the uniform labeling of normal fibrin fibrils by Aβ42 (Figure 3.9F,H) showed that it is also distributed throughout the fibrin lattice. The striking co-localization between fibrin and Aβ42 is not due to the detection of fibrinogen-488 fluorescence in the 555 channel, since clots formed without Aβ42-555 produced no signal in the 555 channel (Figure 3.9, B and D). Furthermore, omitting labeled fibrinogen, but not labeled Aβ42, reproduced the Aβ42-covered fibrin lattice (Figure 3.9, G and H). Replacing 555-Aβ42 with 555-Aβ(1-9), which does not cause delayed fibrinolysis (not shown), eliminated the co-localization (Figure 3.9, I and J), confirming that the labeling reflects specific Aβ-fibrin(ogen) binding and is not a result of nonspecific trapping of the 555-labeled peptides in the forming fibrin network. Clots made without unlabeled Aβ42 but still containing 555-Aβ(1-9) did not have co-localization between fibrin and Aβ(1-9) (not shown), precluding the possibility that unlabeled Aβ42 blocks access of 555-Aβ(1-9) to fibrin. The specific Aβ42-fibrin co-localization found in these experiments, together with the previously described spatial proximity of Aβ42 and plasminogen binding sites on fibrin(ogen)[125,132],

suggested that Aβ42 could block plasmin(ogen) from accessing its binding sites on fibrin. However, another potential mechanism became apparent: Aβ42-influenced fibrin is composed of thinner fibers arranged in a tighter network than control fibrin (Figure 3.9, A vs. C), which could make it more resistant to fibrinolysis[138,156-158].

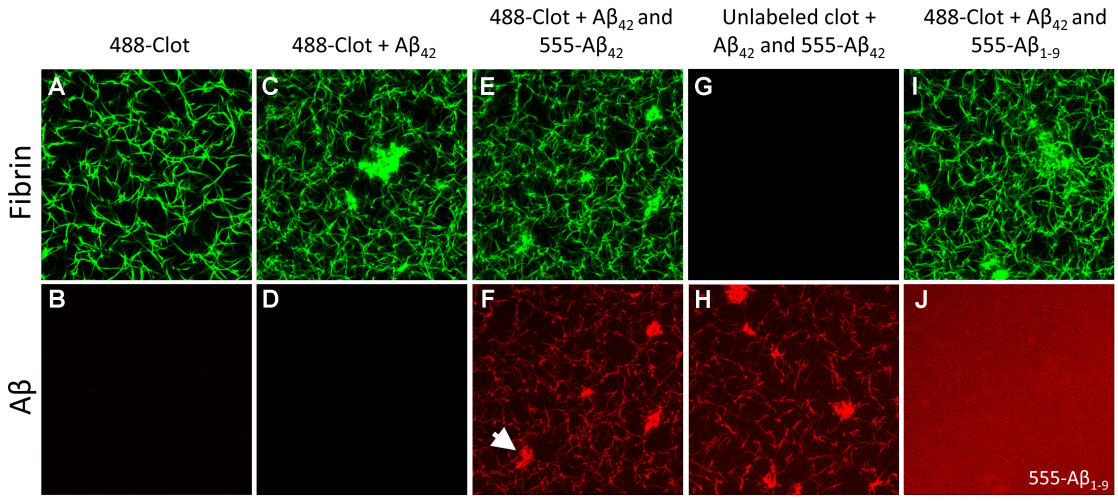

Figure 3.9. Aβ42 binds to fibrin fibrils and alters fibrin structure. Fibrin clots were formed with or without Aβ42 as described in methods to determine the location of Aβ42 binding. (Top row) Fibrin visualized with Alexa-488 labeled fibrinogen (green); (Bottom row) Aβ visualized with HiLyte Fluor 555-labeled Aβ42 (red); (A,B) Control clot. (C,D) Clot with only unlabeled Aβ42 shows that fibrin fibers and irregular clusters do not produce signal in the red channel. (E,F) Clot formed with unlabeled $A\beta_{42}$ and HiLyte Fluor 555 labeled Aβ42 shows co-localization between Aβ42 and fibrin fibers as well as Aβ42 and irregular clusters (arrowhead). (G,H). Clot formed without Alexa-488 labeled fibrinogen but with both unlabeled and labeled Aβ42 shows Aβ42 signal in the fibrin fiber pattern, confirming that Aβ42 signal is not Alexa-488 signal detected in the red channel. (I,J) Clot formed with unlabeled Aβ42 and HiLyte Fluor 555-labeled Aβ(1-9) does not have Aβ(1-9) signal along fibrin fibers or in aggregates, indicating that the Aβ42 signal represents specific Aβ42-fibrin(ogen) binding and not fluorophore entrapment. Images are representative of ≥3 experiments.

3.9. Binding of plasminogen to fibrin and plasmin generation are decreased in the presence of Aβ42

I next tested if Aβ42 binding to fibrin affected the ability of plasminogen to bind to fibrin using two complementary approaches: confocal microscopy of clots formed with FITC labeled plasminogen and ELISA with an antibody against plasminogen. Confocal microscopy of clots formed with FITC-plasminogen showed plasminogen binding as fluorescence in the pattern of the fibrin network to which it was bound (Figure 3.10A). Fluorescence was decreased in clots containing Aβ42 (Figure 3.10B), suggesting that less plasminogen was bound to the fibrin network (plasminogen does not bind to Aβ; not shown). The amount of plasminogen binding was quantified as total fluorescence intensity per slice, since fluorescence intensity is greater for FITC-labeled proteins bound to their target than for FITC-labeled proteins in solution[168]. Total fluorescence was significantly lower for Aβ42-containing clots (Figure 3.10C). These results demonstrate that Aβ42-modified fibrin binds less plasminogen, but they do not prove that Aβ is blocking plasminogen's access to fibrin, since changes in fibrin fiber thickness may be an alternative explanation. To avoid the possible modification of fibrin fibers by Aβ42 during fibrin formation, I used an immobilized fibrin monolayer overlaid with Aβ or vehicle as a surface for plasminogen binding. Excluding Aβ42 from fibrin polymerization eliminates the influence of Aβ42 on fibrin thickness, and also changes the binding target for Aβ42 from fibrinogen to fibrin. The binding affinity of Aβ42 for pre-formed fibrin may be different (and possibly lower) than for fibrinogen due to conformational changes near the Aβ binding site on fibrinogen that accompany the fibrinogen-fibrin transition. Nonetheless, Aβ42 overlay of fibrin monolayers decreased the amount of plasminogen bound to fibrin (Figure 3.10D), suggesting that Aβ42 can inhibit plasminogen binding to fibrin by impeding its access to fibrin independently of fibrin fiber thickness.

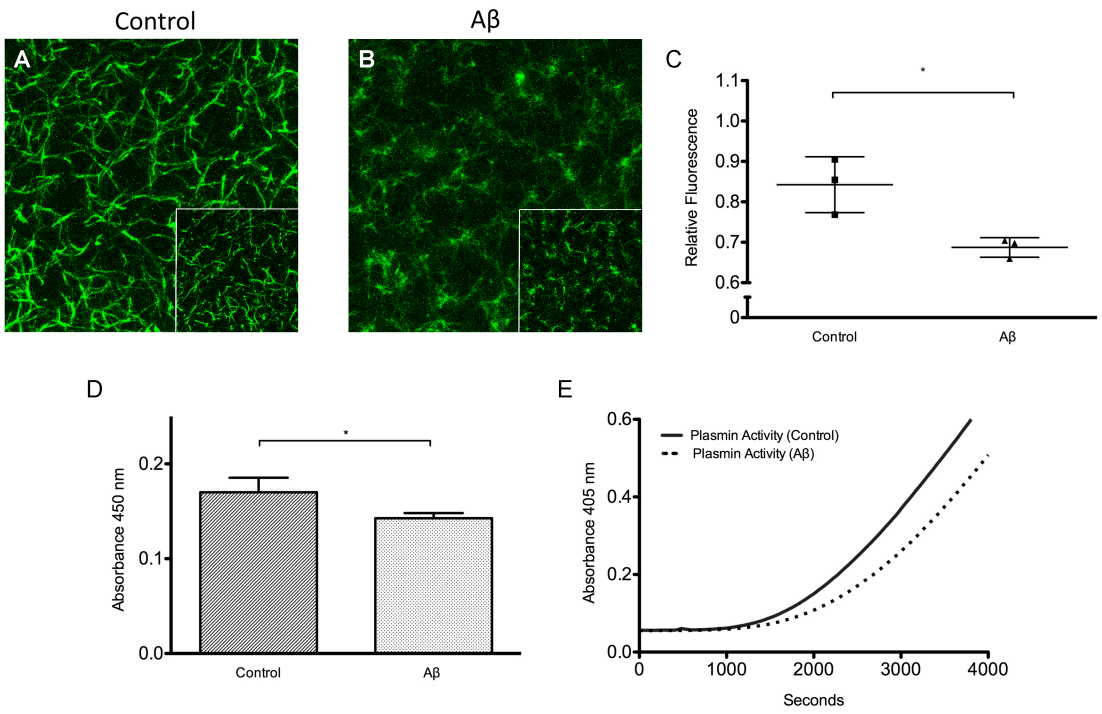

Figure 3.10. Aβ42 inhibits plasminogen binding to fibrin and plasmin generation. Fibrin clots were formed with FITC-plasminogen as described in methods, and 5 μm z-stacks composed of 11 sections were acquired and projected two-dimensionally for control (A) and Aβ42-containing (B) clots. Images of 15 random sections from 3 separate clots were also acquired and used for quantification (insets show representative single sections). (A) Control clots formed with FITC-plasminogen show plasminogen fluorescence in the pattern of the fibrin network. (B) Clots formed with Aβ42 have less FITC-plasminogen fluorescence. (C) Fluorescence intensity relative to maximum intensity recorded was significantly lower ($p=0.02$) for Aβ42-containing clots. (D) Plasminogen binding to fibrin monolayers exposed to 2 μM Aβ42 or vehicle was measured by ELISA and normalized to samples not containing plasminogen. Plasminogen binding was decreased in the presence of Aβ42 ($p = 0.04$). (E) Plasmin generation was measured by overlaying tPA, plasminogen, and chromogenic substrate Pefa-5329 on fibrin monolayers exposed to 2 μM Aβ42 or vehicle and recording absorbance at 405 nm. Plasmin generation on fibrin monolayers exposed to Aβ42 was attenuated.

To test whether the decrease in plasminogen binding translates to decreased plasmin generation, fibrin monolayers were exposed to Aβ42 or vehicle, and the rate of plasminogen activation by tPA was measured using chromogenic substrate Pefa-5329. Plasmin activity was decreased in fibrin monolayers that had been exposed to Aβ42 (Figure 3.10E). The activation of plasminogen by tPA was fibrin-dependent, since identical reactions in wells that did not contain fibrin monolayers produced negligible amounts of plasmin (not shown). This confirms that fibrin in the presence of Aβ is a weaker enhancer of plasminogen activation by tPA (as in Figure 3.7), but without the differences in clot structure as a confounding factor.

3.10. Aβ42 overlaid onto pre-formed clots delays fibrinolysis

I next tested whether Aβ42 can delay fibrinolysis independently of its effect on clot structure. Clots prepared without Aβ42, and therefore having normal structure, were overlaid with a solution containing Aβ or vehicle for 1 hour, after which the solutions were removed and the clot surfaces washed. The clots were then overlaid with a tPA solution to initiate fibrinolysis. Aβ42 overlay significantly delayed half-lysis of clots compared to control (Figure 3.11A,B), indicating that Aβ-mediated alterations in clot structure are not necessary for Aβ42-mediated clot lysis delay.

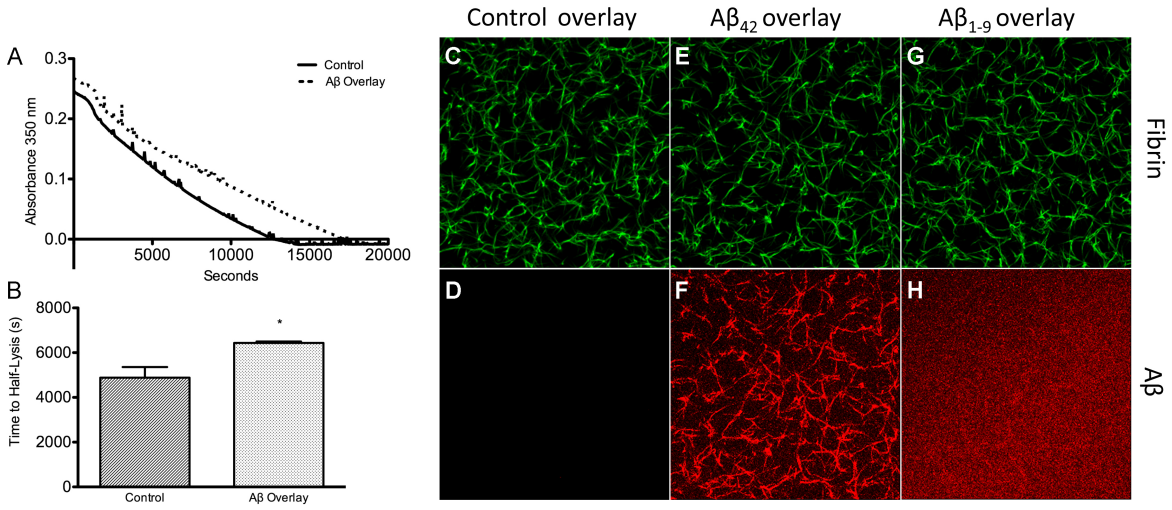

Figure 3.11. Pre-formed clots overlaid with Aβ42 are resistant to lysis. (A) Pre-formed clots (prepared as described in methods) containing no Aβ were overlaid with 5 μM Aβ42 (dashed line) or control buffer (solid line) for 1 hr, the overlays removed, and the clot surfaces washed. All clots were then overlaid with 10 nM tPA to initiate lysis. (B) Half lysis of clots that had been overlaid with Aβ was significantly delayed compared to control clots ($p = 0.012$). (C-H) Confocal microscopy of clots using Alexa Fluor-488 labeled fibrinogen and HiLyte Fluor-555 labeled Aβ. (C,D) Normal clot overlaid with buffer. (E,F) Normal clot overlaid with 555-Aβ42 (3 μM) for 1 hr contained fibrin-bound Aβ42 (G,H). Normal clot overlaid with 555-Aβ(1-9) (3 μM) for 1 hr did not show specific co-localization between fibrin and Aβ(1-9). Images are representative of ≥3 experiments.

I examined if the delay in lysis provoked by overlaid Aβ42 results from its ability to penetrate the clot and bind to fibrin after clot formation. Clots formed without Aβ42 were overlaid with Aβ42-555 and incubated for 1 hour. After removal of the overlay and washing, the interior of the clots was visualized. No structural alterations of the Aβ-overlaid fibrin network were found (Figure 3.11C,E). However, Aβ42-555 labeling of the fibrin fibers was observed (Figure 3.11F), indicating that Aβ had penetrated the clot and accumulated on the fibrin lattice. Overlays with Aβ(1-9)-555 did not lead to specific 555-labeling of fibrin, but produced diffuse fluorescence corresponding to non-specific penetration of Aβ(1-9)-555 into the clot (Figure 3.11H). The delay in lysis in these structurally normal clots could thus result from Aβ-mediated blockage of plasmin(ogen)'s access to fibrin (Figure 3.10).

Taken together, these results show that generation of plasmin is slowed, and that plasmin-mediated degradation of clots is attenuated in clots formed with Aβ42. This occurs through Aβ42-mediated hindrance of plasmin(ogen)'s access to fibrin and from Aβ-induced tightening of the fibrin network, and not through the direct effect of Aβ42 on fibrinolytic enzyme activity. Inhibiting the binding between Aβ42 and fibrinogen could therefore normalize fibrin clot lysis and possibly reduce the prothrombotic phenotype observed in AD patients and mouse models.

3.11. Aβ42 aggregation state: effects on clot structure fibrinolysis

Aβ42 aggregates into oligomers, protofibrils, and fibrils, a process that may be accelerated in the presence of fibrin(ogen)[125]. To determine whether the aggregation state of Aβ42 modulates its effect on fibrin clot structure and fibrinolysis, preparations of Aβ42 with varying potential for aggregation were used. Aβ42 I31P is unable to form aggregates with beta-sheet structure[152], a characteristic of Aβ fibrils. Incubation of Aβ42 I31P for 24 hours at 37^{o}C resulted in much less aggregated material by TEM compared to Aβ42 (Figure 3.12A,B). Aβ I31P was able to bind fibrinogen, as demonstrated by pulldown assay using biotinylated

fibrinogen FragD (Figure 3.3A) and via ELISA to fibrin monolayer (not shown). Unlike fibrin clots formed in the presence of Aβ42, clots formed in the presence of Aβ42 I31P were not characterized by clumps and a thinner network of fibers or differ in any other way from clots formed with vehicle (Figure 3.12D-F). Furthermore, clots formed in the presence of Aβ42 I31P had similar susceptibility to lysis as clots formed with vehicle (Figure 3.12, G and H), suggesting that Aβ42 aggregates/structures need to attain a certain size threshold in order for their binding to fibrin(ogen) to affect clot structure and susceptibility to lysis.

Unlike Aβ42, Aβ42 labeled with the fluorophore 555 Hylite Fluor (Aβ42-555) forms oligomers and protofibrils but does not assemble into fibrils following incubation (Figure 3.12A,C). Aβ42-555 is able to bind to fibrin(ogen), as shown by the colocalization of the peptide with the fibrin network (Figure 3.12J) and pulldown assay (not shown). Clots formed in the presence of Aβ42-555 have a thinner network of fibrin than control clots but lack the clumps seen in clots formed with Aβ42 (Figure 3.12H,I). Furthermore, Aβ42-555-influenced clots are more resistant to fibrinolysis than control clots, which is not a function of the fluorophore, since Aβ(1-9)-555 had no effect on clot lysis (Figure 3.12K).

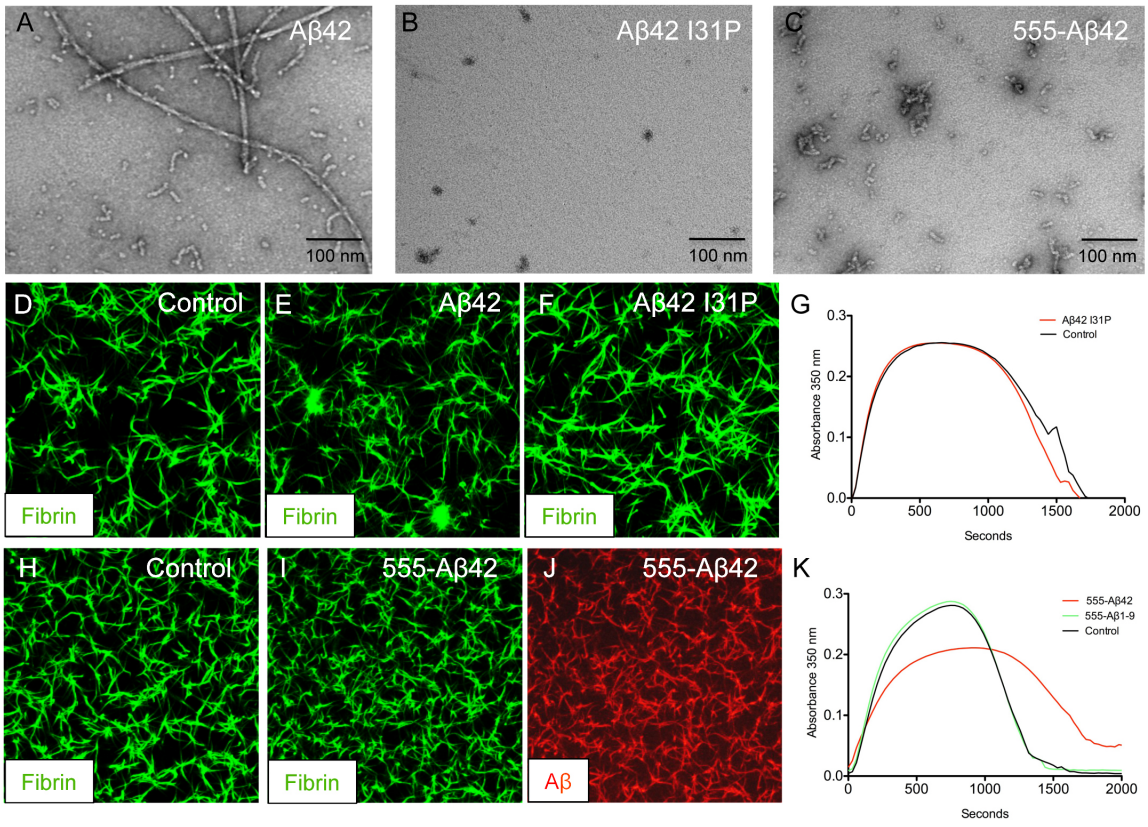

Figure 3.12. Aβ42 aggregation state differentially affects fibrin structure and lysis. (A) TEM of Aβ42 showing oligomers, protofibrils, and fibrils. (B) TEM of Aβ42 I31P mutant showing a lack of oligomers and fibrils. Monomers are too small to be visualized by EM. (C) TEM of 555-Aβ42 showing oligomers but no fibrils. (D-F) Fibrin clots prepared in the presence of vehicle (D), Aβ42 (E), or Aβ42 I31P (F). Fibrin fibers are shown in green. (G) Fibrinolysis is not delayed in the presence of Aβ42 I31P. (H-J) Fibrin clots prepared in the presence of vehicle (H) or 555-Aβ42 (I,J). Fibrin (green) is shown in H and I, while 555-Aβ42 (red) is shown in J. (K) Fibrinolysis is delayed in the presence of Aβ42-555 but not Aβ(1-9)-555, indicating that fibrinolysis is not inhibited by the fluorophore conjugated to Aβ42.

CHAPTER 4. Aβ42 is prothrombotic via activation of the FXII-driven intrinsic coagulation pathway

4.1. Aβ42 promotes thrombin generation in plasma

A prothrombotic state may be achieved not only by decreased fibrinolysis, as described in Chapter 3, but also by over-activation of the coagulation cascade. To test if Aβ42 could promote coagulation, I quantified thrombin generation in human plasma using the Calibrated Automated Thrombogram method (CAT)[144] in the presence of oligomeric Aβ42, a toxic assembly that correlates with disease severity[169]. The oligomeric composition of my Aβ42 preparation (Methods 2.15) was confirmed by electron microscopy (Figure 4.1A). In the absence of exogenous activators, a small thrombin burst is detectable after a long lag period (Vehicle, Figure 4.1B-D). Addition of Aβ42 to platelet rich plasma promoted thrombin generation in a dose-dependent manner, as indicated by a shortening of the lag time to thrombin burst and an increase in peak height (maximum thrombin formed) (Figure 4.1B). A similar prothrombotic effect was observed in platelet poor plasma (Figure 4.1C), indicating that platelets are not required. However, Aβ42 had no effect in microparticle- and exosome-free plasma prepared by ultracentrifugation (Figure 4.1D). Supplementing ultracentrifuged plasma with phospholipids restored Aβ42's ability to trigger thrombin generation (Figure 4.1D), indicating that the presence of phospholipid surfaces (found on platelets, microparticles, or exosomes) is required for Aβ42-mediated thrombin generation. The prothrombotic effect is specific to Aβ42, since amylin, another amyloid-forming peptide, failed to induce thrombin generation (Figure 4.1E).

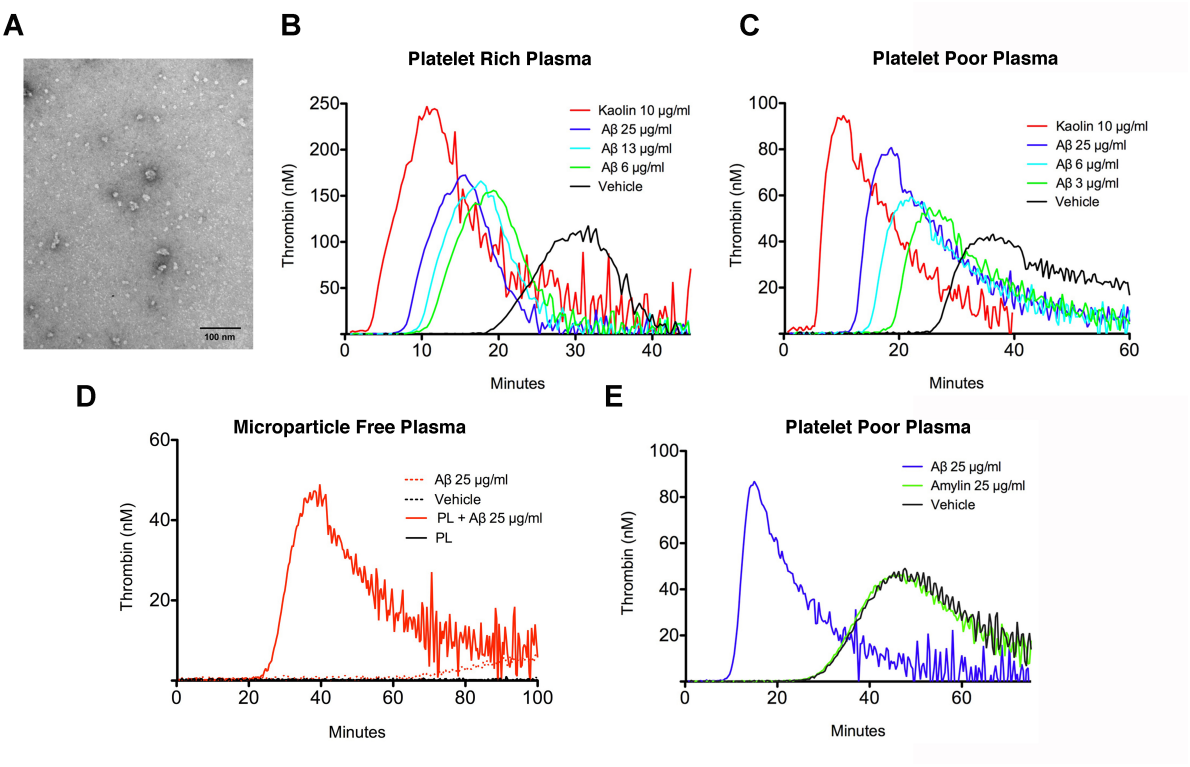

Figure 4.1. Aβ42 triggers thrombin generation in human plasma. (A) Representative TEM image of Aβ42 oligomers used. (B-E) Real-time thrombin generation was measured by CAT. (B) Platelet rich plasma (PRP) was incubated with Aβ42 at concentrations indicated or kaolin (a known activator of thrombin generation). Lag time to thrombin generation was decreased and thrombin peak was increased in the presence of Aβ42 in a dose-dependent manner. (C) As in (B), except platelet poor plasma (PPP) was used. (D) Aβ42 had no effect in plasma lacking platelets microparticles, and exosomes (labeled as Microparticle Free Plasma). Addition of phospholipids (PL; 4 µM) restored Aβ42's ability to trigger thrombin generation. (E) Lag time to thrombin generation was decreased and maximum peak height was increased in PPP with Aβ42 but not amylin. All experiments were performed in duplicate, and averaged curves are presented.

4.2. Aβ42-mediated thrombin generation is FXII-dependent

Thrombin is generated through the activation of either the intrinsic (FXII-driven) or extrinsic (tissue factor; TF-driven) pathways of coagulation (Figure 4.2A). To determine which pathway is activated by Aβ42, CAT experiments were performed in the presence of either a FXIIa function blocking antibody[145] (to block the intrinsic pathway), or with active site-inhibited factor VII (ASIS; to block the extrinsic pathway). The FXIIa antibody abolished Aβ42-induced thrombin generation (Figure 4.2B), whereas ASIS had no effect (Figure 4.2C), suggesting that Aβ42 is prothrombotic via the FXIIa-driven intrinsic coagulation pathway. The specificity of the FXIIa antibody to block FXIIa-mediated thrombin generation was confirmed by showing that it blocked thrombin generation initiated by kaolin, a known activator of FXII, but did not interfere with tissue factor (TF)-initiated thrombin generation. As expected, ASIS inhibited TF-initiated thrombin generation (not shown).

To further examine the role of FXII in Aβ42-mediated thrombin generation, I analyzed the effect of Aβ42 in plasma obtained from an individual deficient in FXII, having no detectable plasma FXII antigen (Figure 4.2D inset). Aβ42 failed to trigger thrombin generation in FXII-deficient human plasma (Figure 4.2D, dashed curves). To examine the role of Aβ42 in a system where FXII is completely absent, I tested plasma from mice that do not express any FXII ($FXII^{-/-}$). While Aβ42 promoted thrombin generation in WT mouse plasma, no effect was seen in $FXII^{-/-}$ mouse plasma (Figure 4.2E), corroborating results obtained from plasma in which FXIIa was blocked by antibody (Figure 4.2B) and from FXII-deficient human plasma (Figure 4.2D).

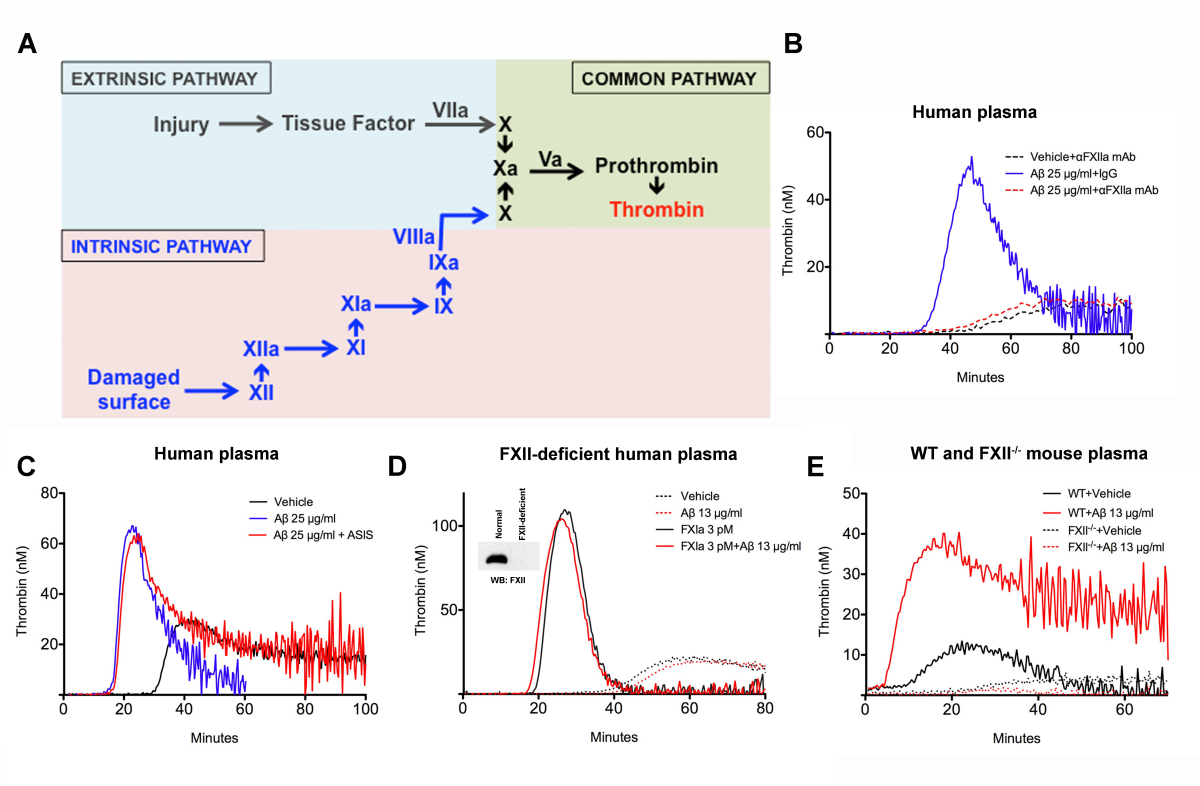

Figure 4.2. Aβ42 promotes thrombin generation in a FXII-dependent manner. (A) Intrinsic and extrinsic pathways of coagulation. (B-E) Real-time thrombin generation was analyzed by CAT. (B) Aβ42-induced thrombin generation was blocked by a monoclonal antibody against FXIIa (4 μM), but not by IgG. (C) Aβ42's enhancement of thrombin generation was not affected by the extrinsic coagulation pathway inhibitor ASIS (60 nM). (D) Thrombin generation was not enhanced in human plasma from a FXII-deficient individual in the presence of Aβ42. Deficiency of FXII in this plasma was confirmed by Western blot (WB; inset). Aβ42 had no effect when thrombin generation was triggered by 3 pM FXIa. (E) Thrombin generation was enhanced in WT mouse plasma but not FXII-/- mouse plasma in the presence of Aβ42. Mouse plasma contained 240 nM ASIS to block TF-mediated thrombin generation stemming from TF contamination during blood draw. ASIS does not affect Aβ42-mediated enhancement of thrombin generation (Figure 4.2C). All experiments were performed in duplicate, and averaged curves are presented.

Since FXII-deficient or -neutralized plasmas have normal levels of FXI, FIX, FX, FVII, and prothrombin, the results also indicate that thrombin generation is not driven through direct activation of any of these factors by Aβ42. However, it is possible that Aβ42 may potentiate these factors when they are in the activated state, low levels of which may be induced by minute FXII activation triggered by contact with the well surface or during sampling and storage (e.g. the background thrombin signal in Figure 4.1B-D). To address this possibility, thrombin generation in FXII-deficient human plasma was measured following addition of low levels of FXIa, which can activate the remaining members of the coagulation cascade (Figure 4.2A). Aβ42 had no effect on thrombin generation in plasma activated with FXIa (Figure 4.2D, solid curves), indicating that it does not enhance the activity of FXIa or any downstream factors. Furthermore, Aβ42 had no effect on thrombin generation in plasma from mice that have normal levels of FXII but do not express FXI (not shown), confirming that the pathway enhanced by Aβ42 involves FXIIa-mediated activation of FXI and not FXIIa-mediated activation of another substrate.

4.3. Aβ42 oligomers trigger FXII-dependent FXI activation *in vitro*

FXII undergoes autoactivation on negatively charged surfaces to generate FXIIa. Since autoactivation of FXII has only been shown with fibrillar Aβ and in the presence of $ZnCl_2$[121], I first determined that Aβ42 oligomers can bind FXII (Figure 4.3A, first panel) and directly induce FXII autoactivation (Figure 4.3B). Physiologically, contact system activation takes place in the presence of prekallikrein, which is activated by FXIIa to kallikrein, which in turn activates additional FXII, amplifying the reaction (feedback activation; Figure 1.2). Aβ42 dose-dependently promoted FXII activation in the presence of prekallikrein (Figure 4.3C), as seen through the reduction of FXII zymogen levels (80 kDa) and the appearance of the heavy chain fragment of FXIIa (52 kDa).

The activation of FXI by FXIIa requires co-localization of the two factors on the activating surface. A pulldown assay revealed that Aβ42 binds both FXI and FXII (Figure 4.3A), indicating that Aβ42 oligomers are a surface capable of co-localizing FXII and FXI, thereby facilitating FXIIa-mediated FXI activation. Indeed, Aβ42 led to robust FXIIa-dependent FXIa generation compared to vehicle in the absence (Figure 4.3D) and presence (Figure 4.3E) of prekallikrein, indicating that FXII activated by Aβ42 is capable of cleaving its substrate FXI. Interestingly, the relationship between the concentration of Aβ42 oligomers and the level of FXII-dependent FXI activation was not linear. FXI activation peaked at ~500 nM Aβ42, with further increases to Aβ42 concentration resulting in diminished FXI activation (Figure 4.3F). This behavior is consistent with a template-like mechanism for this process, where there is an optimal concentration of Aβ42 that allows FXII and FXI to bind the same Aβ42 molecule. Too much Aβ42 separates FXII and FXI to different Aβ42 molecules, resulting in less intermolecular interaction and decreased activation.

Previously, FXIIa-dependent FXI activation and procoagulant effects were not detected when Aβ42 was tested as an activator[122]. The main difference between our experiments is that Maas et al. used “amorphous aggregates” of Aβ42 with the Dutch mutation (E22Q) instead of the oligomeric Aβ42 tested here. This discrepancy prompted me to analyze the ability of Aβ42 in different states of aggregation as well as other Aβ variants to trigger FXII-dependent FXI activation. My results demonstrate that Aβ42 oligomers had a much greater ability to trigger FXII-dependent FXI activation compared to freshly dissolved Aβ42 and Aβ40 (Figure 4.3G,H). No FXI activity was detected in the presence of Aβ42 fibrils (Figure 4.3G). However, even when the most active (oligomeric) form of Aβ42 Dutch was tested, it was substantially less potent than oligomeric Aβ42 in stimulating FXII-dependent FXI activation (Figure 4.3I), indicating that the discrepancy between our results is a function of the use of Aβ42 Dutch in the Maas et al. study.

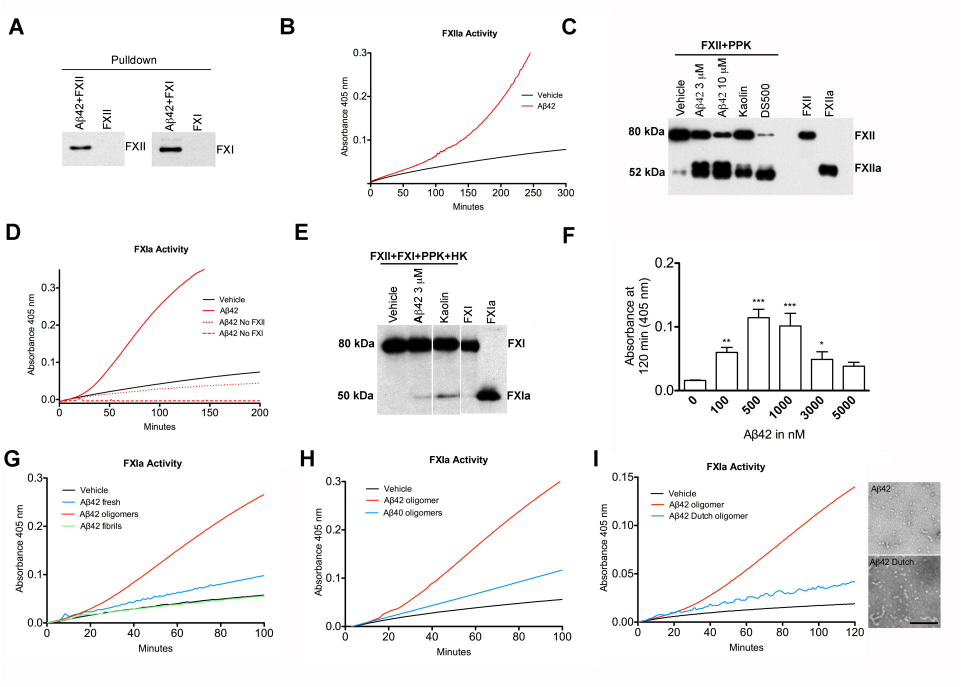

Figure 4.3. Aβ42 promotes FXII-dependent FXI activation *in vitro*. (A) Western blot showing results of pulldown assay with biotinylated Aβ42 oligomers and purified FXII (left panel) or FXI (right panel). Western blots were probed with anti-FXII and FXI antibodies, respectively. (B) Aβ42 triggered autoactivation of FXII by chromogenic substrate assay. (C) In the presence of both FXII and prekallikrein, Aβ42 dose-dependently promoted activation of FXII as seen through the reduction of FXII zymogen level at 80 kDa and appearance of the FXIIa heavy chain at 52 kDa. Dextran sulfate 500 kDa (DS500) and kaolin were used as positive controls. (D) Aβ42 triggered FXII-dependent FXIa generation by chromogenic substrate assay. The signal was not due to non-specific cleavage of chromogenic substrate by FXIIa, or by autoactivation of FXI, as seen in controls where FXII or FXI were omitted. (E) FXI activation can be seen through the appearance of the 50 kDa FXIa heavy chain band following incubation of FXII, FXI, prekallikrein (PPK), and HK with Aβ42 or kaolin. (F) FXII-dependent FXI activation was analyzed with various concentrations of Aβ42 oligomers by chromogenic substrate assay and absorbance after 2 hours analyzed. Significance is with respect to vehicle (0 nM Aβ42). (G) Aβ42 oligomers were more potent in promoting FXII-dependent FXI activation than freshly dissolved Aβ42. Aβ42 fibrils had no effect. (H) Aβ42 oligomers were more potent than Aβ40 oligomers in promoting FXII-dependent FXI activation. (I) Aβ42 oligomers (TEM image, top inset) promoted FXII-dependent FXI activation much more strongly than Aβ42 Dutch oligomers (TEM image, bottom inset).

4.4. Aβ42 oligomers trigger FXII-dependent FXI activation in plasma

To investigate the relevance of FXII-mediated FXI activation by Aβ42 to a more complex environment, I examined this process in human plasma. Biotinylated Aβ42, but not biotinylated amylin, was able to bind FXII in plasma as shown by pulldown assay (Figure 4.4A), demonstrating that the Aβ42-FXII interaction is specific and occurs in the presence of plasma proteins. This interaction leads to FXII activation, since plasma incubated with Aβ42 had decreased FXII zymogen and increased FXIIa heavy chain compared to incubation with vehicle (Figure 4.4B). While Western blotting cannot sensitively detect FXI activation, plasma FXIa can be measured by quantifying FXIa-inhibitor complex formation, since FXIa generated in plasma is rapidly bound by inhibitors[170]. Incubation of plasma with Aβ42 but not Aβ42 Dutch resulted in significantly increased levels FXIa-C1 inhibitor (C1inh) complex than when plasma was incubated with vehicle (Figure 4.4C; $p < 0.001$). The activation of FXI by Aβ42 was FXII-dependent, since incubation of FXII-deficient plasma with Aβ42 did not result in increased FXIa-C1inh complex formation. Because multiple inhibitors neutralize FXIa in plasma, I tested whether FXIa generated in plasma following Aβ42-mediated activation of FXII is bound by other inhibitors in addition to C1inh. The level of FXIa-α1 antitrypsin (α1AT) complex in plasma following activation with Aβ42 was also increased relative to vehicle (Figure 4.4D; $p<0.0001$).

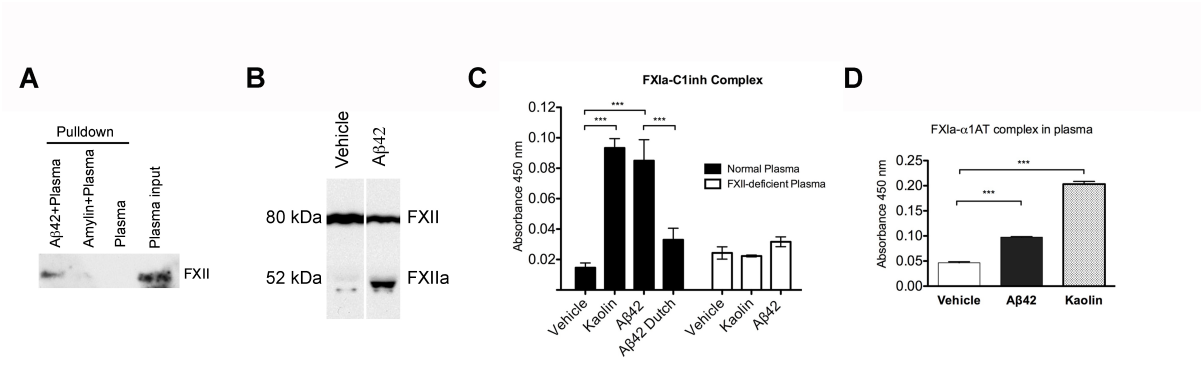

Figure 4.4. Aβ42 promotes FXII-dependent FXI activation in plasma. (A) Western blot demonstrating that biotinylated Aβ42 oligomers bind FXII in human plasma. (B) Aβ42 oligomers incubated with human plasma lead to FXII activation. (C) ELISA measuring FXIa-C1inh complex formation in normal and FXII-deficient human plasma. Oligomers of Aβ42 but not Aβ42 Dutch promoted the formation of more FXIa-C1inh than vehicle ($p < 0.001$) (D) ELISA measuring FXIa-α1AT complex formation in normal human plasma. Aβ42 oligomers resulted in increased complex formation compared to vehicle ($p < 0.0001$). Results are presented as mean ± SD of experiments performed in triplicate.

4.5. Levels of FXI zymogen and C1inh are decreased in AD patient plasma

In vivo, increased activation of plasma FXI can be detected as decreased plasma FXI zymogen levels, often observed in disease states accompanied by FXI activation[171-173]. Decreased plasma FXI zymogen levels could reflect continuous consumption of FXI due to its activation and clearance. Levels of FXI zymogen normalized to transferrin loading control, plasma levels of which are not altered in AD[174], were analyzed by Western blot in two sets of AD patient and non-demented control (ND) plasmas obtained from two AD tissue banks (see Methods 2.21). Ten AD and 10 ND cases in Group 1 were age-, gender-, and ApoE genotype-matched, while 10 AD and 10 ND cases in Group 2 were age-matched. AD plasma had decreased levels of FXI zymogen compared to ND plasma in both Group 1 (0.43 ± 0.07 vs. 0.69 ± 0.20, $p = 0.008$; Figure 4.5A,B) and Group 2 (0.85 ± 0.25 vs. 1.44 ± 0.28, $p = 0.0003$, $p < 0.0001$; Figure 4.5D,E). If AD plasma FXI levels are decreased due to its activation and clearance, levels of its main inhibitor C1inh[170] would also be expected to decrease. Indeed, C1inh levels were decreased in AD vs. ND plasma in both Group 1 (0.59 ± 0.20 vs. 1.33 ± 0.43, $p = 0.0008$; Figure 4.5A,C) and Group 2 (1.0 ± 0.12 vs. 1.2 ± 0.18, $p = 0.012$; Figure 4.5D,F), suggesting its consumption due to increased activation of FXIIa, kallikrein, and/or FXIa.

Activation of the intrinsic pathway of coagulation would be expected to result in increased thrombosis and fibrin formation. Indeed, plasma fibrin levels (as determined by monoclonal antibody 59D8 against fibrin[175]) were elevated in AD patients from Group 2 compared to controls (0.97 ± 0.17 vs. 0.74 ± 0.15, $p = 0.009$; Figure 4.5G,H). Levels of fibrin were inversely correlated with FXI levels ($r = -0.46$, $p = 0.04$; Figure 4.5I), suggesting that activation and subsequent clearance of FXI results in thrombin generation and fibrin formation. In Group 1, there was a non-significant trend toward increased fibrin levels in AD plasma (not shown), which could be due to differences in blood draw and anticoagulation

methods between the groups (see Methods 2.21). Another possible explanation stems from the more advanced disease stage of AD patients in Group 1 compared to Group 2 as determined by clinical dementia rating score (2.0 ± 1.1 vs. 1.0 ± 0.6, $p = 0.028$). Since Group 1 patients are likely to have been exposed to FXI activation for longer due to more advanced disease, the fibrin formed may have been progressively deposited, thereby depleting soluble fibrin monomers from plasma.

Figure 4.5. AD patient plasma has lower levels of FXI and C1inh. (A) Non-reducing Western blot analysis of FXI, C1inh, and transferrin loading control in plasma of 10 AD patients and 10 ND controls from Group 1. Lanes loaded with FXI purified protein (FXI) and FXI-deficient human plasma (FXI-def) show that the band just above the FXI band is non-specific. (B) FXI levels normalized to transferrin were lower in AD than ND plasma (p=0.008). (C) C1inh levels were lower in AD than ND plasma (p = 0.0008). (D) Levels of FXI, C1inh, and transferrin were analyzed in 10 AD and 10 ND plasmas from Group 2. (E) FXI levels were lower in AD than ND plasma (p = 0.0003). (F) C1inh levels were lower in AD than ND plasma (p = 0.01). (G) Levels of fibrin monomer were analyzed under reducing conditions in 10 AD and 10 ND plasma samples from Group 2 using antibody 59D8 specific for fibrin beta chain[175]. (H) Fibrin levels were increased in AD plasma compared to control (p = 0.009). (I) Fibrin levels were negatively correlated with FXI levels in samples from Group 2 (r = -0.46; p = 0.04).

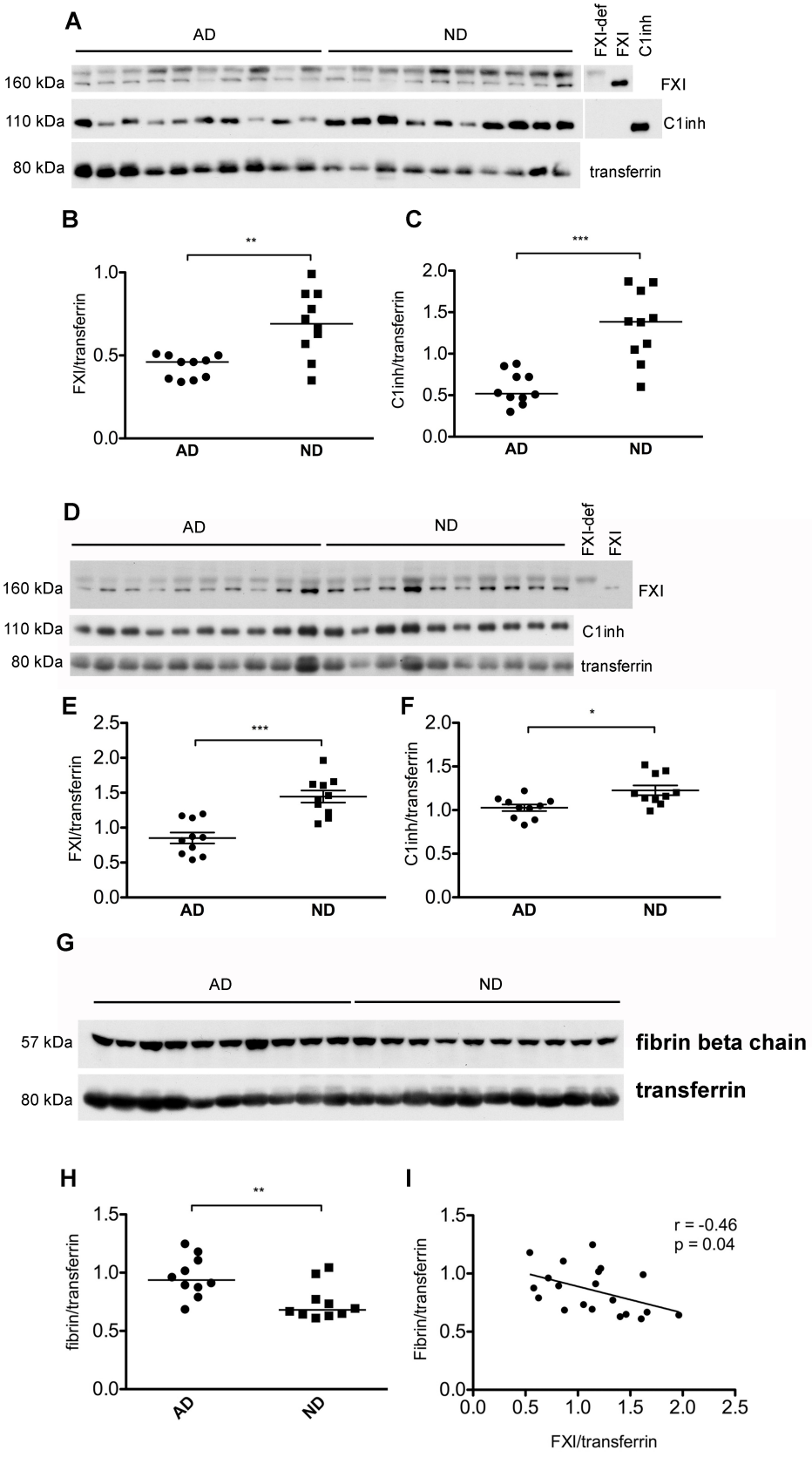
A
AD
ND
FXI-def
FXI
C1inh
160 kDa
FXI
110 kDa
C1inh
80 kDa
transferrin
B
**
FXI/transferrin
1.0
0.5
0.0
AD
ND
C
***
C1inh/transferrin
2.0
1.5
1.0
0.5
0.0
AD
ND
D
AD
ND
FXI-def
FXI
160 kDa
FXI
110 kDa
C1inh
80 kDa
transferrin
E
***
FXI/transferrin
2.5
2.0
1.5
1.0
0.5
0.0
AD
ND
F
*
C1inh/transferrin
2.0
1.5
1.0
0.5
0.0
AD
ND
G
AD
ND
57 kDa
fibrin beta chain
80 kDa
transferrin
H
**
fibrin/transferrin
1.5
1.0
0.5
0.0
AD
ND
I
r = -0.46
p = 0.04
Fibrin/transferrin
1.5
1.0
0.5
0.0
0.0
0.5
1.0
1.5
2.0
2.5
FXI/transferrin

CHAPTER 5. Aβ42 is proinflammatory via activation of FXII in the AD circulation and brain parenchyma

5.1. Aβ42 promotes FXII-dependent kallikrein-kinin system activation in plasma

I have shown that Aβ42-mediated activation of FXII can result in FXI activation and thrombin generation, and that this may occur in AD patient plasma (Chapter 4). Thrombin generation is not the only possible outcome of Aβ-mediated FXII activation, since FXIIa can also activate the proinflammatory kallikrein-kinin system (Figure 1.2). Indeed, Aβ has been shown to trigger FXII-dependent kallikrein generation and HK cleavage *in vitro*[121,122,176], and increased cleavage of HK occurs in AD patient CSF[176]. However, activation of the FXII-driven kallikrein-kinin system has not been shown with oligomeric Aβ42 or in AD patient plasma.

Since Aβ-mediated contact activation appears to be sensitive to small changes in the makeup of Aβ preparations (Figure 4.3), I first confirmed the ability of my preparation of oligomeric Aβ42 to trigger FXII-dependent prekallikrein activation in a purified protein system (Figure 5.1A). Prekallikrein activation in the presence of Aβ42 was also observed in normal plasma, as seen through the reduction in 86 kDa prekallikrein zymogen levels (Figure 5.1B). Incubation of plasma with Aβ42 generated functional kallikrein that cleaved its substrate HK in a dose-dependent manner, seen as diminished signal intensity of single chain (uncleaved) HK bands at 120 kDa (Figure 5.1C). Decreases in uncleaved HK levels were accompanied by the appearance of cleaved HK fragments: the light chain band migrating at 56 kDa and an additional 45 kDa band representing a degradation product of 56 kDa HK light chain. Aβ42-initiated HK cleavage in plasma was FXII-dependent, since Aβ42 had no effect on HK cleavage in FXII-deficient plasma (Figure 5.1C).

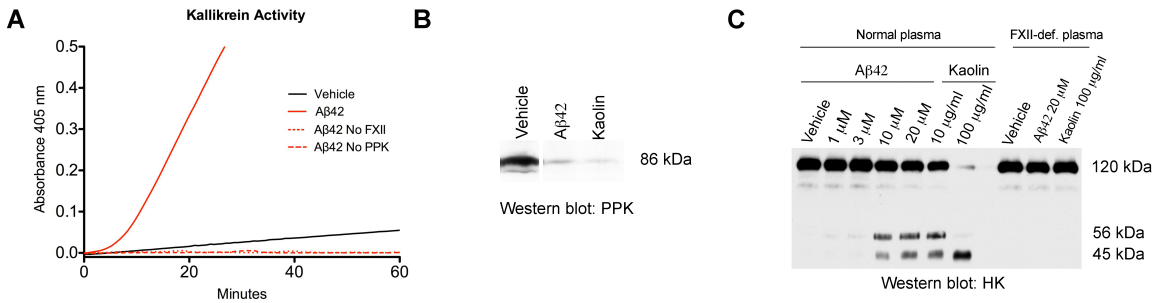

Figure 5.1. Aβ42 triggers FXII-dependent prekallikrein activation and HK cleavage. (A) Aβ42 (3 μM) promoted kallikrein generation in the presence of FXII (10 nM) and prekallikrein (PPK; 10 nM) as measured by chromogenic substrate Pefachrome PK. The specificity of Pefachrome PK for detecting kallikrein and not FXIIa activity was confirmed by testing 10 nM FXIIa (maximum amount of FXIIa generated in the assay) with no prekallikrein, which did not result in any substrate cleavage (not shown). (B) Aβ42 (20 μM) and kaolin (100 μg/ml) promoted PPK activation in human plasma. (C) Aβ42 promoted HK cleavage in a dose-dependent manner in normal but not FXII-deficient human plasma.

5.2. Increased contact system activation in AD patient plasma (Group 1)

If activation of the FXII-driven kallikrein-kinin system by Aβ occurs *in vivo,* AD patient plasma may show evidence of this process. Plasma from AD patients and controls was obtained from two tissue banks (Methods 2.21). Samples from the University of Kentucky Sanders-Brown Center on Aging (Group 1) consisted of 18 AD and 11 ND samples matched with respect to age and gender (Table 1). The extent of dementia in these individual had been assessed using Clinical Dementia Rating (CDR) scores, where 0 = no dementia and 3 = severe dementia[177], as well as Mini Mental State Examination (MMSE) scores, where 30 = no dementia and 0 = severe dementia[178]. At the time of blood draw, Group 1 AD cases had an average CDR score of 1.6 ± 1.3 (range 0-3) and an average MMSE score of 16.5 ± 9.6 (range 0-30), corresponding to moderate dementia. The presence of CDR 0 and MMSE 30 individuals in this group can be attributed to the fact that several (n = 3) were diagnosed with MCI or AD after blood draw. Upon autopsy, the majority of Group 1 AD cases (77.8%) were Braak stage 5 or 6, corresponding to severe dementia (Table 1)[179].

Plasma FXII activation in Group 1 AD patients and ND controls was analyzed under reducing conditions, with results reported after normalization to transferrin loading control. Cleavage of the FXII zymogen (80 kDa) and the appearance of a heavy chain band at 52 kDa were detected in 13 of 18 AD plasmas and 2 of 11 ND plasmas in Group 1 (Figure 5.2A). Levels of the 52 kDa heavy chain fragment, the generation of which typically corresponds to FXII activation, were higher in AD than in ND cases (0.47 vs. 0.07, p=0.029; Figure 5.2B).

Table 5.1. Characteristics of AD and ND cases from Group 1

	AD (18)	ND (11)
Gender (% Male)	61	64
Mean age at blood draw (years; SD)	82.4 (9.1)	82.5 (6.3)
Mean CDR at blood draw (score; SD)	1.56 (1.28)	0 (0.2)
Mean MMSE at blood draw (score; SD)	16.5 (9.6)	28.5 (1.5)
CERAD (%)		
None	0	100
B	27.8	0
C	72.2	0
Braak stage (%)		
0-2	16.7	100
3-4	5.6	0
5-6	77.8	0
History of (%)		
Hypertension	50	63.6
Atrial Fibrillation	5.6	18.2
Stroke	27.8	0
Diabetes	5.6	18.2
Hypercholesterolemia	38.5[#]	45.5
Myocardial Infarction	11.1	27.3

History of hypercholesterolemia data was available for only 13 AD cases.

Figure 5.2. Contact system activation in AD patient plasma from Group 1. (A) Western blot analysis of FXIIa and transferrin loading control in plasma of 18 AD patients and 11 ND controls from Group 1 (representative samples shown). FXII zymogen is observed at 80 kDa and the αFXIIa heavy chain at 52 kDa. Lane loaded with FXII-deficient human plasma (FXII-def) shows that the bands just below and above the FXIIa band are non-specific. (B) FXIIa levels normalized to transferrin were higher in AD ($p = 0.029$) than ND plasma. When AD cases with a history of stroke ($n = 5$) were excluded from the analysis, FXIIa levels in AD with stroke-excluded cases (AD SE) remained significantly higher than in ND plasma ($p = 0.018$). (C) Western blot analysis of HK in representative samples: uncleaved HK is observed at 120 kDa, HK light chain at 56 kDa, and light chain fragment at 45 kDa. (D) Uncleaved HK levels normalized to transferrin were significantly lower in AD ($p < 0.0001$) than ND plasma. When AD cases with a history of stroke ($n = 5$) were excluded from the analysis, uncleaved HK levels in AD with stroke excluded cases (AD SE) remained significantly lower than in ND plasma ($p = 0.0002$). Red points represent individuals who developed cognitive decline at least one year after blood draw. (E) Kallikrein-like activity was higher in AD plasma compared to ND ($p = 0.0006$). (F) Kallikrein-like activity was correlated with HK levels ($r = 0.81$, $p < 0.0001$). (G) HK levels normalized to transferrin were higher in both individuals with CERAD score B ($p = 0.003$) and CERAD score C ($p < 0.0001$) than in individuals with CERAD score 0. Samples were analyzed 3 separate times with similar results. Results are presented as vertical scatter plots with medians, with statistical significance determined using the Mann-Whitney test for two-group comparisons and the Kruskal-Wallis test with Dunn's Multiple Comparison post-test for comparisons between multiple groups.

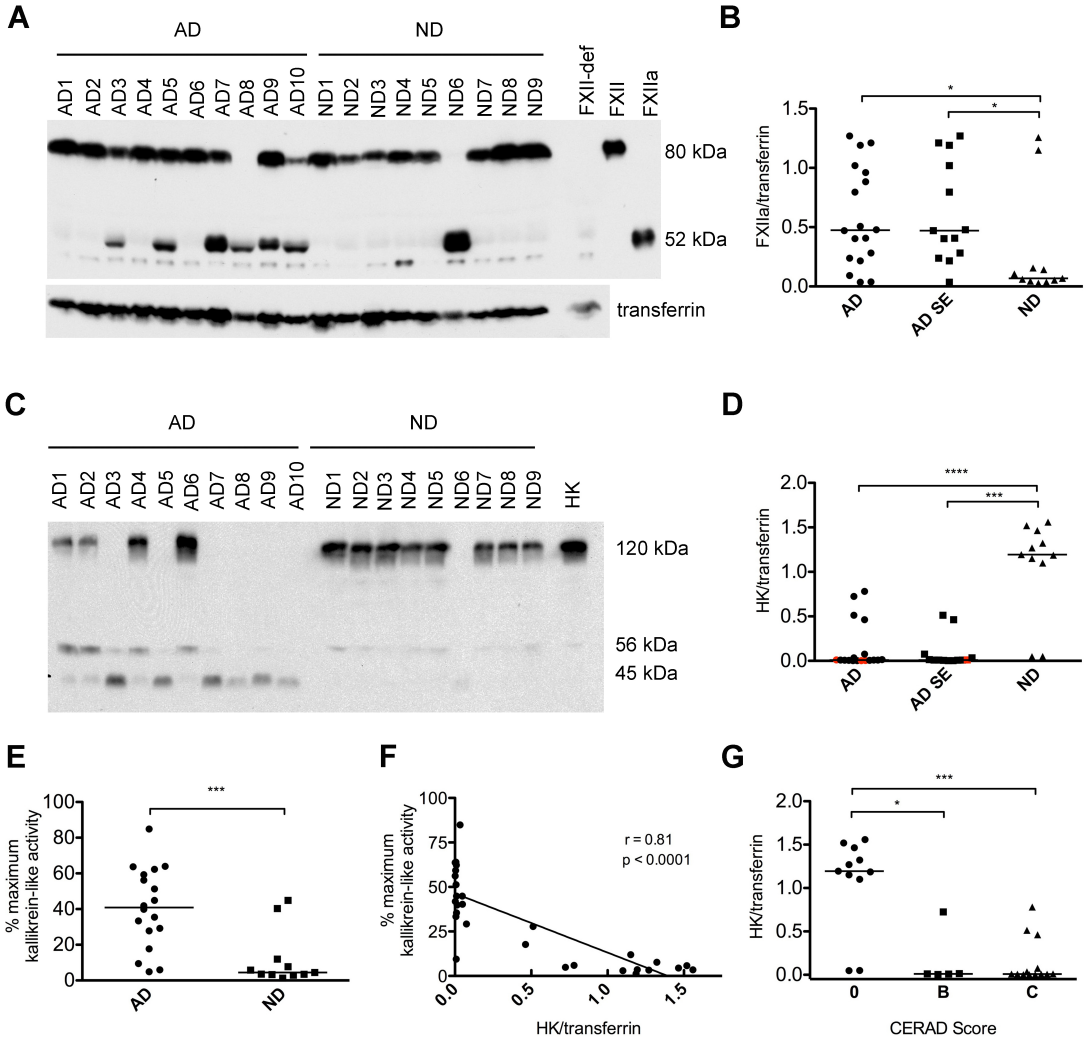
A
AD
ND
AD1
AD2
AD3
AD4
AD5
AD6
AD7
AD8
AD9
AD10
ND1
ND2
ND3
ND4
ND5
ND6
ND7
ND8
ND9
FXII-def
FXII
FXIIa
80 kDa
52 kDa
transferrin
B
FXIIa/transferrin
AD
AD SE
ND
C
AD
ND
HK
120 kDa
56 kDa
45 kDa
D
HK/transferrin
E
% maximum kallikrein-like activity
F
% maximum kallikrein-like activity
r = 0.81
p < 0.0001
HK/transferrin
G
HK/transferrin
0
B
C
CERAD Score

Activation of FXII may occur in conjunction with co-morbidities present in AD patients that are absent in controls. However, records of self- or caregiver-reported medical conditions indicate that AD cases did not have higher levels of hypertension, hypercholesterolemia, diabetes, myocardial infarction, or atrial fibrillation than controls (Table 1), arguing against a role for these co-morbidities in the increased FXIIa levels observed in AD patient plasma. Interestingly, history of stroke was found in 5 of 18 (almost 30%) of AD cases, but was absent in ND cases. Stroke is mediated by thrombosis and/or vessel rupture, both of which generate surfaces for FXII activation such as polyphosphates[180] and RNA[181]. However, excluding AD cases with history of stroke did not substantially change the FXIIa levels in AD and ND groups (0.47 vs. 0.07 respectively, $p = 0.018$; Figure 5.2B).

The presence of FXIIa in AD patient plasma in Group 1 (Figure 5.2A) was accompanied by HK cleavage (decreased intensity of bands at 120 kDa; Figure 5.2C). AD plasma as a group had much lower levels of uncleaved HK than ND plasma (0.01 vs. 1.19, $p < 0.0001$; Figure 5.2D), even when AD cases with history of stroke were excluded (0.01 vs. 1.19, $p = 0.0002$; Figure 5.2D). Decreases in uncleaved HK levels were accompanied by the appearance of cleaved HK fragments at 56 kDa and 45 kDa. Because HK cleavage products are rapidly degraded[182], samples with high levels of HK cleavage did not necessarily have proportionally higher levels of HK light chain, making quantification of the HK breakdown products uninformative. Interestingly, some samples (e.g. AD1 and AD2) that did not have detectable FXIIa showed evidence of HK cleavage, demonstrating that HK cleavage is a more sensitive indicator of contact activation than FXII activation.

To determine whether the reduction in uncleaved HK levels observed by Western blot is a result of contact system activation, I measured the activity of plasma kallikrein, the enzyme responsible for HK cleavage. Kallikrein-like activity, measured by chromogenic

substrate assay, was higher in AD vs. ND plasma (40.9% vs. 4.5% of fully activated plasma, p = 0.0006; Figure 5.2E) and correlated with HK cleavage as detected by Western blot (r = 0.81, p <0.0001; Figure 5.2F). Since kallikrein generation is triggered by FXIIa, this result also indicates that FXII cleavage detected by Western blot represents FXII activation.

When HK levels were plotted as a function of CERAD score (a measure of Aβ plaque pathology in the brain on autopsy: 0 = normal brain; B = probable AD; C = definite AD[147]), plasma from individuals with a CERAD score of 0 had higher levels of uncleaved HK compared to plasma from individuals with a CERAD score of B (1.19 vs. 0.01, p <0.05) or C (1.19 vs. 0.01, p <0.001) (Figure 5.2E). The fact that HK cleavage is apparent in the plasma of individuals with CERAD B and does not increase further in those with CERAD C suggests that FXIIa-driven inflammation begins early in disease progression and is mostly developed by the time individuals reach CERAD B status. The idea that HK cleavage is an early event in AD is also suggested by its presence in plasma from 3 individuals who were cognitively normal at time of blood draw but went on to develop cognitive impairment (red points in Figure 5.2D).

5.3. Increased contact system activation in AD patients plasma (Group 2)

Samples from the Washington University Knight Alzheimer's Disease Research Center (Group 2) consisted of 10 AD and 10 ND samples matched with respect to age (Table 2). AD cases in Group 2 had an average CDR score of 1.0 ± 0.6 at the time of blood draw, with the majority (80%) being CDR 0.5 or 1 (Table 2), corresponding to very mild to mild dementia[177]. Group 2 individuals are still living and therefore Braak stages and CERAD scores are not available.

While FXIIa was not detected in AD or ND plasma from Group 2 (not shown), uncleaved HK levels were lower in AD than ND (0.59 vs. 0.85; p <0.0001; Figure 5.3A,B). Kallikrein-like

activity was also increased in AD plasma from Group 2 (1.2% vs. 0.96% of fully activated plasma, p = 0.03; Figure 5.3C), corroborating the decreased levels of uncleaved HK seen by Western blot.

Levels of CSF Aβ42, total tau (tau), and phosphorylated tau (p-tau) in Group 2 were available from the Washington University Alzheimer's Disease Research Center. Decreased CSF Aβ42 levels are thought to be the earliest CSF marker of incipient AD, appearing as early as ~15 years prior to onset of symptoms and remaining low as disease progresses, while CSF tau and p-tau levels (related to neurofibrillary tangle formation and neurodegeneration) begin to rise closer to the appearance of cognitive decline (reviewed in [183]). We therefore performed correlation analyses for these CSF biomarkers and uncleaved HK levels. Levels of uncleaved plasma HK were positively correlated with CSF Aβ42 (r = 0.63; p = 0.003; Figure 5.3C), consistent with increased HK cleavage in the plasma of individuals with lower CSF Aβ42. Uncleaved plasma HK did not correlate with CSF tau (r = -0.11; p = 0.64; Figure 5.3D) or p-tau (r = -0.25; p = 0.28; Figure 5.3E), suggesting that increased HK cleavage may be an early event in AD progression that precedes substantial changes to neuronal injury markers.

Undetectable FXIIa and less dramatic HK cleavage in Group 2 than Group 1 may stem from the earlier disease stage of Group 2 cases (CDR score Group 2, 1.0 ± 0.6 vs. Group 1,1.6 ± 1.3) and from differences in blood collection. While I show that the degree of contact system activation may increase with disease progression (Figure 5.3D), the method of blood collection appears to also play a role, since ND plasma in Group 2 had lower kallikrein activity than ND plasma in Group 1 (Figures 5.2E, 5.3C).

Table 5.2. Characteristics of AD and ND cases from Group 2

	AD (10)	ND (10)
Gender (% Male)	30	50
Mean age at blood draw (years; SD)	73.6 (5.8)	70.5 (3.9)
Mean CDR at blood draw (score; SD)	1.0 (0.6)	0 (0)
CDR (%)		
0	0	100
0.5	40	0
1	40	0
2	20	0

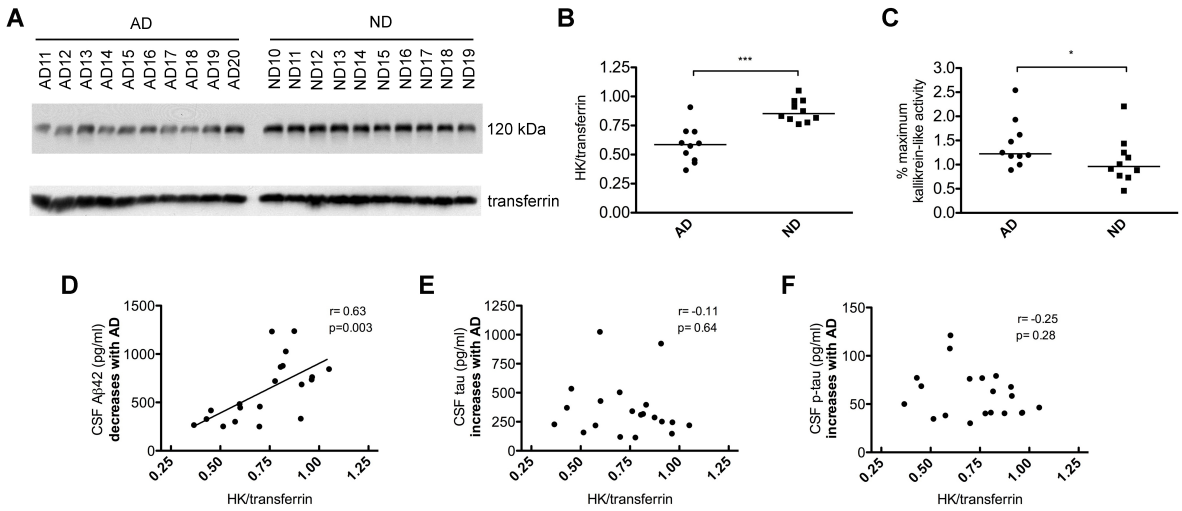

Figure 5.3. Contact system activation in AD patient plasma from Group 2. (A) Western blot analysis of HK and transferrin loading control in plasma of 10 AD patients and 10 ND controls from Group 2. (B) Uncleaved HK levels normalized to transferrin were significantly lower in AD ($p < 0.0001$) compared to ND plasma. (C) Kallikrein-like activity was higher in AD plasma compared to ND ($p = 0.03$). (D) Levels of CSF Aβ42, which decrease with AD, were positively correlated with uncleaved HK levels ($r = 0.63$, $p = 0.003$). (E) Levels of CSF tau, which increase with AD, were not correlated with uncleaved HK levels ($r = -0.11$, $p = 0.64$). (F) Levels of CSF p-tau, which increase with AD, were not correlated with uncleaved HK levels ($r = -0.25$, $p = 0.28$). Samples were analyzed 3 separate times with similar results. Results are presented as vertical scatter plots with medians, with statistical significance determined using the Mann-Whitney test.

5.4. Blood draw method and detection of contact system activation

In Group 1, blood was drawn into plastic heparinized Vacutainer tubes via vacuum, while Group 2 blood was drawn into EDTA-coated syringes via aspiration. Heparin can promote contact system activation in a purified protein system[184] and in plasma diluted to 30%[185], but not in plasma diluted to 90%[186], arguing against heparin-mediated activation of undiluted blood during collection. On the other hand, EDTA is a Zn^{++} chelator and may therefore prevent ongoing contact activation after blood collection, resulting in detection of less FXIIa and uncleaved HK in Group 2. To test these possibilities, I evaluated the activation potential of blood from WT mice collected into heparin or EDTA (in collaboration with Zu-Lin Chen in the Strickland laboratory). Both EDTA- and heparin-anticoagulated plasma treated with the FXII activator dextran sulfate had comparably decreased levels of uncleaved HK (Figure 5.4), indicating that heparin-mediated promotion or EDTA-mediated inhibition of *ex-vivo* FXII activation cannot explain the differences between Groups 1 and 2. However, the possibility remains that long-term storage of frozen plasma with EDTA vs. heparin could lead to differences *in ex-vivo* contact activation.

Another possible explanation is that collection of blood into Vacutainer tubes is more likely to trigger FXII activation compared to slower blood draw into syringes (personal communication, Thomas Renné; Karolinska Institute). Indeed, plasma collected into Vacutainer tubes (with vacuum) has increased FXII-driven thrombin generation[187] and earlier clot formation[188] compared to blood drawn into S-Monovette tubes, which employ a syringe-like mechanism. Thus, blood draw methods used for Group 1 may have resulted in *ex-vivo* amplification of smaller differences in contact factor activation present *in vivo,* which did not occur in Group 2.

It is important to note that there are limitations to my analysis of AD patient and ND control plasma inherent to the discontinuous chain of custody of the samples and potential

variability in sample storage, which could both play a role in *ex-vivo* activation of plasma proteins. While storage times were similar between AD and ND samples in Group 2, Group 1 AD samples were (on average) stored for a longer time than ND samples. However, excluding some samples (AD = 3; ND = 3), and thereby equalizing average storage times between AD and control samples, did not alter the results (not shown).

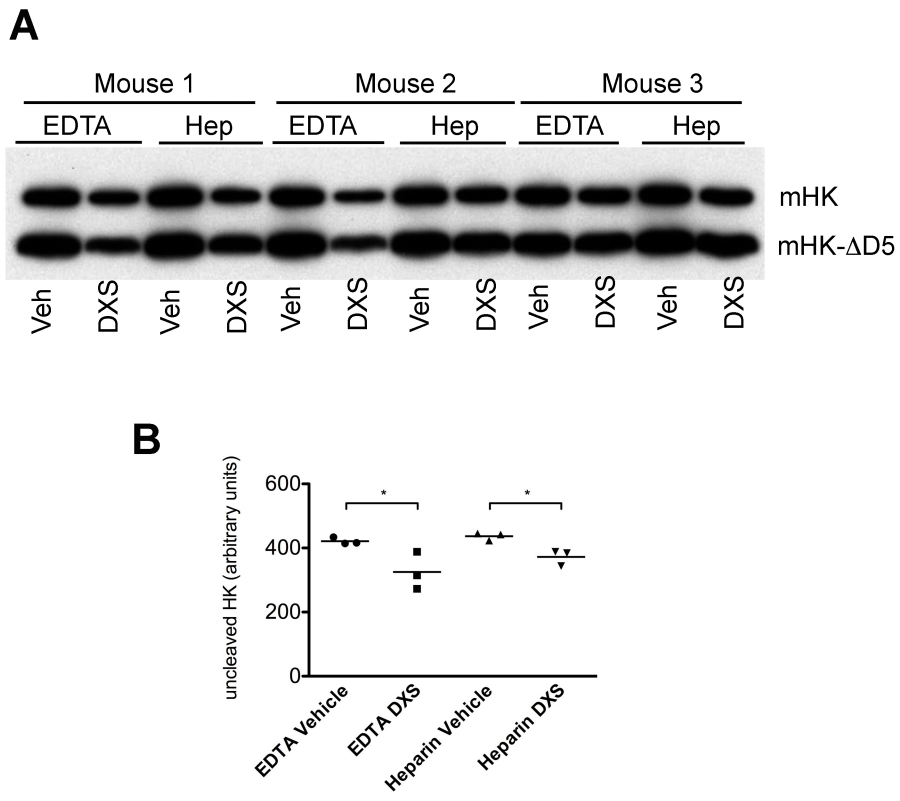

Figure 5.4. Blood draw into EDTA or heparin does not affect *ex-vivo* contact activation. Blood from C57Bl/6 mice (n = 3) was drawn with EDTA or heparin anticoagulants as described in Methods 2.24. Plasma was activated with dextran sulfate (DXS), 0.1 µg/ml final concentration, or vehicle for 20 min at 37°C, and reactions stopped with reducing sample buffer. (A) Western blot analysis of plasma with an antibody against mouse HK (mHK). Mouse plasma contains mHK and mHK-ΔD5 (mHK lacking domain 5)[189], observed at ~110 kDa and 82 kDa, respectively. (B) Uncleaved (sum of both mHK and mHK-ΔD5 bands) is decreased in samples activated with DXS compared to vehicle in both EDTA and heparin conditions ($p < 0.05$).

5.5. Contact system activation in AD mice and in WT mice injected with Aβ42

AD patients are a heterogeneous population with various disease etiologies and comorbidities. To analyze HK cleavage in a more homogeneous model, we examined plasma from the Tg6799 mouse model of AD, in which AD pathology is driven by the overexpression of human $A\beta^{142}$ (hereafter referred to as AD mice; mouse experiments were done in collaboration with Zu-Lin Chen). Since detection of FXIIa by Western blot in mouse plasma is technically challenging given the poor ability of antibodies to recognize murine FXIIa fragments (not shown), we focused on HK cleavage as a marker of contact system activation. Compared to non-transgenic wild type littermate controls (WT), AD mice had decreased levels of uncleaved HK (2.0 vs. 1.6, $p = 0.0012$; Figure 5.5A,B). These data corroborate HK cleavage in human AD patient plasma and also support the idea that the increased HK cleavage in AD patient plasma is related to Aβ-driven AD pathology and not to comorbidities present in AD patients.

We next investigated whether the increased HK cleavage found in AD patient and mouse model plasma could be mediated by Aβ42, an aggregation-prone, negatively-charged peptide. To control for non-specific effects, scrambled Aβ42 as well as amylin, another aggregating peptide, were used. Peptide preparations were shown by TEM to be composed of similar sized structures (Figure 5.5C). Incubation of Aβ42 but not scrambled Aβ42, amylin, or vehicle with WT mouse plasma resulted in HK cleavage (not shown), confirming results obtained with human plasma[121,123]. Wild type (WT; C57BL/6) mice were then intravenously injected with the same peptides or vehicle. Plasma from mice injected with Aβ42 but not scrambled Aβ42 or amylin had decreased levels of uncleaved HK (2.8 ± 0.8 vs. 4.5 ± 1.0, $p < 0.01$; Figure 5.5D,E) and increased kallikrein-like activity (73.0 ± 38.2% vs. 4.9 ± 1.9% of fully activated plasma, $p < 0.001$; Figure 5.5F) compared to plasma from mice injected with vehicle. The presence of Aβ42 in the blood of injected mice was

confirmed by ELISA (17.1 ± 9.0 ng/ml in Aβ42-injected mice compared to undetectable levels in vehicle-injected mice; lower limit of detection = 0.0156 ng/ml; Figure 5.5G). Aβ42-mediated activation of the contact system *in vivo* (as determined by kallikrein activity in plasma) was both dose (r = 0.92, p <0.0001; Fig. 5.5H) and FXII-dependent, since injection of Aβ42 into $FXII^{-/-}$ mice did not result in increased kallikrein activity (Fig. 5.5I). Our combined results indicate that circulating Aβ42 functions as a FXII contact activator capable of triggering kallikrein activity and HK cleavage *in vivo,* and support the hypothesis that increased HK cleavage in AD patient and mouse model plasma is due to Aβ42-mediated FXII activation.

Figure 5.5. Contact system activation in plasma from an AD mice and from wild type mice injected with Aβ42. (A) Plasma from AD mice (n = 7) and littermate controls (WT; n = 7) was analyzed by Western blot with an antibody against mHK; representative lanes shown. (B) Levels of uncleaved mHK (sum of both mHK and mHK-ΔD5 bands) normalized to transferrin were lower in AD than WT mice (p = 0.0012). (C) Representative TEM images of Aβ42, scrambled (scr) Aβ42, and amylin used for injections. Scale bar = 100 nm. (D) Representative lanes from blot probed with an antibody against mHK light chain showing C57BL/6 mice injected with vehicle, Aβ42, Aβ42 scr, or amylin. (E) The level of uncleaved HK normalized to transferrin was significantly lower (p <0.001) in mice injected with Aβ42 than in vehicle-, Aβ42 scr-, or amylin-injected mice. (F) Kallikrein activity as measured by chromogenic substrate was increased in plasma from mice injected with Aβ42 but not Aβ42 scr or amylin compared plasma from mice injected with vehicle (p <0.001). (G) Plasma Aβ42 levels in C57BL/6 mice injected with Aβ42 were significantly higher than in mice injected with vehicle (p = 0.001). In mice injected with vehicle, levels of Aβ42 were below the detection limit of the ELISA (0.0156 ng/ml). (H) The dose of Aβ42 (0, 3, 6, or 9 mg/kg Aβ42) injected into WT mice (n = 4 per dose) correlated with kallikrein activity levels in plasma (r = 0.92, p <0.0001). (I) Kallikrein activity was increased in WT (n = 4 per group; p <0.01) but not in $FXII^{-/-}$ mice injected with 6 mg/kg Aβ42 (n = 6 per group). Results are presented as vertical scatter plots with medians for panels B, G, and I, and with means for panels E and F, with statistical significance determined using the Mann-Whitney test for panels B and G, ANOVA with Dunnett's post-test for E and F, and Kruskal-Wallis with Dunn's post-test for I.

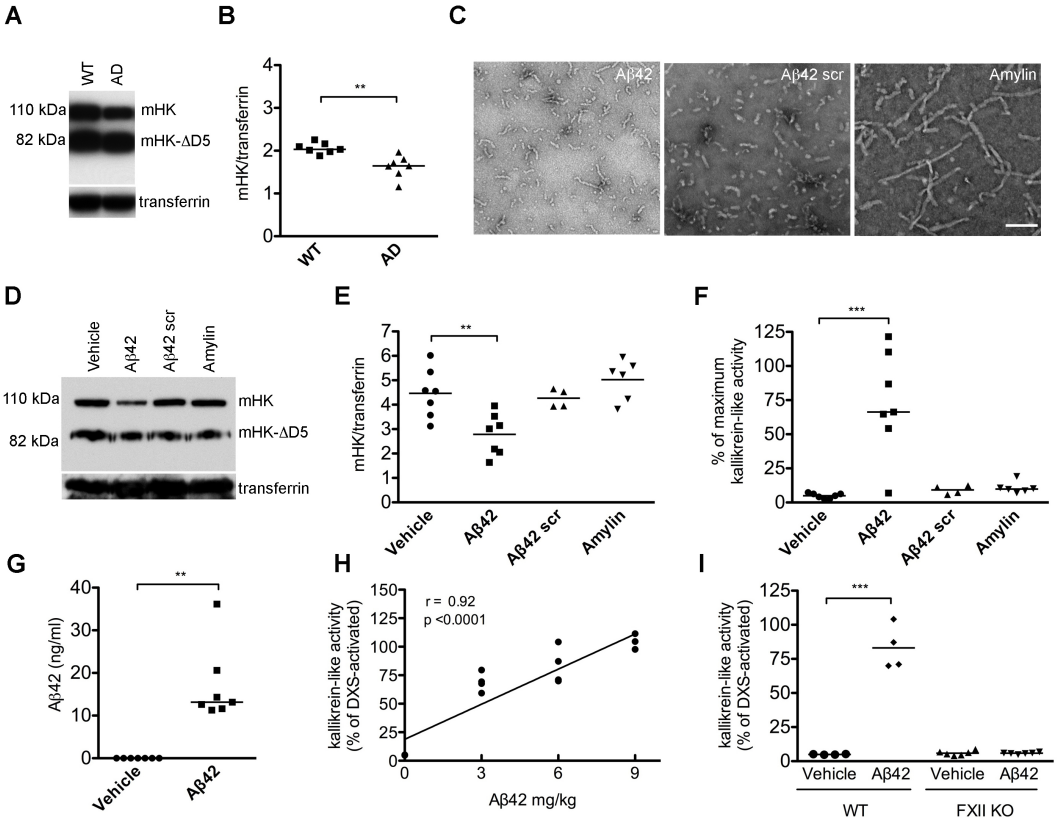
A
B
C
WT
AD
110 kDa
82 kDa
mHK
mHK-ΔD5
transferrin
mHK/transferrin
**
WT
AD
Aβ42
Aβ42 scr
Amylin
D
Vehicle
Aβ42
Aβ42 scr
Amylin
110 kDa
82 kDa
mHK
mHK-ΔD5
transferrin
E
mHK/transferrin
**
Vehicle
Aβ42
Aβ42 scr
Amylin
F
% of maximum kallikrein-like activity
***
Vehicle
Aβ42
Aβ42 scr
Amylin
G
Aβ42 (ng/ml)
**
Vehicle
Aβ42
H
kallikrein-like activity (% of DXS-activated)
r = 0.92
p <0.0001
Aβ42 mg/kg
I
kallikrein-like activity (% of DXS-activated)
***
Vehicle
Aβ42
Vehicle
Aβ42
WT
FXII KO

5.6. Contact system activation in AD brain parenchyma

Activation of FXII by Aβ42 may occur not only in the circulation, but also in the brain parenchyma, where many components of the contact activation system are found[190-194]. Evidence of activation of these systems in AD is limited to increased plasma kallikrein activity in brain parenchyma[193] and elevated levels of cleaved HK in CSF[176]. However, the presence and cleavage of HK in the AD brain parenchyma has not been investigated.

Two mouse models of AD (TgCRND8 and Tg6799, see Methods 2.17 for details) were used to analyze contact system activation in the brain parenchyma as a function of age and hence disease progression. Marta Cortes-Canteli from the Strickland laboratory provided brain tissue and homogenates for all experiments described below. FXII was detected in both TgCRND8 and Tg6799 but not WT littermate control brains by immunofluorescence (Figure 5.6A; representative images from 35 week old Tg6799 mice and littermate controls probed with two anti-FXII antibodies are shown). FXII immunoreactivity surrounded Aβ immunoreactive regions in a halo-like pattern (Figure 5.6A), suggesting that FXII interacts with Aβ and corroborating results in AD patient brains[190]. The co-localization of FXII and Aβ was detected at 16 weeks of age in the TgCRND8 model (Figure 5.6B), around the time cognitive dysfunction first begins to appear, suggesting that FXII presence in the brain is not a consequence of late-stage disease. The presence of FXII in the brain at earlier time points has not yet been analyzed. Whether the FXII detected is produced locally or is a result of plasma protein extravasation across the BBB is unclear, although the presence of diffuse FXII immunoreactivity in WT brains (WT panels in Figure 5.6A,B) together with previous identification of FXII mRNA in the brain[190,192] argues for local production.

Co-localization between Aβ and FXII suggests that contact activation occurs in AD mouse model brains, which could result in bradykinin release from HK. While no HK was detected by Western blot in TgCRND8 (AD) or littermate control (WT) brains at 4- and 15

weeks (Figure 5.6C), increased HK levels were found in 58- and 82 week old AD vs. WT brains (Figure 5.6D, $p < 0.01$ at 58 weeks, $p < 0.001$ at 82 weeks). It is possible that differences in brain HK levels exist at or before 15 weeks, but that the antibodies used are not sufficiently sensitive to detect them. The presence of HK in AD mouse brain was confirmed by HK immunofluorescence, where it also co-localized with regions of Aβ accumulation (not shown). When the same samples were analyzed under reducing conditions (which separate the heavy and light chains of cleaved HK, clearly demonstrating HK cleavage), no signal was detected in AD or WT mice at any age. This suggests that the HK detected under non-reducing conditions represents cleaved HK, light chain fragments of which are rapidly degraded under reducing conditions (see for example the low level of HK light chain fragment in lane AD10, Figure 5.3C; when that blot is run under non-reducing conditions, lane AD10 shows a very strong HK signal, not shown).

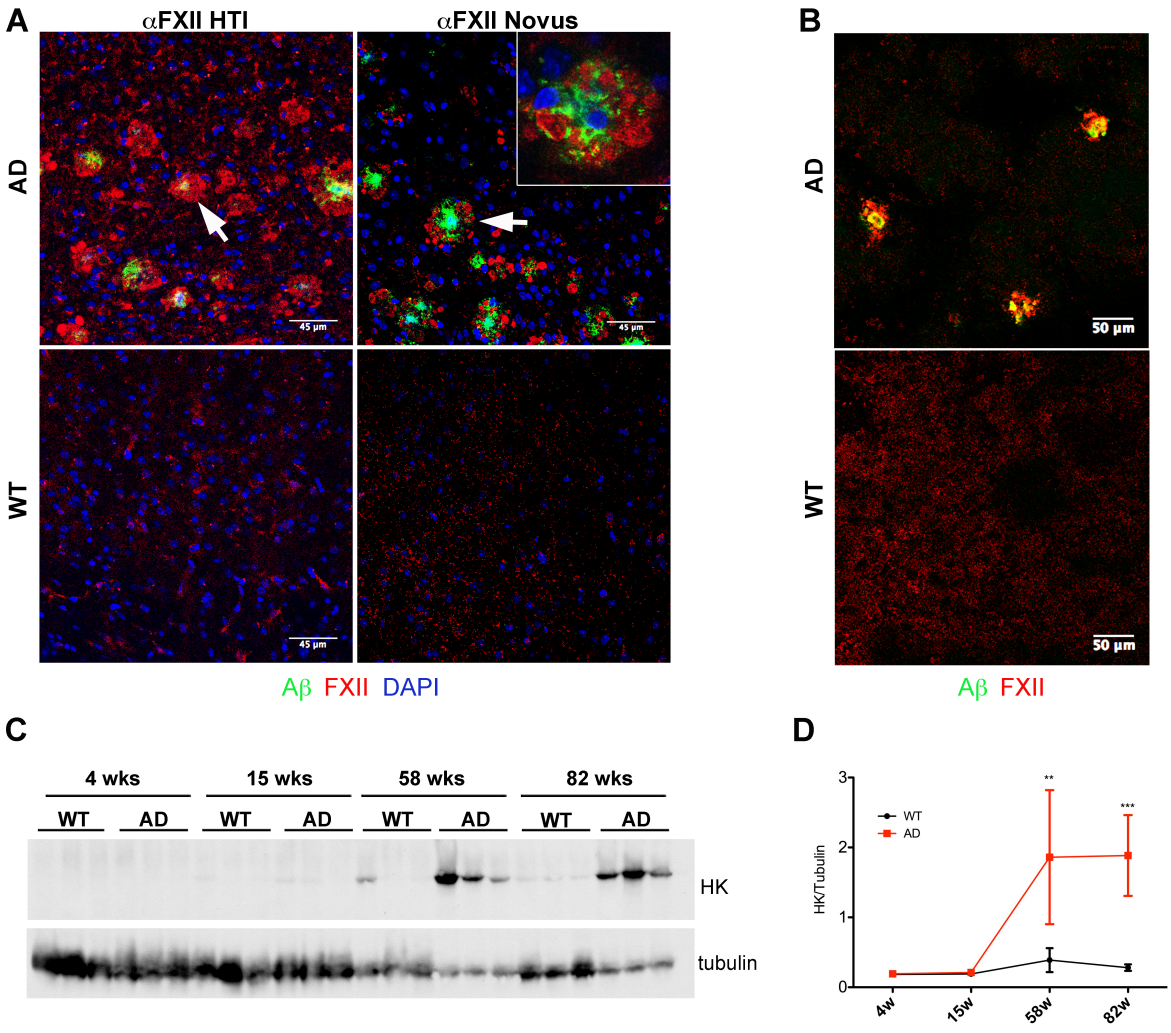

Figure 5.6. FXII and HK in AD mouse model brain. (A) Representative confocal microscopy images of cortex from 35 week old Tg6799 (AD) and littermate control (WT) mice stained with antibodies against Aβ (green) and FXII (red – two different antibodies shown). DAPI staining is in blue. (B) Representative confocal microscopy images of cortex from 16 week old TgCRND8 (AD) and littermate control (WT) mice stained with antibodies against Aβ (green) and FXII (red). (C) Non-reducing Western blot analysis of soluble fraction from whole brain homogenates of TgCRND8 (AD) or littermate control (WT) mice at different ages (n = 3 for each group). Blots were probed with antibodies against mouse HK and tubulin as loading control. Under non-reducing conditions, mHK and mHK-ΔD5 migrate together. (D) Levels of HK normalized to tubulin were increased in AD vs. WT mice at 58- ($p < 0.01$) and 82 weeks ($p < 0.001$) by 2-way ANOVA with Bonferroni post-test.

5.7. HK accumulation and cleavage in AD patient brain parenchyma

The presence and cleavage of HK in human AD brain was analyzed in brain tissue from the Harvard Brain Tissue Resource Center obtained and processed by Marta Cortes-Canteli. AD patients were defined as being Braak stage 3-6, while ND controls were Braak stage 0-2[195] and matched with respect to age. Homogenates were prepared from the temporal pole region, which is strongly affected by Aβ plaques, tau pathology, and neuronal loss in AD[196,197].

Reducing western blot analysis of the soluble protein fraction from temporal pole tissue showed both uncleaved HK at 120 kDa and cleaved portions of the HK light chain (HKa) in AD and ND brains (Figure 5.7A, top panel). Levels of total HK (cleaved and uncleaved) normalized to actin were dramatically increased in AD brains ($p = 0.012$; Figure 5.7B) and correlated with Braak stage ($r = 0.77$, $p < 0.0001$; Figure 5.7C). Brain HK accumulation was accompanied by HK cleavage, as seen through the appearance of cleaved HK light chain bands (Figure 5.7A), levels of which were significantly increased in Braak 6 AD brains compared to ND ($p < 0.05$; Figure 5.7D) and correlated with Braak stage ($r = 0.57$, $p = 0.008$; Figure 5.7E). Cleaved HK levels in all AD vs. ND brains almost achieved significance ($p = 0.053$), and would likely do so with more samples. Interestingly, the ND sample in lane 4 (arrow) that had the highest level of cleaved HK fragments was at Braak stage 2, which is one stage prior to what is defined as clinical AD[195]. Together, these results suggest that HK accumulation and cleavage in the temporal pole are linked to disease onset and progression, and may be an early process in AD development.

HK is an abundant plasma protein, and its increased presence in the AD brain could be explained by extravasation across a pathologically permeable BBB, known to occur in AD[38]. Brain levels of the plasma protein albumin also correlated with Braak stage (Figure 5.6A, third panel and 5.7F; $r = 0.87$, $p < 0.0001$), supporting increased plasma protein

extravasation in AD. Although not widely reported, microglia have been shown to express albumin *in vitro* and in human AD brain tissue, and this expression is increased following microglial activation by Aβ42[198]. Thus, AD brains (which are characterized by Aβ42 accumulation) would be expected to have higher levels of albumin independent of BBB permeability. Indeed, levels of other plasma proteins such as hemoglobin and fibrinogen are not increased in AD brains (Figure 5.7A, fourth and fifth panels), indicating that non-specific extravasation of plasma proteins in AD cannot account for the increased brain HK levels observed.

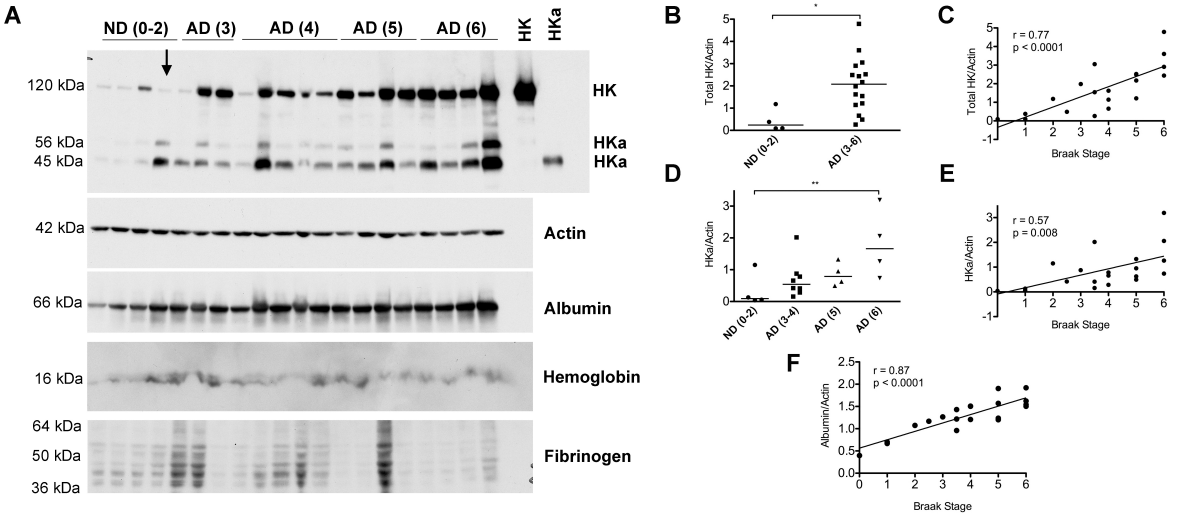

Figure 5.7. Increased HK accumulation and cleavage in AD patient brain. (A) Reducing Western blot analysis of the soluble fraction from the temporal pole in AD (Braak stage 3-6) and ND (Braak stage 0-2) brains. Purified uncleaved HK and cleaved HK (HKa) were loaded as controls. Blots were probed with antibodies against HK, actin, albumin, hemoglobin, and fibrinogen. A possible concern is that uncleaved HK may be absent in the first two ND samples because it has been fully cleaved and HKa bands further degraded. Non-reducing Western blot confirmed that the first two ND samples had very low levels of HK, and that cleaved HK was not being missed (not shown). (B) Levels of total HK (sum of uncleaved and both cleaved bands) normalized to actin were higher in AD vs. ND brains ($p = 0.0123$). (C) Total HK normalized to actin correlated with Braak stage ($r = 0.77$, $p < 0.0001$). (D) Levels of cleaved HK normalized to actin were increased in Braak 6 AD patients compared to ND controls ($p < 0.05$) and were trending higher in other AD groups. (E) Levels of cleaved HK normalized to actin correlated with Braak stage ($r = 0.57$, $p = 0.008$). (F) Levels of albumin normalized to actin correlated with Braak stage ($r = 0.87$, $p < 0.0001$).

CHAPTER 6. DISCUSSION

6.1. Overview

In this thesis, I established the ability of Aβ to initiate prothrombotic and inflammatory processes via activation of the FXII-driven contact system, and provided evidence for these processes in AD patients and mouse models. I also defined the regions involved in Aβ42-fibrinogen binding and elucidated the mechanism by which this interaction results in delayed fibrinolysis. Together, these results provide a basis for a novel hypothesis for the etiology of the vascular dysfunction that may play a key role in AD onset and progression. I will first discuss the results independently, then present the hypothesis derived from my combined findings.

6.2. The Aβ-fibrin(ogen) interaction and Aβ's role in clot susceptibility to fibrinolysis

The Strickland laboratory has identified Aβ42 as a novel factor capable of modulating fibrin clot structure and stability. Results in Chapter 3 defined mechanisms by which fibrin clots formed in the presence of Aβ42 become more resistant to fibrinolysis and suggested mechanisms by which clot structure is altered. Structural and biochemical evidence supports the following hypothetical model (Figure 6.1) for the Aβ-fibrinogen interaction: The C-terminal half of Aβ42 (residues 17-42) binds to fragment D of fibrinogen on the globular domain of its beta chain, near the b-hole (β366-414; Figures 3.1-3.3). Since the b-hole is involved in the lateral aggregation of fibrin protofibrils[199], Aβ binding to this region may interfere with thickening of the fibrin network during clot formation, resulting in a thinner network (Figure 3.9). From the b-hole, Aβ stretches along the coiled-coil portion of fragment D, with the N-terminal portion of Aβ contacting the α-chain within this coiled-coil region. Since Aβ binds to fibrin fibers throughout the network (Figure 3.9) and not just to clumps as previously thought[59], it could hinder the binding of plasminogen to fibrin at residues α148-160[160], thereby reducing network-wide plasmin generation and function.

Aβ may be introduced into fibrin clots in two ways, by intercalation into fibrin fibers during clot formation and by penetration into pre-formed clots**.** This is an important point, indicating that Aβ released from activated platelets[126,200] can alter fibrin's susceptibility to lysis after the clot has formed. The oligomeric state of Aβ42 required for delayed fibrinolysis has also been clarified: While Aβ oligomerization is necessary for delayed fibrinolysis (Figure 3.12), the formation of Aβ42 fibrils, which appear to induce clumping of the fibrin network (Figure 3.12E,I), is not. Although we previously hypothesized that clumps mediate delayed fibrinolysis[59], my current *in vitro* data indicate that two other mechanisms are responsible for the increased stability of Aβ42-influenced clots: thinning/tightening of the fibrin network and Aβ42-mediated hindrance of plasmin(ogen)'s access to fibrin.

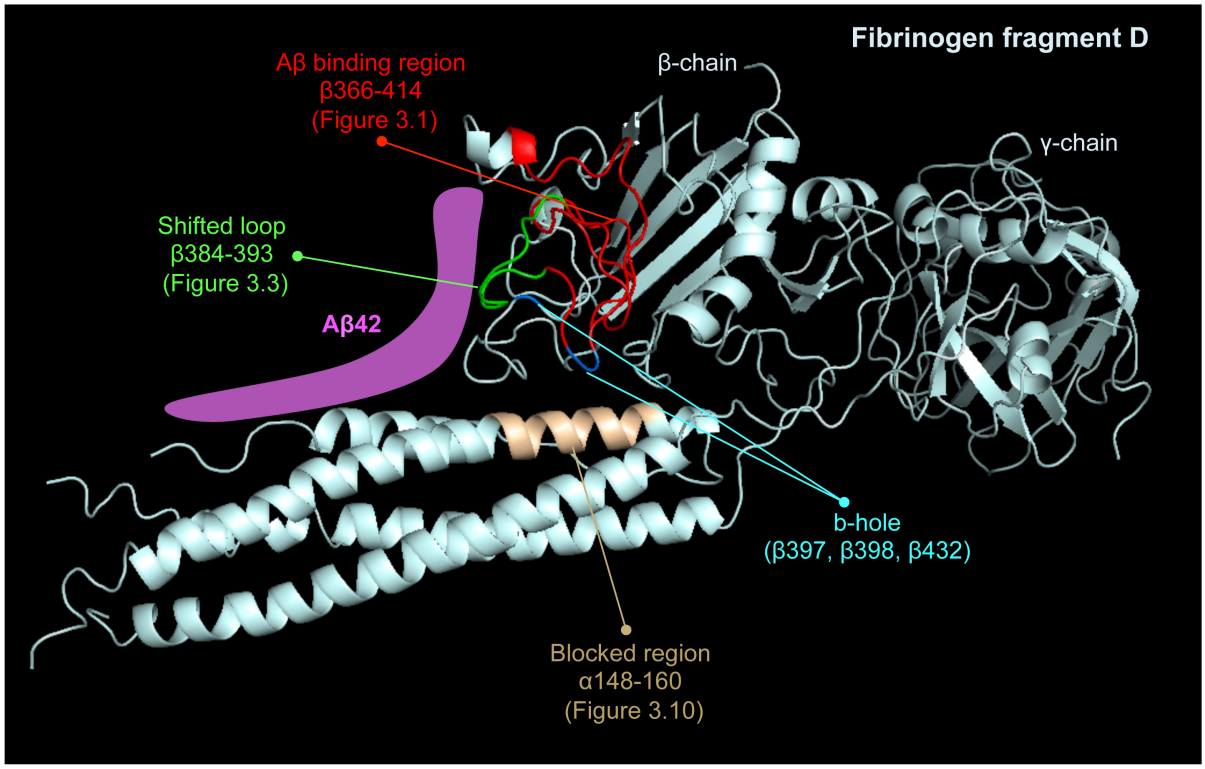

Figure 6.1. Model of the interaction between Aβ42 and fibrinogen fragment D. A ribbon diagram of fibrinogen fragment D (PDB 1FZA; light blue)[132] with the 49 amino acid binding region (β366-414) for Aβ labeled in red and the β-chain loop that undergoes a shift in the presence of Aβ (β384-393) labeled in green. Alpha-chain residues implicated in plasminogen binding (α 148-160), which is inhibited in the presence of Aβ, are in gold. My combined results suggest that Aβ (hypothetical position represented in pink) binds to β366-414 (red) with its C-terminal end, which results in a shift of the loop defined by β384-393 (green). The N-terminal end of Aβ extends toward the coiled-coil region of fragment D, thereby blocking α148-160 (gold) necessary for plasminogen binding. The b-hole, centered around residues β397, β398[201], and β432[202] (teal), is implicated in lateral aggregation of fibrin protofibrils. Blocking of the b-hole by Aβ may contribute to the formation of thinner fibrin fibers.

The interaction between Aβ and fibrin(ogen) in the cerebral circulation and brain parenchyma may therefore support increased thrombosis and fibrin accumulation, which are obstructive and proinflammatory, thereby contributing to AD pathology[59,203]. Indeed, vessel narrowing and occlusion caused by persistent fibrin(ogen) deposits co-localizing with Aβ were shown to contribute to impaired perfusion and reduced density of functional cortical microvessels in a mouse model of AD[204]. Furthermore, increased fibrin accumulation in the AD brain negatively affects synaptic health, and genetically decreasing fibrinogen in an AD mouse model ameliorates synaptic dysfunction and neuronal death[205]. The relevance of the Aβ-fibrinogen interaction to these processes is supported by studies demonstrating that inhibiting this interaction results in restored fibrinolysis *in vitro* and amelioration of pro-thrombotic phenotype, microgliosis, and cognitive performance in a mouse model of AD[206].

6.3. Aβ is a prothrombotic factor via activation of FXII

My results identify Aβ42 as a prothrombotic factor based not only on its ability to delay fibrinolysis (Chapter 3), but also on its ability to trigger thrombin generation via the intrinsic coagulation pathway (Chapter 4). Aβ42 oligomers triggered FXII-dependent activation of FXI, the first step of the intrinsic pathway, via a template mechanism (Figure 4.3), i.e. by binding and co-localizing contact activation factors. Aβ42-induced thrombin generation required the presence of phospholipids (Figure 4.1D), suggesting that while Aβ42 can serve as a surface for FXII-dependent FXI activation, phospholipid surfaces (necessary for efficient assembly of downstream coagulation cascade complexes) are required in order for thrombin generation to proceed.

Aβ42-mediated, FXII-dependent FXI activation was previously not found[122], likely due to the fact that amorphous aggregates of Aβ42 with the Dutch mutation (E22Q) were used. While Maas et al. found absolutely no FXI activation with Aβ42 Dutch amorphous aggregates, my results with Aβ42 Dutch oligomers showed low levels of FXII-dependent FXI

activation (Figure 4.3I). Thus, the assembly state of Aβ42 Dutch (amorphous aggregates vs. oligomers) plays an important role in determining its ability to induce FXI activation, a relationship also observed for Aβ42 (Figure 4.3G). Aβ42 oligomers were still much more potent in FXII-dependent FXI activation than Aβ42 Dutch oligomers, which may stem from differences in peptide charge (-2.7 for Aβ42 vs. -1.7 for Aβ42 Dutch at pH 7). A specific negative charge and/or the presence of glutamic acid at position 22 of Aβ42 therefore appears crucial for its interaction with and/or activation of FXII and FXI. Although the role of negative charge in Aβ's ability to bind and activate FXII remains to be established, preliminary results suggest that the binding of Aβ42 to FXII is not negative charge-dependent, but its ability to activate FXII is (not shown).

Other physiological surfaces such as collagen[207], polyphosphates[180], and RNA[181] have been shown to stimulate FXII-dependent FXI activation and thrombin generation. These surfaces are brought into contact with circulating FXII during vascular injury, cell death, and platelet activation. Aβ, however, is constantly present in the circulation, where it exists in a dynamic equilibrium with brain Aβ[208]. In AD, circulating Aβ may contribute to continuous low-level FXII-dependent FXI activation, a hypothesis supported by decreased plasma levels of FXI zymogen and its inhibitor C1inh in AD patients compared to controls (Figure 4.5). Decreased levels of FXI and C1inh could reflect the clearance of the FXIa-C1inh complex following FXI activation[209]. Chronic FXI activation in AD could mediate the production of low "idling" levels of thrombin, which may contribute to the maintenance of a prothrombotic state in AD.

The ability of circulating Aβ to trigger thrombin generation via FXII adds to its previously identified prothrombotic roles, including Aβ-mediated formation of fibrinolysis-resistant fibrin clots (See section 6.2) and Aβ-mediated platelet activation[210-212]. A combination of these

effects may participate in the establishment of the prothrombotic state observed in AD (Section 1.4).

6.4. Aβ is a proinflammatory factor via activation of FXII

FXII-dependent prekallikrein activation and subsequent HK cleavage by some Aβ40 and Aβ42 preparations has been shown *in vitro*[121-123]. In Chapter 5, I established that oligomeric Aβ42 is also capable of FXII-dependent prekallikrein activation and HK cleavage (Figure 5.1), and showed for the first time increased FXII activation, kallikrein activity, and HK cleavage in AD patient circulation. HK cleavage correlated with early CSF biomarkers of AD (Figures 5.2, 5.3), suggesting that FXII-mediated kallikrein-kinin system activation is an early process in disease development that plateaus at more advanced stages. In collaboration with Dr. Zu-Lin Chen, I demonstrated that Aβ42 injected intravenously triggers kallikrein-kinin system activation in mice, providing a mechanism for increased plasma HK cleavage in AD patients and mouse models (Figure 5.5). Previously, HK cleavage in AD patient plasma was not detected[176], possibly due to the inclusion of polybrene in blood collection tubes in that study. Thus, chronic activation of the FXII-driven kallikrein-kinin system by Aβ42 in the AD circulation may induce constant low levels of bradykinin-mediated inflammatory processes, including increased BBB permeability, increased extravasation of plasma proteins in the brain parenchyma, and cytokine up-regulation[106,213], all observed in AD[24,38].

My results suggest that activation of the FXII-driven kallikrein-kinin system by Aβ may contribute to AD pathology not only in the circulation, but also in the brain parenchyma. The co-localization of FXII with Aβ deposits in the cortex of AD mice (Figure 5.6A) and AD patients[190] implicates Aβ-mediated FXII activation in the brain, supported by higher kallikrein activity in AD brain[193] and by increased HK cleavage AD CSF[214]. My results indicate that HK accumulation and cleavage in the brains of AD mice (Figure 5.6C,D) and patients (Figure 5.7) correlate with disease progression, suggesting that activation of the kallikrein-kinin

system may play a pathological role. It is unclear whether HK accumulation results from non-specific plasma protein extravasation through a more permeable BBB in AD[38] or arises through other mechanisms, since not all plasma proteins tested were observed to accumulate in the brain with disease progression (Figure 5.6).

6.5. Aβ levels in AD patients

My hypothesis that Aβ42 contributes to thrombosis and inflammation by interacting with FXII requires the co-localization of Aβ42 with FXII at sufficient levels in the brain parenchyma and/or circulation. FXII is abundant in the circulation and has been found in the brain parenchyma[190], thus being available in both compartments relevant to my data. Levels of Aβ42 in AD brain tissue are higher than in the ND brain[215] and may begin to accumulate up to 20 years before disease onset[216,217], allowing the Aβ-FXII interaction to be an early disease process. In plasma, reported concentrations of Aβ are in the picomolar range[215], but these levels are likely to be underestimated due to binding of Aβ to plasma proteins and erythrocytes[218]. Indeed, techniques that measure total bound and unbound plasma Aβ have found concentrations in the nanomolar range[218], similar to doses used to demonstrate a prothrombotic effect (Figure 4.1). Furthermore, much lower concentrations of Aβ than those required to demonstrate an acute effect *in vitro* may have significant effects on thrombosis and inflammation over the many years of AD development.

If increased contact system activation observed in AD patient plasma is a result of Aβ42-mediated FXII activation, levels of plasma Aβ42 would be expected to be elevated prior to AD onset and during AD development. While studies of high-risk populations for AD (Down syndrome patients, familial AD patients, and family members of AD patients) demonstrate increased plasma Aβ42 concentrations compared to controls[219,220], the relationship between circulating Aβ42 levels and sporadic AD progression is less clear: cross-sectional studies of plasma Aβ42 have produced inconsistent results, while longitudinal studies have generally

found higher Aβ42 levels prior to and just at the onset of AD symptoms with a subsequent decrease[219-221]. This suggests that increases in plasma Aβ42 are early event in AD development, and supports Aβ42-mediated FXII activation as an early pathological process preceding the onset of symptoms.

While elevated levels of Aβ42 prior to AD onset would directly facilitate contact system activation, its levels in more advanced disease stages do not necessarily need to be elevated, since changes to the vasculature that precede and accompany AD[42] may create an environment that allows Aβ42 levels that cannot activate FXII in normal individuals to produce a pathological effect.

6.6. A new role for circulating Aβ in the development of vascular dysfunction and AD

The model illustrated in Figure 6.2 presents new mechanisms by which circulating Aβ may lead to vascular dysfunction and contribute to AD onset through FXII-dependent prothrombotic and inflammatory processes. Inflammation and coagulation are highly regulated systems that are typically activated in response to injury. In the proposed model, FXII activation by Aβ induces mild but chronic inflammation and thrombosis in the absence of injury, which, in the presence of subtle age- or disease-related inflammatory processes, can rise above threshold levels and contribute to AD onset and progression.

Age- and genetics-associated decreases in the ability of clearance mechanisms to balance brain Aβ production[9,222,223] may result in compensatory increased transport of Aβ across the BBB into the circulation. Elevated plasma Aβ levels, a risk factor for AD[224-227], initiate pathological processes by triggering FXII activation, leading to the generation of thrombin and bradykinin (Figure 6.2, Stage 1A). Alternatively, AD risk factors such as advanced age and vascular disease states may set the stage for AD development by producing changes in vessel wall biology[34,42,47], inflammatory potential[228], and platelet

activation state[229]. The resulting reduction in the thromboresistance of the vascular endothelium, increased activation of inflammatory pathways, and facilitated coagulation factor assembly on the surface of pre-activated platelets could allow normal levels of circulating Aβ to have prothrombotic effects (Figure 6.2, Stage 1B).

At this point, thrombin and bradykinin induce small, localized changes to endothelial function and BBB permeability, further contributing to the prothrombotic and inflammatory environment[99,100,104,106] (Figure 6.2, stage 2). Due to significant cross-talk between prothrombotic and inflammatory processes[104,230-232], activation of inflammation and coagulation by Aβ is mutually reinforcing. Non-occlusive fibrin clot formation resulting from limited activation of the intrinsic coagulation and platelets may occur at these early levels of endothelial cell modification[233] (Figure 6.2, Stage 3). Fibrin clots forming in the presence of Aβ would have increased resistance to fibrinolysis, enhancing their procoagulant and inflammatory potential. Initial non-occlusive thrombus formation aggravates endothelial dysfunction[234], BBB permeability[235] and inflammatory state[236], and the resulting leakage of plasma components into the vessel wall leads to stiffening of the vessel and narrowing of the lumen, which decrease CBF and induce hypoperfusion[28,115,237]. Vessel stiffening combined with CBF disturbances also decrease the drainage of brain interstitial fluid along perivascular spaces, promoting Aβ accumulation in the brain[238,239].

Severe endothelial dysfunction combined with accumulating procoagulant factors can result in occlusive clot formation (Figure 6.2, Stage 4), which exacerbates hypoxic conditions and plasma protein extravasation into the brain parenchyma[240]. The combined effects of hypoxia and plasma protein leakage can induce astrocyte and microglial activation[241-243]. Glial activation[87] and CBF disruption[244,245] are early events in AD development that can directly contribute to brain Aβ deposition, neurofibrillary tangle formation, and neuronal dysfunction[24,29,46,49,50], the pathological hallmarks of AD.

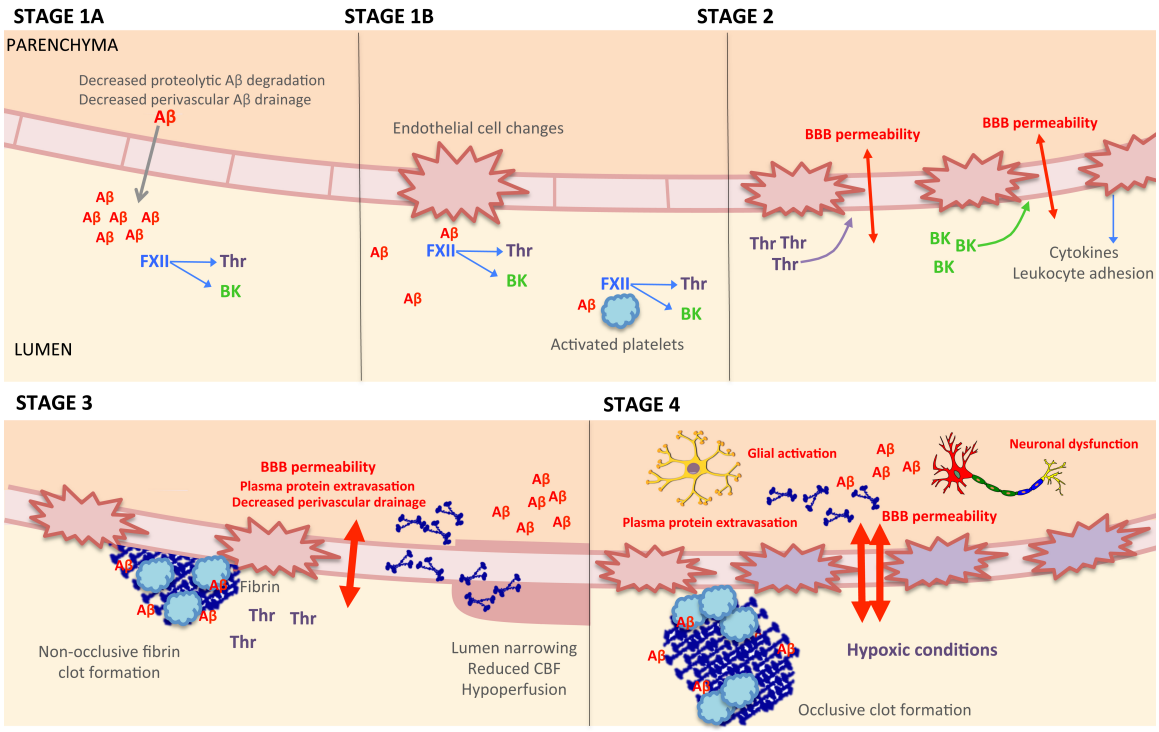

Figure 6.2. Model schematic. Stage1A. Increased transport of Aβ across the BBB due to age-related dysregulation of other clearance mechanisms results in elevated local levels of circulating Aβ, which lead to thrombin (Thr) and bradykinin (BK) generation through FXII-driven contact system activation. **Stage 1B.** Alternatively, changes to vascular biology, inflammatory potential, and platelet activation state caused by aging and/or vascular risk factors create an environment where normal levels of Aβ trigger FXII activation. **Stage 2.** Thrombin and bradykinin induce increased BBB dysfunction, BBB permeability, and cytokine release via interactions with their receptors on endothelial cells. **Stage 3.** Once a threshold level of platelet- and intrinsic coagulation pathway activation is achieved, non-occlusive clots begin to form. These clots are more resistant to degradation due to Aβ-mediated stabilization of the fibrin network (blue mesh), resulting in prolonged proinflammatory and prothrombotic damage to the BBB. Plasma protein extravasation (blue shapes) induces vessel wall changes resulting in dysregulated clearance of Aβ through perivascular drainage and in decreased CBF. **Stage 4.** Occlusive clot formation exacerbates hypoxic conditions, BBB dysfunction, and extravasation of plasma components. Stage 3 and 4 changes can elicit vessel narrowing, decreased CBF, parenchymal Aβ deposition, tau phosphorylation, glial activation, and finally neuronal dysfunction.

6.7. Testing the model with existing evidence

The model proposed above implies that modulating the functional levels of Aβ and/or members of the coagulation and kallikrein-kinin pathways in AD should ameliorate or exacerbate pathological processes initiated by contact system activation (i.e. BBB dysfunction, thrombosis, inflammation, and cognitive decline). Several lines of evidence indicate that this is indeed the case. In an AD mouse model, sequestration of Aβ by active immunization results in restoration of BBB integrity in aged mice and prevents BBB dysfunction when administered to young mice[246]. By contrast, intravenously injected Aβ increases BBB permeability in animal models[247-249]. Chronic cerebroventricular infusion of Aβ into rats induces bradykinin generation and subsequent AD-like pathology[250], and pharmacological inhibition or genetic depletion of bradykinin receptors in AD mice results in reduced inflammation[251], normalized CBF responses, and improved cognitive function[252,253]. Finally, plasma levels of C1 esterase inhibitor (which inhibits FXIIa, kallikrein, and FXIa) are decreased in prodromal AD[254], suggesting that defects in the ability to control contact system activation may participate in disease onset and development, or that ongoing contact activation is depleting its levels.

The end product of the intrinsic pathway of coagulation is thrombin, which induces inflammation and mediates the conversion of fibrinogen to fibrin. Long-term inhibition of thrombin activity in AD mouse models decreases cerebrovascular inflammation[255], reduces Aβ accumulation[76] and improves cognitive function[77]. Inhibiting the coagulation cascade at multiple points with warfarin improves cognitive function in AD patients[73-75]. Inducing persistent fibrin accumulation in an AD mouse model by inhibiting fibrinolysis exacerbates BBB permeability and neuroinflammation, while decreasing fibrinogen levels results in improved BBB function[203] and cognitive performance[59]. Importantly, interfering with the Aβ-fibrinogen interaction reduces thrombotic tendency and improves cognitive performance in

an AD mouse model[206]. Together, these results support a role for Aβ-induced activation of the contact system and for Aβ-mediated fibrin stability in eliciting vascular pathology and cognitive dysfunction in AD.

Additional support for the model comes from striking similarities between the disease course implied by the described mechanisms and the pathological cascade of cerebral small vessel disease (SVD). SVD is associated with AD[256,257], increases AD risk[43], leads to AD pathology in animal models[258] and humans[259], and is found in the majority of AD patients[30,237]. SVD presents with degenerative changes in arteriolar vessel walls in the deep white and deep gray matter. These changes are accompanied by plasma component leakage into the vessel wall and perivascular tissue and can result in stroke and cognitive decline[115]. The trigger for the initiating event in SVD development, which is thought to be endothelial dysfunction[102,115], remains elusive.

Since the development of SVD (through endothelial dysfunction, BBB permeability, and plasma protein extravasation) mirrors the AD mechanism proposed in Figure 6.2, it is possible that SVD is a precursor to AD, and that the mechanisms for these disorders share a common trigger. Recent work has shown that in SVD, stalled erythrocytes accumulate in areas of future BBB breakdown and may thus initiate disease by an unknown mechanism[233]. Given that up to 50% of Aβ is bound to erythrocytes[220], it is tempting to speculate that the elusive trigger for SVD onset is Aβ-mediated contact system activation, which may induce thrombosis and BBB dysfunction (Figure 6.2). This connection is supported by the observation of small non occlusive clots near stases[233] and by correlations between plasma Aβ levels and pathological markers of SVD such as infarcts and white matter lesions[260-262]. Aβ-mediated contact system activation could thus contribute to localized edema, extravasation of plasma components, consequent stenosis of vessels, and hypoperfusion leading to SVD development and subsequent AD onset.

6.8. AD diagnosis and therapy

A definitive AD diagnosis has traditionally been established upon post-mortem histological analysis of the brain, since a clinical diagnosis of cognitive decline is not necessarily specific to AD. Diagnostic challenges have hampered therapeutic efforts: Because clinically-measurable cognitive decline in AD is thought to manifest after significant pathological changes have occured[263], treatment of symptomatic individuals may have limited efficacy (due to the advanced nature of disease processes).

As research has focused on earlier stages of disease, it has become clear that pathological markers of AD, such as parenchymal Aβ accumulation, develop gradually and can precede cognitive and behavioral symptoms by 15-20 years[2,183,216,217]. Recent advances have made it possible to detect changes in Aβ homeostasis in living individuals using amyloid imaging techniques like Positron Emission Tomography with Pittsburgh compound and by measuring Aβ levels in the CSF. A combination of these and other methods now allow a diagnosis of AD to be established during life. However, the required techniques are expensive, invasive, and have limited availability. A more easily accessible biomarker with the ability to provide an AD diagnosis at early stages of disease would therefore be of great benefit to the field. My results indicate that plasma contact system activation has the potential to be one such biomarker. The value of contact system activation as an early indicator of disease is supported by the correlation between CSF Aβ42 levels and plasma HK cleavage as well as by contact system activation in pre-symptomatic individuals (Figure 5.2D, red points).

A definitive AD diagnosis during life is unfortunately of little help to the patient unless clinically meaningful treatment is available. Approved drugs for AD currently include acetylcholinesterase inhibitors and an NMDA receptor antagonist, both of which provide temporary relief by managing symptoms, but do not stop the progression of the disease. In

addition to therapeutic challenges stemming from late diagnosis, a possible reason for such limited success is that AD is a heterogeneous disease with potentially different driving mechanisms in different patients. Patients may therefore need therapy aimed at mechanisms specific to their disease to provide maximum efficacy. In this regard, monitoring the levels of plasma contact system activation could be used as a diagnostic tool to help identify AD patients with inflammatory and thrombotic disease mechanisms. If FXII activation is found to contribute to disease progression, identification of AD patients with this biochemical signature may pave the way for new therapies aimed at neutralizing FXIIa, such as anti-FXIIa antibody 3F7, which specifically blocks FXIIa activity and interferes with FXIIa-driven bradykinin formation in plasma[145].

6.9. Future directions

Role of Aβ-mediated prothrombotic and proinflammatory processes in AD. It will be important to determine whether activation of FXII-dependent intrinsic coagulation and plasma kallikrein-kinin pathways contributes to AD onset and development *in vivo.* The thrombotic potential, AD pathology, and cognitive performance of AD and littermate control mice should be assessed in the presence and absence of FXII. FXII depletion can be accomplished by crossing AD mice with FXII null mice, which are viable and have no obvious phenotype but are protected from thrombosis[264]. Thrombotic potential as measured by CAT[144] or *in vivo* thrombosis assays[59], BBB permeability, neuroinflammatory markers, and cognitive performance should be tested at different ages to determine if and through what mechanisms FXII is involved. The role of Aβ in this process may be defined by intravenous treatment of groups of mice with an anti-Aβ antibody. If FXII deficiency is protective in AD mouse models, the relative contributions of FXI-driven coagulation and kallikrein-driven inflammation can be determined by creating AD lines lacking FXI or kallikrein.

Plasma contact system activation as a biomarker for AD. Increased plasma kallikrein activity and HK cleavage found in AD patients and mouse models (Figures 5.2-5.4) could be an exciting potential biomarker regardless of whether Aβ-mediated FXII activation is determined to be a causative mechanism in AD development. Increased kallikrein activity and HK cleavage will need to be validated in a larger cohort that includes individuals with familial and sporadic AD as well as individuals with other neurodegenerative diseases. Furthermore, blood collection protocols will need to be optimized to take advantage of the potential amplification of *in vivo* contact system activation observed in plasma from Group 1, and standardized to minimize differences in plasma activation during collection and storage. Most likely, HK cleavage would need to be used in conjunction with other disease markers to serve as a diagnostic tool for AD, since FXII activation and HK cleavage may also be features of unrelated disease states. Increased levels of FXIIa have been found in chronic conditions such as systemic amyloidosis[122] and hyperlipidemia[265] as well as following acute conditions such as ischemic stroke[266] and myocardial infarction[267]. Increased cleavage of HK has been observed in chronic conditions like systemic lupus erythematosus[268], certain cancers[269], and during acute attacks in hereditary angioedema[270]. Evaluation of larger populations would help determine appropriate cut-off values for FXII activation and HK cleavage that may differentiate between AD and other disease states. For improved discrimination between AD and other disease states, plasma HK cleavage should also be tested as part of a panel of plasma components associated with AD as in [271-273]. The development of an ELISA capable of distinguishing between cleaved and uncleaved HK would be beneficial to such studies.

Role of contact system activation in the brain parenchyma. My results demonstrating increased levels of cleaved HK in AD patient and mouse model brain parenchyma strongly implicate contact system activation in brain tissue. The origin of contact activation proteins in

the AD brain is unclear. FXII and prekallikrein expression in normal brain tissue have been reported[190,192,193], but HK mRNA was only detected under pathological conditions[192,194]. FXII, prekallikrein, and HK expression should be measured in AD mice and controls as a function of age and AD pathology. If local expression is not found, the mechanisms by which HK (and several other plasma proteins) extravasating across the BBB are retained in the AD brain while others are not will need to be investigated. The effect of HK cleavage in brain tissue on glial and neuronal health should also be investigated. While bradykinin released from HK could have proinflammatory and vasoactive effects, cleaved HK itself has anti-angiogenic properties, and FXII and FXIIa are signaling molecules[274].

Epidemiological studies. AD risk should be assessed in individuals with deficiency in functional FXII, FXI, HK, and prekallikrein. Based on my results and model, these individuals would be expected to be protected from AD. By contrast, AD risk may be elevated in individuals with gain-of-function mutations in FXII or with decreased levels of functional C1 esterase inhibitor.

Aβ-mediated contact system activation and complement. Accumulating evidence implicates complement activation in AD[275,276]. Complement pathways can be activated by Aβ directly[275] or by Aβ-induced FXIIa and kallikrein activity[277]. It would be interesting to determine the relative contributions of direct Aβ-mediated complement activation vs. Aβ-induced, contact system-mediated complement activation in AD. This can be accomplished by blocking FXIIa and kallikrein activity in AD mice using ASOs, inhibitors, or genetics. Most studies have thus far focused on the role of complement in the brain parenchyma. The role of plasma complement activation in vascular pathology and AD development should be investigated.

Aβ40. An interesting consideration is the role of Aβ40 (which is more abundant in the circulation than Aβ42) in the activation of FXII-dependent processes. Preliminary results indicate that Aβ40 can also trigger FXII-dependent FXI activation and HK cleavage in plasma, although not as strongly as Aβ42. It is possible that the combined action of Aβ42 and Aβ40 may be additive or even synergistic in triggering these pathways.

6.10. Conclusion

Cerebrovascular dysfunction and dysregulation of CBF are early processes in AD development, preceding Aβ plaque deposition, neuronal damage, and cognitive decline in AD[28,244,278,279]. Factors modulating CBF and vascular function could therefore have profound effects on disease onset and progression. In this thesis, I provided evidence that Aβ42 could be a driver of cerebrovascular dysfunction through activation of FXII, the primary trigger of both the intrinsic coagulation pathway and the kallikrein-kinin system, and through its interaction with fibrinogen.

Because AD is a complex and multifactorial disease, it is unlikely that a single pathogenic mechanism will emerge. The ability to identify groups of patients with AD driven by specific mechanisms and to treat them accordingly would be a major advance in the field. If contact system activation is found to play a causative role in AD pathogenesis, targeting FXII, which is dispensable for hemostasis[117], could provide novel therapeutic opportunities for individuals with elevated plasma HK cleavage.

REFERENCES

1 Thies, W., Bleiler, L. & Alzheimer's, A. 2013 Alzheimer's disease facts and figures. *Alzheimers Dement* **9**, 208-245, (2013).

2 Weintraub, S., Wicklund, A. H. & Salmon, D. P. The neuropsychological profile of Alzheimer disease. *Cold Spring Harb Perspect Med* **2**, a006171, (2012).

3 Glenner, G. G. & Wong, C. W. Alzheimer's disease: initial report of the purification and characterization of a novel cerebrovascular amyloid protein. *Biochem Biophys Res Commun* **120**, 885-890, (1984).

4 Grundke-Iqbal, I. *et al.* Abnormal phosphorylation of the microtubule-associated protein tau (tau) in Alzheimer cytoskeletal pathology. *Proc Natl Acad Sci U S A* **83**, 4913-4917, (1986).

5 Sisodia, S. S. & St George-Hyslop, P. H. gamma-Secretase, Notch, Abeta and Alzheimer's disease: where do the presenilins fit in? *Nat Rev Neurosci* **3**, 281-290, (2002).

6 Saido, T. & Leissring, M. A. Proteolytic degradation of amyloid beta-protein. *Cold Spring Harb Perspect Med* **2**, a006379, (2012).

7 Paresce, D. M., Ghosh, R. N. & Maxfield, F. R. Microglial cells internalize aggregates of the Alzheimer's disease amyloid beta-protein via a scavenger receptor. *Neuron* **17**, 553-565, (1996).

8 Wyss-Coray, T. *et al.* Adult mouse astrocytes degrade amyloid-beta in vitro and in situ. *Nat Med* **9**, 453-457, (2003).

9 Weller, R. O., Subash, M., Preston, S. D., Mazanti, I. & Carare, R. O. Perivascular drainage of amyloid-beta peptides from the brain and its failure in cerebral amyloid angiopathy and Alzheimer's disease. *Brain pathology* **18**, 253-266, (2008).

10 Deane, R., Bell, R. D., Sagare, A. & Zlokovic, B. V. Clearance of amyloid-beta peptide across the blood-brain barrier: implication for therapies in Alzheimer's disease. *CNS & neurological disorders drug targets* **8**, 16-30, (2009).

11 Selkoe, D. J. Toward a comprehensive theory for Alzheimer's disease. Hypothesis: Alzheimer's disease is caused by the cerebral accumulation and cytotoxicity of amyloid beta-protein. *Ann N Y Acad Sci* **924**, 17-25, (2000).

12 Bateman, R. J. *et al.* Autosomal-dominant Alzheimer's disease: a review and proposal for the prevention of Alzheimer's disease. *Alzheimer's research & therapy* **3**, 1, (2011).

13 Wilcock, D. M. & Griffin, W. S. Down's syndrome, neuroinflammation, and Alzheimer neuropathogenesis. *J Neuroinflammation* **10**, 84, (2013).

14 Selkoe, D. J. Clearing the brain's amyloid cobwebs. *Neuron* **32**, 177-180, (2001).

15 Tanzi, R. E., Moir, R. D. & Wagner, S. L. Clearance of Alzheimer's Abeta peptide: the many roads to perdition. *Neuron* **43**, 605-608, (2004).

16 Mawuenyega, K. G. *et al.* Decreased clearance of CNS beta-amyloid in Alzheimer's disease. *Science* **330**, 1774, (2010).

17 Strittmatter, W. J. *et al.* Apolipoprotein E: high-avidity binding to beta-amyloid and increased frequency of type 4 allele in late-onset familial Alzheimer disease. *Proc Natl Acad Sci U S A* **90**, 1977-1981, (1993).

18 Corder, E. H. *et al.* Gene dose of apolipoprotein E type 4 allele and the risk of Alzheimer's disease in late onset families. *Science* **261**, 921-923, (1993).

19 Deane, R. *et al.* apoE isoform-specific disruption of amyloid beta peptide clearance from mouse brain. *J Clin Invest* **118**, 4002-4013, (2008).

20 Reddy, P. H. & Beal, M. F. Amyloid beta, mitochondrial dysfunction and synaptic damage: implications for cognitive decline in aging and Alzheimer's disease. *Trends in molecular medicine* **14**, 45-53, (2008).

21 Lambert, M. P. *et al.* Diffusible, nonfibrillar ligands derived from Abeta1-42 are potent central nervous system neurotoxins. *Proc Natl Acad Sci U S A* **95**, 6448-6453, (1998).

22 Shankar, G. M. *et al.* Natural oligomers of the Alzheimer amyloid-beta protein induce reversible synapse loss by modulating an NMDA-type glutamate receptor-dependent signaling pathway. *J Neurosci* **27**, 2866-2875, (2007).

23 Klyubin, I. *et al.* Amyloid beta protein dimer-containing human CSF disrupts synaptic plasticity: prevention by systemic passive immunization. *J Neurosci* **28**, 4231-4237, (2008).

24 Wyss-Coray, T. & Rogers, J. Inflammation in Alzheimer disease-a brief review of the basic science and clinical literature. *Cold Spring Harb Perspect Med* **2**, a006346, (2012).

25 Davis, D. G., Schmitt, F. A., Wekstein, D. R. & Markesbery, W. R. Alzheimer neuropathologic alterations in aged cognitively normal subjects. *Journal of neuropathology and experimental neurology* **58**, 376-388, (1999).

26 Schneider, J. A., Arvanitakis, Z., Bang, W. & Bennett, D. A. Mixed brain pathologies account for most dementia cases in community-dwelling older persons. *Neurology* **69**, 2197-2204, (2007).

27 De Meyer, G. *et al.* Diagnosis-independent Alzheimer disease biomarker signature in cognitively normal elderly people. *Arch Neurol* **67**, 949-956, (2010).

28 Zlokovic, B. V. Neurovascular pathways to neurodegeneration in Alzheimer's disease and other disorders. *Nat Rev Neurosci* **12**, 723-738, (2011).

29 de la Torre, J. C. Cerebral hemodynamics and vascular risk factors: setting the stage for Alzheimer's disease. *J Alzheimers Dis* **32**, 553-567, (2012).

30 Kalaria, R. N. & Ballard, C. Overlap between pathology of Alzheimer disease and vascular dementia. *Alzheimer Dis Assoc Disord* **13 Suppl 3**, S115-123, (1999).

31 Miyakawa, T., Uehara, Y., Desaki, J., Kimura, T. & Kuramoto, R. Morphological changes of microvessels in the brain with Alzheimer's disease. *The Japanese journal of psychiatry and neurology* **42**, 819-824, (1988).

32 Attems, J., Jellinger, K., Thal, D. R. & Van Nostrand, W. Review: sporadic cerebral amyloid angiopathy. *Neuropathol Appl Neurobiol* **37**, 75-93, (2011).

33 Hunter, J. M. *et al.* Morphological and pathological evolution of the brain microcirculation in aging and Alzheimer's disease. *PloS one* **7**, e36893, (2012).

34 de la Torre, J. C. Alzheimer disease as a vascular disorder: nosological evidence. *Stroke* **33**, 1152-1162, (2002).

35 Kalaria, R. N. The blood-brain barrier and cerebrovascular pathology in Alzheimer's disease. *Ann N Y Acad Sci* **893**, 113-125, (1999).

36 Kalaria, R. N. The role of cerebral ischemia in Alzheimer's disease. *Neurobiol Aging* **21**, 321-330, (2000).

37 Bowman, G. L. & Quinn, J. F. Alzheimer's disease and the Blood-Brain Barrier: Past, Present and Future. *Aging health* **4**, 47-55, (2008).

38 Farrall, A. J. & Wardlaw, J. M. Blood-brain barrier: ageing and microvascular disease--systematic review and meta-analysis. *Neurobiol Aging* **30**, 337-352, (2009).

39 Sagare, A. P., Bell, R. D. & Zlokovic, B. V. Neurovascular dysfunction and faulty amyloid beta-peptide clearance in Alzheimer disease. *Cold Spring Harb Perspect Med* **2**, (2012).

40 Vermeer, S. E. *et al.* Silent brain infarcts and the risk of dementia and cognitive decline. *N Engl J Med* **348**, 1215-1222, (2003).

41 de la Torre, J. C. Is Alzheimer's disease a neurodegenerative or a vascular disorder? Data, dogma, and dialectics. *Lancet Neurol* **3**, 184-190, (2004).

42 Humpel, C. Chronic mild cerebrovascular dysfunction as a cause for Alzheimer's disease? *Exp Gerontol* **46**, 225-232, (2011).

43 Brickman, A. M. Contemplating Alzheimer's disease and the contribution of white matter hyperintensities. *Current neurology and neuroscience reports* **13**, 415, (2013).

44 Defrancesco, M. *et al.* Impact of white matter lesions and cognitive deficits on conversion from mild cognitive impairment to Alzheimer's disease. *J Alzheimers Dis* **34**, 665-672, (2013).

45 Bell, R. D. & Zlokovic, B. V. Neurovascular mechanisms and blood-brain barrier disorder in Alzheimer's disease. *Acta Neuropathol* **118**, 103-113, (2009).

46 Pimentel-Coelho, P. M. & Rivest, S. The early contribution of cerebrovascular factors to the pathogenesis of Alzheimer's disease. *The European journal of neuroscience* **35**, 1917-1937, (2012).

47 Farkas, E. & Luiten, P. G. Cerebral microvascular pathology in aging and Alzheimer's disease. *Progress in neurobiology* **64**, 575-611, (2001).

48 Velliquette, R. A., O'Connor, T. & Vassar, R. Energy inhibition elevates beta-secretase levels and activity and is potentially amyloidogenic in APP transgenic mice: possible early events in Alzheimer's disease pathogenesis. *J Neurosci* **25**, 10874-10883, (2005).

49 Zhang, X. & Le, W. Pathological role of hypoxia in Alzheimer's disease. *Exp Neurol* **223**, 299-303, (2010).

50 Garcia-Alloza, M. *et al.* Cerebrovascular lesions induce transient beta-amyloid deposition. *Brain* **134**, 3697-3707, (2011).

51 Bolay, H. *et al.* Persistent defect in transmitter release and synapsin phosphorylation in cerebral cortex after transient moderate ischemic injury. *Stroke* **33**, 1369-1375, (2002).

52 Mari, D. *et al.* Hemostasis abnormalities in patients with vascular dementia and Alzheimer's disease. *Thromb Haemost* **75**, 216-218, (1996).

53 Gupta, A. *et al.* Coagulation and inflammatory markers in Alzheimer's and vascular dementia. *Int J Clin Pract* **59**, 52-57, (2005).

54 Sevush, S. *et al.* Platelet activation in Alzheimer disease. *Arch Neurol* **55**, 530-536, (1998).

55 Ciabattoni, G. *et al.* Determinants of platelet activation in Alzheimer's disease. *Neurobiol Aging* **28**, 336-342, (2007).

56 Brundel, M., de Bresser, J., van Dillen, J. J., Kappelle, L. J. & Biessels, G. J. Cerebral microinfarcts: a systematic review of neuropathological studies. *J Cereb Blood Flow Metab* **32**, 425-436, (2012).

57 van Rooden, S. *et al.* Increased number of microinfarcts in Alzheimer disease at 7-T MR imaging. *Radiology* **270**, 205-211, (2014).

58 Chi, N. F., Chien, L. N., Ku, H. L., Hu, C. J. & Chiou, H. Y. Alzheimer disease and risk of stroke: a population-based cohort study. *Neurology* **80**, 705-711, (2013).

59 Cortes-Canteli, M. *et al.* Fibrinogen and beta-Amyloid Association Alters Thrombosis and Fibrinolysis: a Possible Contributing Factor to Alzheimer's Disease. *Neuron* **66**, (2010).

60 Jarre, A. *et al.* Pre-activated blood platelets and a pro-thrombotic phenotype in APP23 mice modeling Alzheimer's disease. *Cellular signalling*, (2014).

61 Stott, D. J. *et al.* Activation of hemostasis and decline in cognitive function in older people. *Arterioscler Thromb Vasc Biol* **30**, 605-611, (2010).

62 Dale, G. L. Coated-platelets: an emerging component of the procoagulant response. *J Thromb Haemost* **3**, 2185-2192, (2005).

63 Prodan, C. I., Ross, E. D., Vincent, A. S. & Dale, G. L. Rate of progression in Alzheimer's disease correlates with coated-platelet levels--a longitudinal study. *Transl Res* **152**, 99-102, (2008).

64 Prodan, C. I. *et al.* Coated-platelet levels and progression from mild cognitive impairment to Alzheimer disease. *Neurology* **76**, 247-252, (2011).

65 Bots, M. L. *et al.* Response to activated protein C in subjects with and without dementia. The Dutch Vascular Factors in Dementia Study. *Haemostasis* **28**, 209-215, (1998).

66 Seshadri, S. *et al.* Plasma homocysteine as a risk factor for dementia and Alzheimer's disease. *N Engl J Med* **346**, 476-483, (2002).

67 Kivipelto, M. *et al.* Homocysteine and holo-transcobalamin and the risk of dementia and Alzheimers disease: a prospective study. *European journal of neurology : the official journal of the European Federation of Neurological Societies* **16**, 808-813, (2009).

68 Hooshmand, B. *et al.* Homocysteine and holotranscobalamin and the risk of Alzheimer disease: a longitudinal study. *Neurology* **75**, 1408-1414, (2010).

69 van Oijen, M., Witteman, J. C., Hofman, A., Koudstaal, P. J. & Breteler, M. M. Fibrinogen is associated with an increased risk of Alzheimer disease and vascular dementia. *Stroke* **36**, 2637-2641, (2005).

70 Kokmen, E., Whisnant, J. P., O'Fallon, W. M., Chu, C. P. & Beard, C. M. Dementia after ischemic stroke: a population-based study in Rochester, Minnesota (1960-1984). *Neurology* **46**, 154-159, (1996).

71 Honig, L. S. *et al.* Stroke and the risk of Alzheimer disease. *Arch Neurol* **60**, 1707-1712, (2003).

72 Cumming, T. B. & Brodtmann, A. Can stroke cause neurodegenerative dementia? *Int J Stroke* **6**, 416-424, (2011).

73 Ratner, J., Rosenberg, G., Kral, V. A. & Engelsmann, F. Anticoagulant therapy for senile dementia. *J Am Geriatr Soc* **20**, 556-559, (1972).

74 Walsh, A. C., Walsh, B. H. & Melaney, C. Senile-presenile dementia: follow-up data on an effective psychotherapy-anticoagulant regimen. *J Am Geriatr Soc* **26**, 467-470, (1978).

75 Walsh, A. C. Anticoagulant therapy for Alzheimer's disease. *J Neuropsychiatry Clin Neurosci* **8**, 361-362, (1996).

76 Bergamaschini, L. *et al.* Peripheral treatment with enoxaparin, a low molecular weight heparin, reduces plaques and beta-amyloid accumulation in a mouse model of Alzheimer's disease. *J Neurosci* **24**, 4181-4186, (2004).

77 Timmer, N. M. *et al.* Enoxaparin treatment administered at both early and late stages of amyloid beta deposition improves cognition of APPswe/PS1dE9 mice with differential effects on brain Abeta levels. *Neurobiol Dis* **40**, 340-347, (2010).

78 Trager, U. & Tabrizi, S. J. Peripheral inflammation in neurodegeneration. *Journal of molecular medicine* **91**, 673-681, (2013).

79 Sofroniew, M. V. & Vinters, H. V. Astrocytes: biology and pathology. *Acta Neuropathol* **119**, 7-35, (2010).

80 Verkhratsky, A., Olabarria, M., Noristani, H. N., Yeh, C. Y. & Rodriguez, J. J. Astrocytes in Alzheimer's disease. *Neurotherapeutics : the journal of the American Society for Experimental NeuroTherapeutics* **7**, 399-412, (2010).

81 Schwab, C. & McGeer, P. L. Inflammatory aspects of Alzheimer disease and other neurodegenerative disorders. *J Alzheimers Dis* **13**, 359-369, (2008).

82 Aisen, P. S. & Davis, K. L. Inflammatory mechanisms in Alzheimer's disease: implications for therapy. *The American journal of psychiatry* **151**, 1105-1113, (1994).

83 Wyss-Coray, T. Inflammation in Alzheimer disease: driving force, bystander or beneficial response? *Nat Med* **12**, 1005-1015, (2006).

84 Rodriguez, J. J., Witton, J., Olabarria, M., Noristani, H. N. & Verkhratsky, A. Increase in the density of resting microglia precedes neuritic plaque formation and microglial activation in a transgenic model of Alzheimer's disease. *Cell death & disease* **1**, e1, (2010).

85 Wright, A. L. *et al.* Neuroinflammation and neuronal loss precede Abeta plaque deposition in the hAPP-J20 mouse model of Alzheimer's disease. *PloS one* **8**, e59586, (2013).

86 Okello, A. *et al.* Microglial activation and amyloid deposition in mild cognitive impairment: a PET study. *Neurology* **72**, 56-62, (2009).

87 Olsson, B. *et al.* Microglial markers are elevated in the prodromal phase of Alzheimer's disease and vascular dementia. *J Alzheimers Dis* **33**, 45-53, (2013).

88 Cagnin, A. *et al.* In-vivo measurement of activated microglia in dementia. *Lancet* **358**, 461-467, (2001).

89 Parachikova, A. *et al.* Inflammatory changes parallel the early stages of Alzheimer disease. *Neurobiol Aging* **28**, 1821-1833, (2007).

90 Engelhart, M. J. *et al.* Inflammatory proteins in plasma and the risk of dementia: the rotterdam study. *Arch Neurol* **61**, 668-672, (2004).

91 Dunn, N., Mullee, M., Perry, V. H. & Holmes, C. Association between dementia and infectious disease: evidence from a case-control study. *Alzheimer Dis Assoc Disord* **19**, 91-94, (2005).

92 Holmes, C. *et al.* Systemic infection, interleukin 1beta, and cognitive decline in Alzheimer's disease. *Journal of neurology, neurosurgery, and psychiatry* **74**, 788-789, (2003).

93 Nishimura, N. & Schaffer, C. B. Big effects from tiny vessels: imaging the impact of microvascular clots and hemorrhages on the brain. *Stroke* **44**, S90-92, (2013).

94 Nguyen, J., Nishimura, N., Fetcho, R. N., Iadecola, C. & Schaffer, C. B. Occlusion of cortical ascending venules causes blood flow decreases, reversals in flow direction, and vessel dilation in upstream capillaries. *J Cereb Blood Flow Metab* **31**, 2243-2254, (2011).

95 Chiu, J. J. & Chien, S. Effects of disturbed flow on vascular endothelium: pathophysiological basis and clinical perspectives. *Physiological reviews* **91**, 327-387, (2011).

96 Garcia, J. G. *et al.* Thrombin-induced increase in albumin permeability across the endothelium. *Journal of cellular physiology* **128**, 96-104, (1986).

97 Aschner, J. L., Lennon, J. M., Fenton, J. W., 2nd, Aschner, M. & Malik, A. B. Enzymatic activity is necessary for thrombin-mediated increase in endothelial permeability. *The American journal of physiology* **259**, L270-275, (1990).

98 Rabiet, M. J. *et al.* Thrombin-induced increase in endothelial permeability is associated with changes in cell-to-cell junction organization. *Arterioscler Thromb Vasc Biol* **16**, 488-496, (1996).

99 Liu, D. Z. *et al.* Blood-brain barrier breakdown and repair by Src after thrombin-induced injury. *Ann Neurol* **67**, 526-533, (2010).

100 Chen, B., Cheng, Q., Yang, K. & Lyden, P. D. Thrombin mediates severe neurovascular injury during ischemia. *Stroke* **41**, 2348-2352, (2010).

101 Wardlaw, J. M. Blood-brain barrier and cerebral small vessel disease. *J Neurol Sci* **299**, 66-71, (2010).

102 Schreiber, S., Bueche, C. Z., Garz, C. & Braun, H. Blood brain barrier breakdown as the starting point of cerebral small vessel disease? - New insights from a rat model. *Experimental & translational stroke medicine* **5**, 4, (2013).

103 Rabiet, M. J., Plantier, J. L. & Dejana, E. Thrombin-induced endothelial cell dysfunction. *British medical bulletin* **50**, 936-945, (1994).

104 Schoenmakers, S. H., Reitsma, P. H. & Spek, C. A. Blood coagulation factors as inflammatory mediators. *Blood Cells Mol Dis* **34**, 30-37, (2005).

105 Abbott, N. J. Inflammatory mediators and modulation of blood-brain barrier permeability. *Cellular and molecular neurobiology* **20**, 131-147, (2000).

106 Leeb-Lundberg, L. M., Marceau, F., Muller-Esterl, W., Pettibone, D. J. & Zuraw, B. L. International union of pharmacology. XLV. Classification of the kinin receptor family: from molecular mechanisms to pathophysiological consequences. *Pharmacol Rev* **57**, 27-77, (2005).

107 Zhang, C. The role of inflammatory cytokines in endothelial dysfunction. *Basic research in cardiology* **103**, 398-406, (2008).

108 Carter, A. M. Complement activation: an emerging player in the pathogenesis of cardiovascular disease. *Scientifica* **2012**, 402783, (2012).

109 Ruan, X. Z. *et al.* Mechanisms of dysregulation of low-density lipoprotein receptor expression in vascular smooth muscle cells by inflammatory cytokines. *Arterioscler Thromb Vasc Biol* **26**, 1150-1155, (2006).

110 McColl, B. W., Rothwell, N. J. & Allan, S. M. Systemic inflammation alters the kinetics of cerebrovascular tight junction disruption after experimental stroke in mice. *J Neurosci* **28**, 9451-9462, (2008).

111 Denes, A., Ferenczi, S. & Kovacs, K. J. Systemic inflammatory challenges compromise survival after experimental stroke via augmenting brain inflammation, blood- brain barrier damage and brain oedema independently of infarct size. *J Neuroinflammation* **8**, 164, (2011).

112 Takeda, S. *et al.* Increased blood-brain barrier vulnerability to systemic inflammation in an Alzheimer disease mouse model. *Neurobiol Aging* **34**, 2064-2070, (2013).

113 Weber, C. & Noels, H. Atherosclerosis: current pathogenesis and therapeutic options. *Nat Med* **17**, 1410-1422, (2011).

114 Markus, H. S. Genes, endothelial function and cerebral small vessel disease in man. *Experimental physiology* **93**, 121-127, (2008).

115 Wardlaw, J. M., Smith, C. & Dichgans, M. Mechanisms of sporadic cerebral small vessel disease: insights from neuroimaging. *Lancet Neurol* **12**, 483-497, (2013).

116 Grinberg, L. T. & Thal, D. R. Vascular pathology in the aged human brain. *Acta Neuropathol* **119**, 277-290, (2010).

117 Renné, T., Schmaier, A. H., Nickel, K. F., Blomback, M. & Maas, C. In vivo roles of factor XII. *Blood* **120**, 4296-4303, (2012).

118 Ghebrehiwet, B., Silverberg, M. & Kaplan, A. P. Activation of the classical pathway of complement by Hageman factor fragment. *J Exp Med* **153**, 665-676, (1981).

119 DiScipio, R. G. The activation of the alternative pathway C3 convertase by human plasma kallikrein. *Immunology* **45**, 587-595, (1982).

120 Amara, U. *et al.* Molecular intercommunication between the complement and coagulation systems. *Journal of immunology* **185**, 5628-5636, (2010).

121 Shibayama, Y. *et al.* Zinc-dependent activation of the plasma kinin-forming cascade by aggregated beta amyloid protein. *Clin Immunol* **90**, 89-99, (1999).

122 Maas, C. *et al.* Misfolded proteins activate factor XII in humans, leading to kallikrein formation without initiating coagulation. *J Clin Invest* **118**, 3208-3218, (2008).

123 Bergamaschini, L. *et al.* The region 1-11 of Alzheimer amyloid-beta is critical for activation of contact-kinin system. *Neurobiol Aging* **22**, 63-69, (2001).

124 Wolberg, A. S. & Campbell, R. A. Thrombin generation, fibrin clot formation and hemostasis. *Transfus Apher Sci* **38**, 15-23, (2008).

125 Ahn, H. J. *et al.* Alzheimer's disease peptide beta-amyloid interacts with fibrinogen and induces its oligomerization. *Proc Natl Acad Sci U S A* **107**, 21812-21817, (2010).

126 Skovronsky, D. M., Lee, V. M. & Pratico, D. Amyloid precursor protein and amyloid beta peptide in human platelets. Role of cyclooxygenase and protein kinase C. *J Biol Chem* **276**, 17036-17043, (2001).

127 Kokjohn, T. A. *et al.* Chemical characterization of pro-inflammatory amyloid-beta peptides in human atherosclerotic lesions and platelets. *Biochim Biophys Acta* **1812**, 1508-1514, (2011).

128 Deutsch, D. G. & Mertz, E. T. Plasminogen: purification from human plasma by affinity chromatography. *Science* **170**, 1095-1096, (1970).

129 Everse, S. J., Pelletier, H. & Doolittle, R. F. Crystallization of fragment D from human fibrinogen. *Protein science : a publication of the Protein Society* **4**, 1013-1016, (1995).

130 Schneider, C. A., Rasband, W. S. & Eliceiri, K. W. NIH Image to ImageJ: 25 years of image analysis. *Nature methods* **9**, 671-675, (2012).

131 Otwinowski, Z. & Minor, W. in *Methods in Enzymology* Vol. Volume 276 (ed Charles W. Carter, Jr.) 307-326 (Academic Press, 1997).

132 Spraggon, G., Everse, S. J. & Doolittle, R. F. Crystal structures of fragment D from human fibrinogen and its crosslinked counterpart from fibrin. *Nature* **389**, 455-462, (1997).

133 Adams, P. D. *et al.* PHENIX: a comprehensive Python-based system for macromolecular structure solution. *Acta crystallographica. Section D, Biological crystallography* **66**, 213-221, (2010).

134 Atwood, C. S. *et al.* Dramatic aggregation of Alzheimer abeta by Cu(II) is induced by conditions representing physiological acidosis. *J Biol Chem* **273**, 12817-12826, (1998).

135 Fleury, V. & Angles-Cano, E. Characterization of the binding of plasminogen to fibrin surfaces: the role of carboxy-terminal lysines. *Biochemistry* **30**, 7630-7638, (1991).

136 Boulaftali, Y. *et al.* Platelet protease nexin-1, a serpin that strongly influences fibrinolysis and thrombolysis. *Circulation* **123**, 1326-1334.

137 Mutch, N. J., Engel, R., Uitte de Willige, S., Philippou, H. & Ariens, R. A. Polyphosphate modifies the fibrin network and down-regulates fibrinolysis by attenuating binding of tPA and plasminogen to fibrin. *Blood* **115**, 3980-3988, (2010).

138 Longstaff, C. *et al.* The interplay between tissue plasminogen activator domains and fibrin structures in the regulation of fibrinolysis: kinetic and microscopic studies. *Blood* **117**, 661-668, (2011).

139 Stine, W. B., Jungbauer, L., Yu, C. & LaDu, M. J. Preparing synthetic Abeta in different aggregation states. *Methods Mol Biol* **670**, 13-32, (2011).

140 Gailani, D., Lasky, N. M. & Broze, G. J., Jr. A murine model of factor XI deficiency. *Blood Coagul Fibrinolysis* **8**, 134-144, (1997).

141 Pauer, H. U. *et al.* Targeted deletion of murine coagulation factor XII gene-a model for contact phase activation in vivo. *Thromb Haemost* **92**, 503-508, (2004).

142 Oakley, H. *et al.* Intraneuronal beta-amyloid aggregates, neurodegeneration, and neuron loss in transgenic mice with five familial Alzheimer's disease mutations: potential factors in amyloid plaque formation. *J Neurosci* **26**, 10129-10140, (2006).

143 Chishti, M. A. *et al.* Early-onset amyloid deposition and cognitive deficits in transgenic mice expressing a double mutant form of amyloid precursor protein 695. *J Biol Chem* **276**, 21562-21570, (2001).

144 Hemker, H. C. *et al.* The calibrated automated thrombogram (CAT): a universal routine test for hyper- and hypocoagulability. *Pathophysiol Haemost Thromb* **32**, 249-253, (2002).

145 Larsson, M. *et al.* A factor XIIa inhibitory antibody provides thromboprotection in extracorporeal circulation without increasing bleeding risk. *Science translational medicine* **6**, 222ra217, (2014).

146 Tchaikovski, S. N., BJ, V. A. N. V., Rosing, J. & Tans, G. Development of a calibrated automated thrombography based thrombin generation test in mouse plasma. *J Thromb Haemost* **5**, 2079-2086, (2007).

147 Mirra, S. S. *et al.* The Consortium to Establish a Registry for Alzheimer's Disease (CERAD). Part II. Standardization of the neuropathologic assessment of Alzheimer's disease. *Neurology* **41**, 479-486, (1991).

148 Fagan, A. M. *et al.* Decreased cerebrospinal fluid Abeta(42) correlates with brain atrophy in cognitively normal elderly. *Ann Neurol* **65**, 176-183, (2009).

149 Gallimore, M. J. & Friberger, P. Simple chromogenic peptide substrate assays for determining prekallikrein, kallikrein inhibition and kallikrein "like" activity in human plasma. *Thromb Res* **25**, 293-298, (1982).

150 Weisel, J. W. Fibrinogen and fibrin. *Advances in protein chemistry* **70**, 247-299, (2005).

151 Kanski, J., Aksenova, M. & Butterfield, D. A. The hydrophobic environment of Met35 of Alzheimer's Abeta(1-42) is important for the neurotoxic and oxidative properties of the peptide. *Neurotoxicity research* **4**, 219-223, (2002).

152 Kanski, J., Aksenova, M., Schoneich, C. & Butterfield, D. A. Substitution of isoleucine-31 by helical-breaking proline abolishes oxidative stress and neurotoxic properties of Alzheimer's amyloid beta-peptide. *Free radical biology & medicine* **32**, 1205-1211, (2002).

153 Everse, S. J., Spraggon, G., Veerapandian, L. & Doolittle, R. F. Conformational changes in fragments D and double-D from human fibrin(ogen) upon binding the peptide ligand Gly-His-Arg-Pro-amide. *Biochemistry* **38**, 2941-2946, (1999).

154 Medved, L. & Nieuwenhuizen, W. Molecular mechanisms of initiation of fibrinolysis by fibrin. *Thromb Haemost* **89**, 409-419, (2003).

155 Schielen, W. J., Voskuilen, M., Tesser, G. I. & Nieuwenhuizen, W. The sequence A alpha-(148-160) in fibrin, but not in fibrinogen, is accessible to monoclonal antibodies. *Proc Natl Acad Sci U S A* **86**, 8951-8954, (1989).

156 Carr, M. E., Jr. & Alving, B. M. Effect of fibrin structure on plasmin-mediated dissolution of plasma clots. *Blood Coagul Fibrinolysis* **6**, 567-573, (1995).

157 Weisel, J. W., Veklich, Y., Collet, J. P. & Francis, C. W. Structural studies of fibrinolysis by electron and light microscopy. *Thromb Haemost* **82**, 277-282, (1999).

158 Collet, J. P. *et al.* Influence of fibrin network conformation and fibrin fiber diameter on fibrinolysis speed: dynamic and structural approaches by confocal microscopy. *Arterioscler Thromb Vasc Biol* **20**, 1354-1361, (2000).

159 Sabovic, M. & Blinc, A. Biochemical and biophysical conditions for blood clot lysis. *Pflugers Arch* **440**, R134-136, (2000).

160 Kolev, K., Tenekedjiev, K., Komorowicz, E. & Machovich, R. Functional evaluation of the structural features of proteases and their substrate in fibrin surface degradation. *J Biol Chem* **272**, 13666-13675, (1997).

161 Lord, S. T. Molecular mechanisms affecting fibrin structure and stability. *Arterioscler Thromb Vasc Biol* **31**, 494-499, (2011).

162 Weisel, J. W. & Medved, L. The structure and function of the alpha C domains of fibrinogen. *Ann N Y Acad Sci* **936**, 312-327, (2001).

163 Collet, J. P., Lesty, C., Montalescot, G. & Weisel, J. W. Dynamic changes of fibrin architecture during fibrin formation and intrinsic fibrinolysis of fibrin-rich clots. *J Biol Chem* **278**, 21331-21335, (2003).

164 Wnendt, S., Wetzels, I. & Gunzler, W. A. Amyloid beta peptides stimulate tissue-type plasminogen activator but not recombinant prourokinase. *Thromb Res* **85**, 217-224, (1997).

165 Kingston, I. B., Castro, M. J. & Anderson, S. In vitro stimulation of tissue-type plasminogen activator by Alzheimer amyloid beta-peptide analogues. *Nat Med* **1**, 138-142, (1995).

166 Kruithof, E. K. & Schleuning, W. D. A comparative study of amyloid-beta (1-42) as a cofactor for plasminogen activation by vampire bat plasminogen activator and recombinant human tissue-type plasminogen activator. *Thromb Haemost* **92**, 559-567, (2004).

167 Boxrud, P. D. & Bock, P. E. Coupling of conformational and proteolytic activation in the kinetic mechanism of plasminogen activation by streptokinase. *J Biol Chem* **279**, 36642-36649, (2004).

168 Aoyagi, S., Imai, R., Sakai, K. & Kudo, M. Reagentless and regenerable immunosensor for monitoring of immunoglobulin G based on non-separation immunoassay. *Biosens Bioelectron* **18**, 791-795, (2003).

169 Watson, D. *et al.* Physicochemical characteristics of soluble oligomeric Abeta and their pathologic role in Alzheimer's disease. *Neurological research* **27**, 869-881, (2005).

170 Wuillemin, W. A. *et al.* Inactivation of factor XIa in human plasma assessed by measuring factor XIa-protease inhibitor complexes: major role for C1-inhibitor. *Blood* **85**, 1517-1526, (1995).

171 Wuillemin, W. A. *et al.* Activation of the intrinsic pathway of coagulation in children with meningococcal septic shock. *Thromb Haemost* **74**, 1436-1441, (1995).

172 Minnema, M. C. *et al.* Activation of clotting factor XI without detectable contact activation in experimental human endotoxemia. *Blood* **92**, 3294-3301, (1998).

173 Konings, J. *et al.* Ongoing contact activation in patients with hereditary angioedema. *PloS one* **8**, e74043, (2013).

174 Squitti, R. *et al.* Ceruloplasmin/Transferrin ratio changes in Alzheimer's disease. *International journal of Alzheimer's disease* **2011**, 231595, (2010).

175 Hui, K. Y., Haber, E. & Matsueda, G. R. Monoclonal antibodies to a synthetic fibrin-like peptide bind to human fibrin but not fibrinogen. *Science* **222**, 1129-1132, (1983).

176 Bergamaschini, L. *et al.* Activation of the contact system in cerebrospinal fluid of patients with Alzheimer disease. *Alzheimer Dis Assoc Disord* **12**, 102-108, (1998).

177 Morris, J. C. The Clinical Dementia Rating (CDR): current version and scoring rules. *Neurology* **43**, 2412-2414, (1993).

178 Folstein, M. F., Folstein, S. E. & McHugh, P. R. "Mini-mental state". A practical method for grading the cognitive state of patients for the clinician. *Journal of psychiatric research* **12**, 189-198, (1975).

179 Hyman, B. T. New neuropathological criteria for Alzheimer disease. *Arch Neurol* **55**, 1174-1176, (1998).

180 Muller, F. *et al.* Platelet polyphosphates are proinflammatory and procoagulant mediators in vivo. *Cell* **139**, 1143-1156, (2009).

181 Kannemeier, C. *et al.* Extracellular RNA constitutes a natural procoagulant cofactor in blood coagulation. *Proc Natl Acad Sci U S A* **104**, 6388-6393, (2007).

182 Renné, T. in *Hemostasis and Thrombosis. Basic Princeples and Clinical Practice.* Vol. 6 (ed VJ Marder, Aird, WC, Bennett, JS, Schulman S, White, GC II) 242-253 (Wolters Kluwer, 2013).

183 Musiek, E. S. & Holtzman, D. M. Origins of Alzheimer's disease: reconciling cerebrospinal fluid biomarker and neuropathology data regarding the temporal sequence of amyloid-beta and tau involvement. *Current opinion in neurology* **25**, 715-720, (2012).

184 Silverberg, M. & Diehl, S. V. The autoactivation of factor XII (Hageman factor) induced by low-Mr heparin and dextran sulphate. The effect of the Mr of the activating polyanion. *The Biochemical journal* **248**, 715-720, (1987).

185 Hojima, Y., Cochrane, C. G., Wiggins, R. C., Austen, K. F. & Stevens, R. L. In vitro activation of the contact (Hageman factor) system of plasma by heparin and chondroitin sulfate E. *Blood* **63**, 1453-1459, (1984).

186 Pixley, R. A., Cassello, A., De La Cadena, R. A., Kaufman, N. & Colman, R. W. Effect of heparin on the activation of factor XII and the contact system in plasma. *Thromb Haemost* **66**, 540-547, (1991).

187 Loeffen, R. *et al.* Preanalytic variables of thrombin generation: towards a standard procedure and validation of the method. *J Thromb Haemost* **10**, 2544-2554, (2012).

188 Ramstrom, S. Clotting time analysis of citrated blood samples is strongly affected by the tube used for blood sampling. *Blood Coagul Fibrinolysis* **16**, 447-452, (2005).

189 Merkulov, S. *et al.* Deletion of murine kininogen gene 1 (mKng1) causes loss of plasma kininogen and delays thrombosis. *Blood* **111**, 1274-1281, (2008).

190 Yasuhara, O., Walker, D. G. & McGeer, P. L. Hageman factor and its binding sites are present in senile plaques of Alzheimer's disease. *Brain Res* **654**, 234-240, (1994).

191 Cerf, M. E. & Raidoo, D. M. Immunolocalization of plasma kallikrein in human brain. *Metabolic brain disease* **15**, 315-323, (2000).

192 Neth, P., Arnhold, M., Nitschko, H. & Fink, E. The mRNAs of prekallikrein, factors XI and XII, and kininogen, components of the contact phase cascade are differentially expressed in multiple non-hepatic human tissues. *Thromb Haemost* **85**, 1043-1047, (2001).

193 Ashby, E. L., Love, S. & Kehoe, P. G. Assessment of activation of the plasma kallikrein-kinin system in frontal and temporal cortex in Alzheimer's disease and vascular dementia. *Neurobiol Aging* **33**, 1345-1355, (2012).

194 Takano, M., Horie, M., Yayama, K. & Okamoto, H. Lipopolysaccharide injection into the cerebral ventricle evokes kininogen induction in the rat brain. *Brain Res* **978**, 72-82, (2003).

195 Braak, H. & Braak, E. Staging of Alzheimer's disease-related neurofibrillary changes. *Neurobiol Aging* **16**, 271-278; discussion 278-284, (1995).

196 Arnold, S. E., Hyman, B. T., Flory, J., Damasio, A. R. & Van Hoesen, G. W. The topographical and neuroanatomical distribution of neurofibrillary tangles and neuritic plaques in the cerebral cortex of patients with Alzheimer's disease. *Cerebral cortex* **1**, 103-116, (1991).

197 Arnold, S. E., Hyman, B. T. & Van Hoesen, G. W. Neuropathologic changes of the temporal pole in Alzheimer's disease and Pick's disease. *Arch Neurol* **51**, 145-150, (1994).

198 Ahn, S. M. *et al.* Human microglial cells synthesize albumin in brain. *PloS one* **3**, e2829, (2008).

199 Yang, Z., Mochalkin, I. & Doolittle, R. F. A model of fibrin formation based on crystal structures of fibrinogen and fibrin fragments complexed with synthetic peptides. *Proc Natl Acad Sci U S A* **97**, 14156-14161, (2000).

200 Smith, C. C. Stimulated release of the beta-amyloid protein of Alzheimer's disease by normal human platelets. *Neuroscience letters* **235**, 157-159, (1997).

201 Kostelansky, M. S., Bolliger-Stucki, B., Betts, L., Gorkun, O. V. & Lord, S. T. B beta Glu397 and B beta Asp398 but not B beta Asp432 are required for "B:b" interactions. *Biochemistry* **43**, 2465-2474, (2004).

202 Bowley, S. R. & Lord, S. T. Fibrinogen variant BbetaD432A has normal polymerization but does not bind knob "B". *Blood* **113**, 4425-4430, (2009).

203 Paul, J., Strickland, S. & Melchor, J. P. Fibrin deposition accelerates neurovascular damage and neuroinflammation in mouse models of Alzheimer's disease. *J Exp Med* **204**, 1999-2008, (2007).

204 Klohs, J. *et al.* Contrast-enhanced magnetic resonance microangiography reveals remodeling of the cerebral microvasculature in transgenic ArcAbeta mice. *J Neurosci* **32**, 1705-1713, (2012).

205 Cortes-Canteli, M., Mattei, L., Richards, A. T., Norris, E. H. & Strickland, S. Fibrin deposited in the Alzheimer's disease brain promotes neuronal degeneration. *Neurobiol Aging* **36**, 608-617, (2015).

206 Ahn, H. J. *et al.* A novel Abeta-fibrinogen interaction inhibitor rescues altered thrombosis and cognitive decline in Alzheimer's disease mice. *J Exp Med* **211**, 1049-1062, (2014).

207 van der Meijden, P. E. *et al.* Dual role of collagen in factor XII-dependent thrombus formation. *Blood* **114**, 881-890, (2009).

208 Deane, R., Wu, Z. & Zlokovic, B. V. RAGE (yin) versus LRP (yang) balance regulates alzheimer amyloid beta-peptide clearance through transport across the blood-brain barrier. *Stroke* **35**, 2628-2631, (2004).

209 Wuillemin, W. A. *et al.* Clearance of human factor XIa-inhibitor complexes in rats. *British journal of haematology* **93**, 950-954, (1996).

210 Herczenik, E. *et al.* Activation of human platelets by misfolded proteins. *Arterioscler Thromb Vasc Biol* **27**, 1657-1665, (2007).

211 Shen, M. Y. *et al.* Amyloid beta peptide-activated signal pathways in human platelets. *Eur J Pharmacol* **588**, 259-266, (2008).

212 Canobbio, I. *et al.* Amyloid beta-peptide-dependent activation of human platelets: essential role for Ca2+ and ADP in aggregation and thrombus formation. *The Biochemical journal* **462**, 513-523, (2014).

213 Wahl, M. *et al.* Vasomotor and permeability effects of bradykinin in the cerebral microcirculation. *Immunopharmacology* **33**, 257-263, (1996).

214 Bergamaschini, L., Donarini, C., Gobbo, G., Parnetti, L. & Gallai, V. Activation of complement and contact system in Alzheimer's disease. *Mech Ageing Dev* **122**, 1971-1983, (2001).

215 Roher, A. E. *et al.* Amyloid beta peptides in human plasma and tissues and their significance for Alzheimer's disease. *Alzheimers Dement* **5**, 18-29, (2009).

216 Jack, C. R., Jr. *et al.* Serial PIB and MRI in normal, mild cognitive impairment and Alzheimer's disease: implications for sequence of pathological events in Alzheimer's disease. *Brain* **132**, 1355-1365, (2009).

217 Bateman, R. J. *et al.* Clinical and biomarker changes in dominantly inherited Alzheimer's disease. *N Engl J Med* **367**, 795-804, (2012).

218 Kuo, Y. M. *et al.* Amyloid-beta peptides interact with plasma proteins and erythrocytes: implications for their quantitation in plasma. *Biochem Biophys Res Commun* **268**, 750-756, (2000).

219 Mayeux, R. & Schupf, N. Blood-based biomarkers for Alzheimer's disease: plasma Abeta40 and Abeta42, and genetic variants. *Neurobiol Aging* **32 Suppl 1**, S10-19, (2011).

220 Pesini, P. *et al.* Reliable Measurements of the beta-Amyloid Pool in Blood Could Help in the Early Diagnosis of AD. *International journal of Alzheimer's disease* **2012**, 604141, (2012).

221 Gabelle, A. *et al.* Plasma amyloid-beta levels and prognosis in incident dementia cases of the 3-City Study. *J Alzheimers Dis* **33**, 381-391, (2013).

222 Caccamo, A., Oddo, S., Sugarman, M. C., Akbari, Y. & LaFerla, F. M. Age- and region-dependent alterations in Abeta-degrading enzymes: implications for Abeta-induced disorders. *Neurobiol Aging* **26**, 645-654, (2005).

223 Hawkes, C. A. *et al.* Regional differences in the morphological and functional effects of aging on cerebral basement membranes and perivascular drainage of amyloid-beta from the mouse brain. *Aging cell* **12**, 224-236, (2013).

224 Mayeux, R. *et al.* Plasma A[beta]40 and A[beta]42 and Alzheimer's disease: relation to age, mortality, and risk. *Neurology* **61**, 1185-1190, (2003).

225 Blasko, I. *et al.* Conversion from cognitive health to mild cognitive impairment and Alzheimer's disease: prediction by plasma amyloid beta 42, medial temporal lobe atrophy and homocysteine. *Neurobiol Aging* **29**, 1-11, (2008).

226 Blasko, I. *et al.* Plasma amyloid beta-42 independently predicts both late-onset depression and Alzheimer disease. *The American journal of geriatric psychiatry : official journal of the American Association for Geriatric Psychiatry* **18**, 973-982, (2010).

227 Schupf, N. *et al.* Peripheral Abeta subspecies as risk biomarkers of Alzheimer's disease. *Proc Natl Acad Sci U S A* **105**, 14052-14057, (2008).

228 Sullivan, G. W., Sarembock, I. J. & Linden, J. The role of inflammation in vascular diseases. *Journal of leukocyte biology* **67**, 591-602, (2000).

229 Oberheiden, T. *et al.* Activation of platelets and cellular coagulation in cerebral small-vessel disease. *Blood Coagul Fibrinolysis* **21**, 729-735, (2010).

230 Levi, M., van der Poll, T. & Buller, H. R. Bidirectional relation between inflammation and coagulation. *Circulation* **109**, 2698-2704, (2004).

231 Verhamme, P. & Hoylaerts, M. F. Hemostasis and inflammation: two of a kind? *Thrombosis journal* **7**, 15, (2009).

232 Cortes-Canteli, M., Zamolodchikov, D., Ahn, H. J., Strickland, S. & Norris, E. H. Fibrinogen and altered hemostasis in Alzheimer's disease. *J Alzheimers Dis* **32**, 599-608, (2012).

233 Braun, H. *et al.* Stases are associated with blood-brain barrier damage and a restricted activation of coagulation in SHRSP. *J Neurol Sci* **322**, 71-76, (2012).

234 Kashyap, V. S. *et al.* Acute arterial thrombosis causes endothelial dysfunction: a new paradigm for thrombolytic therapy. *Journal of vascular surgery* **34**, 323-329, (2001).

235 Dietrich, W. D., Prado, R., Halley, M. & Watson, B. D. Microvascular and neuronal consequences of common carotid artery thrombosis and platelet embolization in rats. *Journal of neuropathology and experimental neurology* **52**, 351-360, (1993).

236 Davalos, D. & Akassoglou, K. Fibrinogen as a key regulator of inflammation in disease. *Semin Immunopathol* **34**, 43-62, (2012).

237 Brun, A. & Englund, E. A white matter disorder in dementia of the Alzheimer type: a pathoanatomical study. *Ann Neurol* **19**, 253-262, (1986).

238 Schley, D., Carare-Nnadi, R., Please, C. P., Perry, V. H. & Weller, R. O. Mechanisms to explain the reverse perivascular transport of solutes out of the brain. *Journal of theoretical biology* **238**, 962-974, (2006).

239 Arbel-Ornath, M. *et al.* Interstitial fluid drainage is impaired in ischemic stroke and Alzheimer's disease mouse models. *Acta Neuropathol* **126**, 353-364, (2013).

240 Kim, D. E., Schellingerhout, D., Jaffer, F. A., Weissleder, R. & Tung, C. H. Near-infrared fluorescent imaging of cerebral thrombi and blood-brain barrier disruption in a mouse model of cerebral venous sinus thrombosis. *J Cereb Blood Flow Metab* **25**, 226-233, (2005).

241 Nordborg, C., Sokrab, T. E. & Johansson, B. B. The relationship between plasma protein extravasation and remote tissue changes after experimental brain infarction. *Acta Neuropathol* **82**, 118-126, (1991).

242 Ryu, J. K., Davalos, D. & Akassoglou, K. Fibrinogen signal transduction in the nervous system. *J Thromb Haemost* **7 Suppl 1**, 151-154, (2009).

243 Sofroniew, M. V. Molecular dissection of reactive astrogliosis and glial scar formation. *Trends in neurosciences* **32**, 638-647, (2009).

244 Johnson, K. A. & Albert, M. S. Perfusion abnormalities in prodromal AD. *Neurobiol Aging* **21**, 289-292, (2000).

245 Wierenga, C. E., Hays, C. C. & Zlatar, Z. Z. Cerebral Blood Flow Measured by Arterial Spin Labeling MRI as a Preclinical Marker of Alzheimer's Disease. *J Alzheimers Dis*, (2014).

246 Dickstein, D. L. *et al.* Abeta peptide immunization restores blood-brain barrier integrity in Alzheimer disease. *FASEB journal : official publication of the Federation of American Societies for Experimental Biology* **20**, 426-433, (2006).

247 Su, G. C., Arendash, G. W., Kalaria, R. N., Bjugstad, K. B. & Mullan, M. Intravascular infusions of soluble beta-amyloid compromise the blood-brain barrier, activate CNS glial cells and induce peripheral hemorrhage. *Brain Res* **818**, 105-117, (1999).

248 Jancso, G. *et al.* Beta-amyloid (1-42) peptide impairs blood-brain barrier function after intracarotid infusion in rats. *Neuroscience letters* **253**, 139-141, (1998).

249 Farkas, I. G. *et al.* Beta-amyloid peptide-induced blood-brain barrier disruption facilitates T-cell entry into the rat brain. *Acta histochemica* **105**, 115-125, (2003).

250 Iores-Marcal, L. M. *et al.* Bradykinin release and inactivation in brain of rats submitted to an experimental model of Alzheimer's disease. *Peptides* **27**, 3363-3369, (2006).

251 Passos, G. F. *et al.* The bradykinin B1 receptor regulates Abeta deposition and neuroinflammation in Tg-SwDI mice. *The American journal of pathology* **182**, 1740-1749, (2013).

252 Lacoste, B., Tong, X. K., Lahjouji, K., Couture, R. & Hamel, E. Cognitive and cerebrovascular improvements following kinin B1 receptor blockade in Alzheimer's disease mice. *J Neuroinflammation* **10**, 57, (2013).

253 Prediger, R. D. *et al.* Genetic deletion or antagonism of kinin B(1) and B(2) receptors improves cognitive deficits in a mouse model of Alzheimer's disease. *Neuroscience* **151**, 631-643, (2008).

254 Muenchhoff, J. *et al.* Plasma Protein Profiling of Mild Cognitive Impairment and Alzheimer's Disease Across Two Independent Cohorts. *J Alzheimers Dis*, (2014).

255 Tripathy, D. *et al.* Thrombin, a mediator of cerebrovascular inflammation in AD and hypoxia. *Frontiers in aging neuroscience* **5**, 19, (2013).

256 Utter, S. *et al.* Cerebral small vessel disease-induced apolipoprotein E leakage is associated with Alzheimer disease and the accumulation of amyloid beta-protein in perivascular astrocytes. *Journal of neuropathology and experimental neurology* **67**, 842-856, (2008).

257 Kester, M. I. *et al.* Associations between cerebral small-vessel disease and Alzheimer disease pathology as measured by cerebrospinal fluid biomarkers. *JAMA neurology* **71**, 855-862, (2014).

258 Schreiber, S. *et al.* Interplay between age, cerebral small vessel disease, parenchymal amyloid-beta, and tau pathology: longitudinal studies in hypertensive stroke-prone rats. *J Alzheimers Dis* **42 Suppl 3**, S205-215, (2014).

259 Grimmer, T. *et al.* White matter hyperintensities predict amyloid increase in Alzheimer's disease. *Neurobiol Aging* **33**, 2766-2773, (2012).

260 Toledo, J. B. *et al.* Factors affecting Abeta plasma levels and their utility as biomarkers in ADNI. *Acta Neuropathol* **122**, 401-413, (2011).

261 van Dijk, E. J. *et al.* Plasma amyloid beta, apolipoprotein E, lacunar infarcts, and white matter lesions. *Ann Neurol* **55**, 570-575, (2004).

262 Gurol, M. E. *et al.* Plasma beta-amyloid and white matter lesions in AD, MCI, and cerebral amyloid angiopathy. *Neurology* **66**, 23-29, (2006).

263 Jack, C. R., Jr. *et al.* Hypothetical model of dynamic biomarkers of the Alzheimer's pathological cascade. *Lancet Neurol* **9**, 119-128, (2010).

264 Renne, T. *et al.* Defective thrombus formation in mice lacking coagulation factor XII. *J Exp Med* **202**, 271-281, (2005).

265 Cardigan, R. A., Crook, M., Mackie, I. J. & Machin, S. J. Plasma levels of factor XIIa and factor VIIa are increased but not related in primary hyperlipidaemia. *Blood Coagul Fibrinolysis* **12**, 187-192, (2001).

266 Siegerink, B., Govers-Riemslag, J. W., Rosendaal, F. R., Ten Cate, H. & Algra, A. Intrinsic coagulation activation and the risk of arterial thrombosis in young women: results from the Risk of Arterial Thrombosis in relation to Oral contraceptives (RATIO) case-control study. *Circulation* **122**, 1854-1861, (2010).

267 Kohler, H. P., Carter, A. M., Stickland, M. H. & Grant, P. J. Levels of activated FXII in survivors of myocardial infarction--association with circulating risk factors and extent of coronary artery disease. *Thromb Haemost* **79**, 14-18, (1998).

268 Weiser, P. *et al.* Activated contact system and abnormal glycosaminoglycans in lupus and other auto- and non-autoimmune diseases. *Prog Mol Biol Transl Sci* **93**, 443-472, (2010).

269 Pan, J. *et al.* Glycosaminoglycans and activated contact system in cancer patient plasmas. *Prog Mol Biol Transl Sci* **93**, 473-495, (2010).

270 Cugno, M. *et al.* Activation of the coagulation cascade in C1-inhibitor deficiencies. *Blood* **89**, 3213-3218, (1997).

271 Doecke, J. D. *et al.* Blood-based protein biomarkers for diagnosis of Alzheimer disease. *Arch Neurol* **69**, 1318-1325, (2012).

272 Mapstone, M. *et al.* Plasma phospholipids identify antecedent memory impairment in older adults. *Nat Med* **20**, 415-418, (2014).

273 Noguchi, M. *et al.* Roles of serum fibrinogen alpha chain-derived peptides in Alzheimer's disease. *Int J Geriatr Psychiatry* **29**, 808-818, (2014).

274 Schmaier, A. H. Physiologic activities of the contact activation system. *Thromb Res* **133 Suppl 1**, S41-44, (2014).

275 Aiyaz, M., Lupton, M. K., Proitsi, P., Powell, J. F. & Lovestone, S. Complement activation as a biomarker for Alzheimer's disease. *Immunobiology* **217**, 204-215, (2012).

276 Crehan, H., Hardy, J. & Pocock, J. Microglia, Alzheimer's disease, and complement. *International journal of Alzheimer's disease* **2012**, 983640, (2012).

277 Schmaier, A. H. The elusive physiologic role of Factor XII. *J Clin Invest* **118**, 3006-3009, (2008).

278 Niwa, K., Kazama, K., Younkin, S. G., Carlson, G. A. & Iadecola, C. Alterations in cerebral blood flow and glucose utilization in mice overexpressing the amyloid precursor protein. *Neurobiol Dis* **9**, 61-68, (2002).

279 Iadecola, C. Neurovascular regulation in the normal brain and in Alzheimer's disease. *Nat Rev Neurosci* **5**, 347-360, (2004).